Doctoral Dissertation

Preparation and Evaluation of Catalytic Properties of Myoglobins Reconstituted with Abiological Prosthetic Groups Toward Development of an Artificial Metalloenzyme

Hiroyuki Meichin

January, 2018

Graduate School of Engineering,

Osaka University

Doctoral Dissertation

Preparation and Evaluation of Catalytic Properties of Myoglobins Reconstituted with Abiological Prosthetic Groups Toward Development of an Artificial Metalloenzyme

(人工生体触媒の開発に向けた非天然金属錯体含有再構成ミオグロビンの調製と触媒反応挙動の解析)

Hiroyuki Meichin

January, 2018

Graduate School of Engineering,

Osaka University

Acknowledgements

The study presented in this thesis has been carried out at Department of Applied Chemistry, Graduate School of Engineering. Osaka University from April 2012 to March 2018. The author would like to express his best gratitude to Professor Takashi Hayashi for his continuous guidance, kind suggestion, constant discussions and warm encouragement throughout this research. The author would like to deeply thank Dr. Koji Oohora for his valuable suggestions and helpful discussions.

The author would like to express his gratitude to Professor Nicolai Lehnert at the University of Michigan for his kind suggestions and warm encouragement. The author also acknowledges Professor Susumu Kuwabata and Professor Satoshi Minakata for reviewing the thesis and their valuable suggestions.

The author expresses his great gratitude to Professor Jun-ya Hasegawa, Dr. Akira Nakayama and Ms. Zhao Liming at Hokkaido University for their assistance with DFT calculations. The author also acknowledges Professor Yoshitsugu Shiro at Riken and University of Hyogo and Dr. Hiroshi Sugimoto at Riken for their support in X-ray crystal structural analysis. The author would like to deeply thank Professor Hiroshi Fujii at Nara Women's University and Dr. Takuya Kurahashi at Institute for Molecular Science for their fruitful discussions for EPR measurements.

The author would like to express his great gratitude to Dr. Akira Onoda for his helpful suggestions and constant discussions. Acknowledgement is also made to all members at Professor Takashi Hayashi's group and Professor Nicolai Lehnert's group for their encouragements and friendship in their laboratories.

The author would like to express his great gratitude to his family for their assistance.

Finally, The author is grateful for financial supports by the program of leading graduate schools at Osaka University; Interdisciplinary Program for Biomedical Sciences.

Hiroyuki Meichin

January 2018

Contents

General Introduction

1-1. Metalloenzyme

Metalloenzymes, which contain one or more metal ions or complexes in the protein matrix, account for approximately 30% of the total enzymes. For example, cytochrome P450 has iron protoporphyrin IX complex (heme *b*) and it is responsible for biosynthesis of various natural product and detoxification of xenobiotics (Figure 1-1).[1a,b] Methyl coenzyme M reductase found in some methanogenic archaea contains a nickel corphin complex (F430) and promotes the formation of a hetero disulfide bond between coenzyme M and coenzyme B with concomitant production of methane.[2a,b] Methane monooxygenase includes a dinuclear iron complex coordinated by multiple carboxylate ligands and catalyzes monooxygenation reaction of methane to yield methanol using molecular dioxygen as an oxidant.[3a,b] Under mild conditions, the natural metalloenzymes promote the chemical reactions, whereas these reactions intrinsically require harsh conditions in a laboratory level. However, natural metalloenzymes generally show poor reactivities toward unnatural substrates because of the high substrate specificity. Furthermore, scope of the reactions catalyzed by natural metalloenzymes is limited to biological reactions. Various efforts to overcome these disadvantages of natural enzymes have been reported in the field of protein engineering. In particular, development of artificial metalloenzymes with broader scopes for substrates and reactions has been attracting much interest.

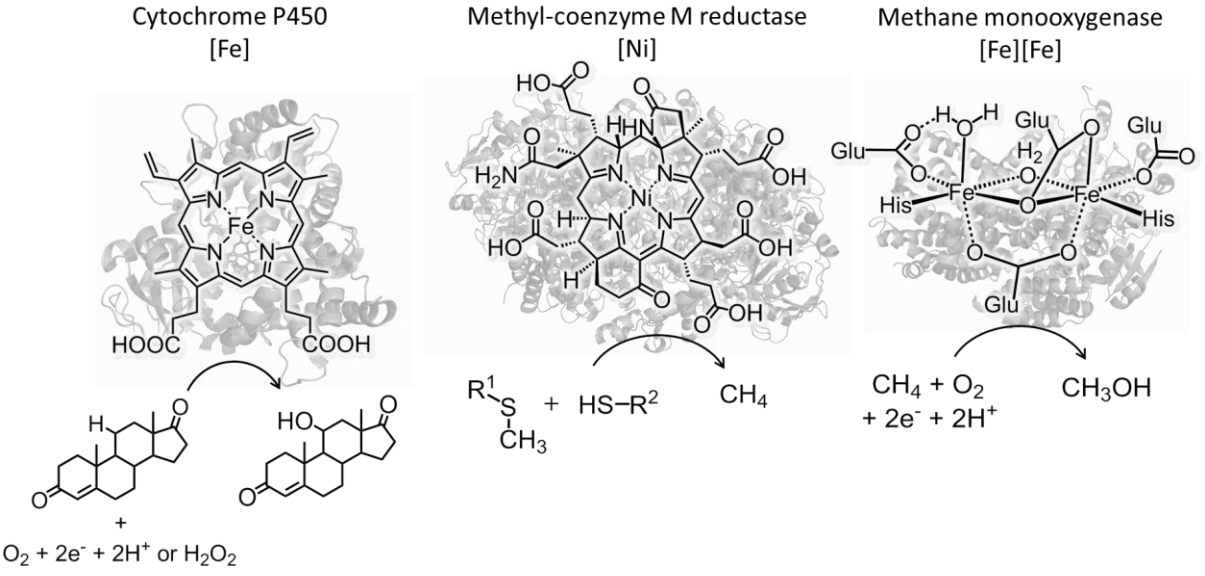

Figure 1-1. Structures and reactions of natural metalloenzymes and molecular structures of active sites containing metal ions. (PDB ID: 1OG2, 1MRO, and 1XU3 for cytochrome P450, methyl coenzyme M reductase, and methane monooxygenase, respectively).

1-2. Artificial Metalloenzyme

Incorporation of artificial metal complexes into protein matrices is a useful strategy for creating artificial metalloenzymes (Figure 1-2), because the metal complexes are able to work as an abiological prosthetic groups within the protein. The first example of an artificial metalloenzyme was reported by Whiteside in 1978.[4] He focused on avidin, a natural protein with a barrel-like structure, tightly binds a biotin moiety with a dissociation constant of ~10^{-15} M,[5] and prepared a biotinylated rhodium diphosphine complex which was able to be incorporated into the cavity of avidin. Obtained rhodium-immobilized avidin was found to promote the hydrogenation of several olefins with 41% enantiomeric excess of the product. Despite the fascinating aspect of their research, no major progress has been made in the next few decades because of limited tools for both organometallic chemistry and protein engineering. Being inspired by the pioneering work, in recent years, various artificial metalloenzymes have been developed. Representative chemical reactions catalyzed by artificial metalloenzymes are summarized as follows (Figure 1-3).

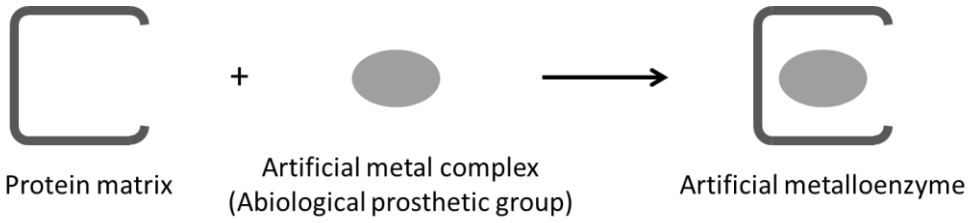

Figure 1-2. A concept of development of an artificial metalloenzyme.

1-3. Reaction Scope of Artificial Metalloenzymes

In recent years, artificial metalloenzymes toward various reactions have been developed. Representative reactions catalyzed by artificial metalloenzymes are categorized as follows and examples are summarized in Figure 1-3: (a) hydrogenation,[6,7] (b) hydrogen evolution,[8-10] (c) polymerization,[11-13] (d) Diels-Alder reaction,[14,15] (e) and (f) Suzuki-Miyaura coupling,[16,17] (g) monooxygenation of sulfinde,[18,19] and (h) hydroxylation.[20]

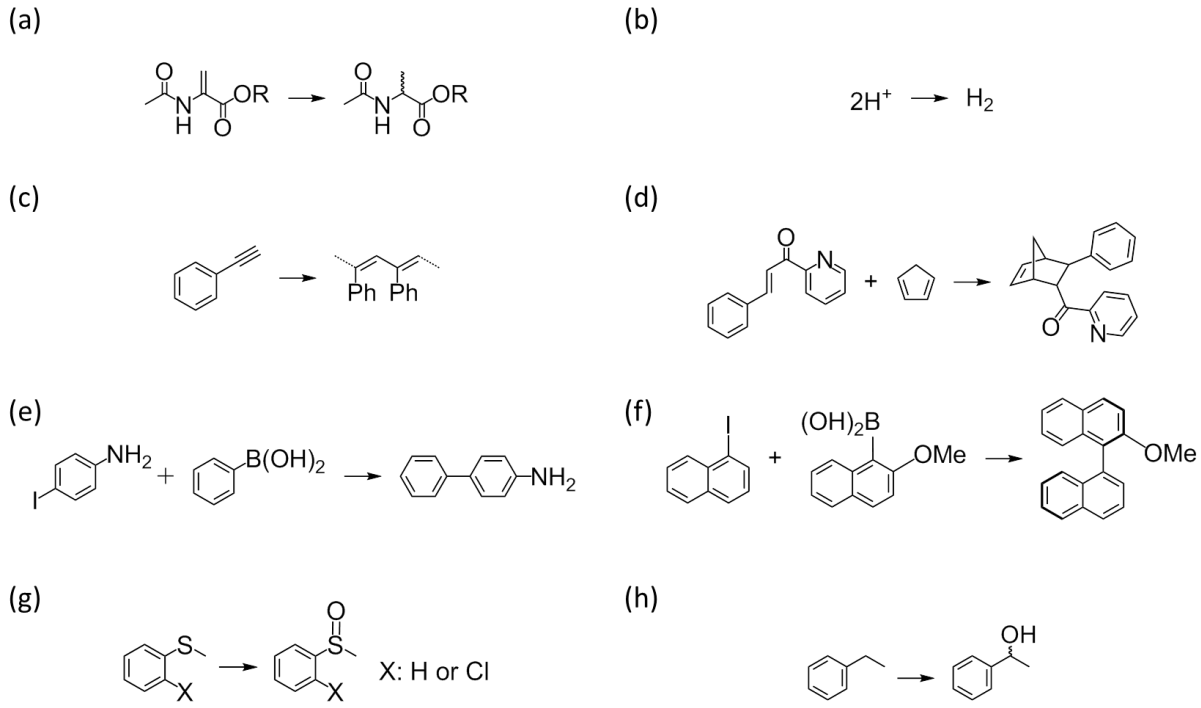

Figure 1-3. Reaction scope by artificial metalloenzymes. (a) Hydrogenation of dehydroamino acid derivatives, (b) hydrogen evolution, (c) polymerization of phenylacetylene, (d) Diels-Alder reaction of azachalcone with cyclopentadiene, (e), cross-coupling of iodoaniline with phenylboronic acid, (f) cross-coupling of iodonaphthalene with naphthaleneboronic acid, (g) monooxygenation of thioanisole derivatives, and (h) hydroxylation of ethylbenzene.

(a) Hydrogenation

Ward *et al.* demonstrated asymmetric hydrogenation of dehydroamino acids by employing rhodium-containing streptavidin variants as artificial metalloenzymes.[6] The optimized protein matrix provides 95%*ee* and quantitative formation of the desired product. Zhang *et al.* reported the incorporation of a rhodium complex in the cavity of lipase and investigated the catalytic activity for hydrogenation of dehydroamino acids.[7] The obtained artificial metalloenzyme showed complete consumption of the substrate.

(b) Hydrogen evolution

Bren *et al.* reported that substitution of the iron atom in cytochrome c_{552} with a cobalt atom provides an artificial hydrogenase with turnover number of 27000 for hydrogen evolution.[8] Ghirlanda *et al.* demonstrated light-driven hydrogen generation using a cobalt-substituted myoglobin.[9] The Co-myoglobin showed 4.3-fold increase in turnover number as compared to the free cobalt complex. Hayashi and Onoda *et al.* reported the introduction of a dinuclear iron complex into the cavity of nitrobindin (Nb) and investigated the activity for photocatalytic hydrogen production.[10] The obtained Nb-diiron complex produced molecular hydrogen with turnover number of 130.

(c) Polymerization

In 2009, Watanabe and Ueno *et al.* reported the introduction of a rhodium complex in the cavity of ferritin to examine the catalytic activity for the polymerization of phenylacetylene.[11] Poly(phenylacetylene) produced by the Rh-ferritin showed an average molecular weight (M_w) of 13.1 ± 1.5 × 10^3 g/mol and polydispersity (M_w/M_n) of 2.6 ± 0.3, while poly(phenylacetylene) produced by free rhodium complex showed M_w of 63.7 ± 4 × 10^3 g/mol and M_w/M_n of 21.4 ± 0.4. The narrow molecular weight distribution of the product indicates the polymerization occurring in the protein matrix. More recently, Hayashi *et al.* prepared a rhodium Cp* complex-linked Nb to develop an artificial polymerase.[12] The rhodium complex in an optimized Nb variant with a suitable reaction cavity provided *trans*-selective polymerization of phenylacetylene, while the free rhodium complex showed thermodynamically favorable *cis*-selectivity.[13]

(d) Diels-Alder reaction

In 2006, Reetz *et al.* demonstrated the Diels-Alder reaction of azachalcone with cyclopentadiene catalyzed by serum albumin containing a cupper phthalocyanine complex as an abiological prosthetic group.[14] Okuda *et al.* reported that the tridentate cupper complex immobilized in in the cavity of FhuA, a transmembrane protein of ferric hydroxamate uptake component A, catalyzes the Diels-Alder reaction with excellent *endo*-selectivity.[15]

(e), (f) Suzuki-Miyaura coupling

Reports on development of artificial Suzukiases are relatively limited. Watanabe *et al.* prepared the first artificial Suzukiase by incorporating $[Pd(allyl)Cl]_2$ into ferritin cavity.[16] The resulting Suzukiase promotes the cross-coupling up to TOF of 3500 / hour. More recently, Ward *et al.* reported that streptavidin containing a palladium complex is capable of catalyzing enantioselective Suzuki-Miyaura coupling to afford enantio-enriched binaphtyls.[17]

(g) Oxygenation of sulfides

Ménage *et al.* reported the development of an artificial sulfoxidase by incorporating a manganese salen complex into a human serum albumin (HSA) matrix.[18] In the reaction of thioanisole and sodium hypochlorite, the free manganese salen complex afforded methyl phenyl sulfone as a product, whereas HSA–manganese salen complex led to the formation of sulfoxide product selectively, although no enantioselectivity was observed. A better result was obtained by incorporating a cobalt salen complex into a bovine serum albumin (BSA) as reported by Liang and co-workers. The BSA–cobalt salen complex showed enantioselectivity up to 87%*ee* toward the sulfoxidation of 2-chlorothioanisole using hydrogen peroxide as an oxidant.[19]

(h) Hydroxylation reaction

Activation and functionalization of an inert C–H bond are still a challenging topic. In 2013, Hayashi *et al.* reported C–H bond hydroxylation of ethylbenzene using myoglobin containing a manganese complex as an abiological prosthetic group.[20] The reconstituted protein promotes the reaction with turnover number of 13, whereas the free manganese complex does not promote the catalysis.

Thus, artificial metalloenzymes are capable of not only improving the selectivity such as enantioselectivity and chemoselectivity but also catalyzing the reaction which is not promoted by the corresponding free metal complexes. These studies clarify that the introduction of an appropriate abiological prosthetic group into an appropriate protein matrix as a reaction field enables the development of artificial metalloenzymes with various reactivities.

1-4. Myoglobin as a Promising Protein Matrix

In this doctoral dissertation research, myoglobin (Mb) was utilized as the protein matrix. Mb is an O_2 storage protein containing protoporphyrin IX iron complex (heme) as a natural prosthetic group (Figure 1-4a). In the Mb matrix, an iron atom of the heme molecule is coordinated by histidine 93 and molecular dioxygen in the oxygenated form. The coordinated dioxygen is stabilized by the hydrogen bonding interaction with histidine 64 in the distal side of the heme binding pocket. Native Mb (nMb) also shows peroxidase activity, which is quite lower than that of native peroxidases such as horseradish peroxidase (HRP). However, Mb is a promising scaffold for development of an artificial metalloenzyme because of its simple, rigid and stable structure. More importantly, the prosthetic group of Mb, heme, is easily removed under acidic conditions to afford apoMb. Under neutral pH, a suitable metal complex as an abiological prosthetic group can be inserted into the vacant pocket of apoMb (Figure 1-4b). The obtained protein is called as a reconstituted Mb (rMb).

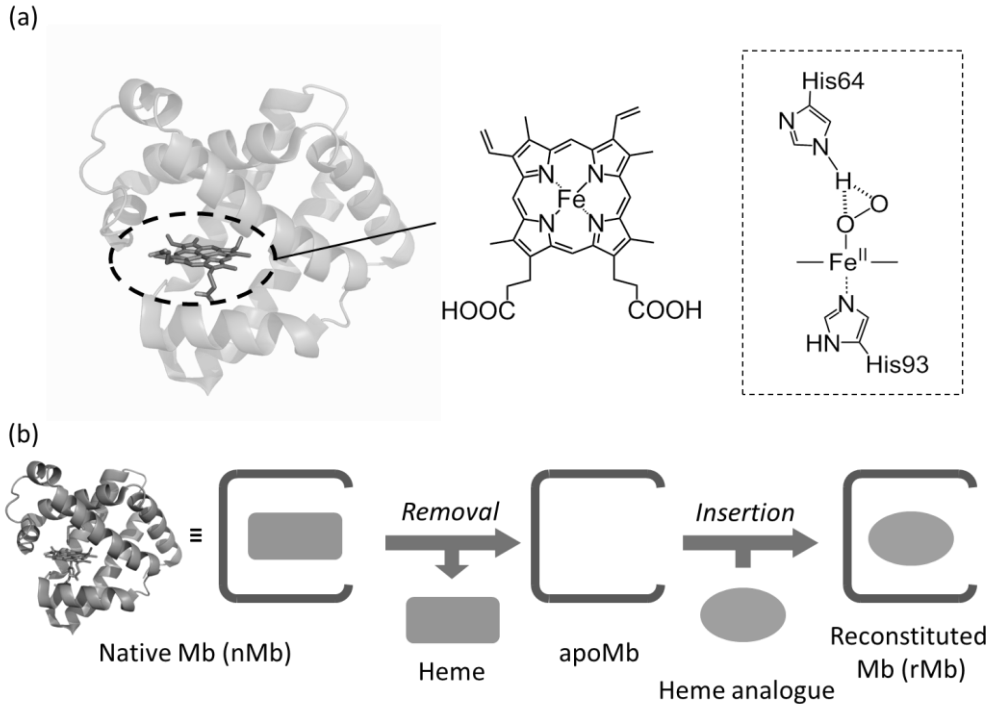

Figure 1-4. (a) Structure of Mb (PDB ID: 1YMB) and heme and hydrogen bonding network between oxygenated heme and distal histidine. (b) Schematic representation of reconstitution of Mb.

1-5. Design of Abiological Prosthetic Groups for Myoglobin

To design a porphyrin-based abiological prosthetic group for Mb, at least three strategies are available (Figure 1-5): (1) modification of peripheral groups, (2) modification of the macrocycle structure and (3) substitution of the metal center.

Figure 1-6 summarizes the examples of abiological prosthetic groups for Mb. In 1999, Ogoshi and Hayashi *et al.* reported that introduction of the substrate binding site to the propionate side chains of native heme of Mb enhanced peroxidase activity by 13-fold for oxidation of 2-methoxyphenol (Figure 1-6a).[21] In that research, the authors also investigated the oxidative reactivity toward neutral substrates such as catechol, hydroquinone, and cationic substrate such as $[Ru(NH_3)_6]^{2+}$.

Asakura *et al.* revealed that Mb reconstituted with 2,4-diformyl porphyrin iron complex showed lower O_2 binding affinity than nMb because of strong electron withdrawing effect of the formyl groups (Figure 1-6b).[22] Although functional modifications of Mb were achieved using abiological prosthetic groups with modified peripheral groups, the changes were moderate.

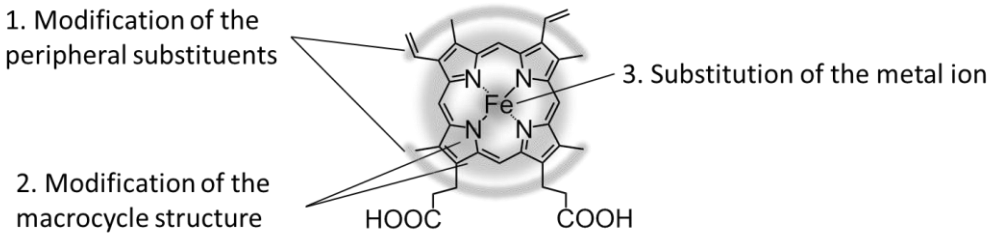

Figure 1-5. Schematic representation for design of abiological prosthetic groups for Mb.

Modifications of the macrocycle structure have been found to dramatically change the function of Mb (strategy 2, Figure 1-6c,d). For example, Hayashi and Hisaeda *et al.* reported that Mb reconstituted with iron porphycene, a constitutional isomer of porphyrin, shows 1400-fold enhancement of O_2 binding affinity compared to nMb.[23] They speculated that the high O_2 affinity is derived from slower O_2 dissociation, whici is mainly caused by the strong axial ligand coordination character. In addition, Mb reconstituted with an iron corrole shows 180-fold increase in peroxidase reactivity toward oxidation of 2-methoxyphenol compared to that of nMb.[24]

Substitution of the metal center is also useful for developing a novel abiological prosthetic group for Mb (strategy 3, Figure 1-6e,f). For instance, Zhang *et al.* reported the first example of Mb reconstituted with a Mn protoporphyrin IX complex capable of epoxidation of a C=C bond of styrene.[25] The authors pointed out that the formation of a high-valent manganese-oxo intermediate accounted for the unique

reactivity. As a fascinating example, Mb variants reconstituted with an iridium porphyrin are known to promote carbene insertion reaction to a C–H bond.[26a] Importantly, Mb variants with an iron porphyrin show no catalytic activity toward C–H insertion reaction. In recent years, several groups have reported the preparation of Mb variants containing various noble metals such as iridium, rhodium, and ruthenium porphyrin.[26a-c] Optimized protein matrices promote the carbene-transfer cyclopropanation reaction of styrene derivatives with good yield, diastereoselectivity, and enantioselectivity.

Thus, the modifications of macrocycle core and/or substitution of the metal center are promising strategies for larger functional changes of Mb than introduction of modified substituents in the peripheral position of iron porphyrin.

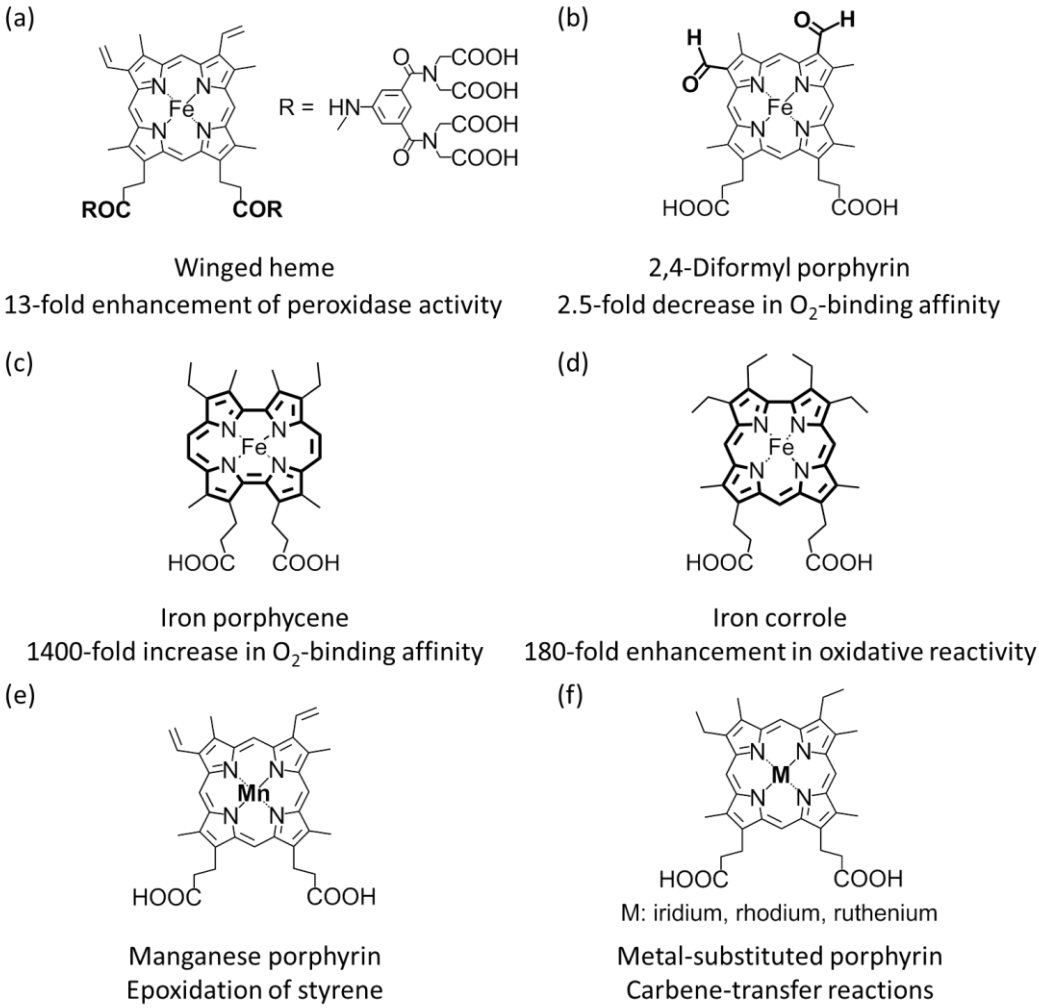

Figure 1-6. Chemical structures of abiological prosthetic groups of Mb.

Outline of This Thesis

This thesis describes the investigation of the reconstituted Mb with the abiological prosthetic groups which were designed by the strategies of structural modifications of macrocycle and/or substitution of the metal center (Figure 1-7). The author constructed a new reconstituted Mb with unique autooxidation and cyanide binding behavior in Chapter 2. In Chapters 3 and 4, evaluations of catalytic properties of reconstituted Mb with cyclopropanation and hydroxylation reactivity are described, respectively.

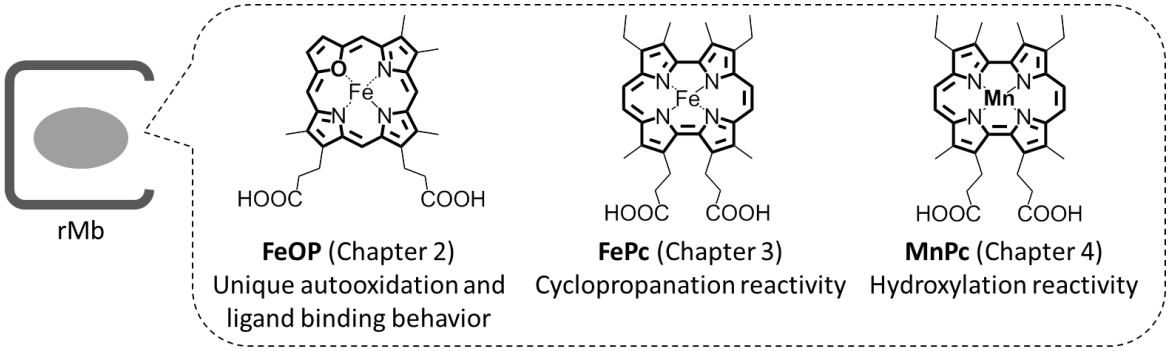

Figure 1-7. Molecular structures of abiological prosthetic groups used in this study.

Chapter 2. *Design, Synthesis, and Characterization of Iron Oxaporphyrin and Evaluation of Physicochemical Properties of Myoglobin Reconstituted with Iron Oxaporphyrin*

The chapter 2 describes design and synthesis of a novel abiological prosthetic group, iron oxaporphyrin (**FeOP**).[27] The electrochemical measurements suggest that the ferrous **FeOP** dimethylester is stable compared to heme moiety. Physicochemical properties of Mb reconstituted with **FeOP** (rMb(**FeOP**)) were also investigated. UV-vis and CD studies suggested that ferric **FeOP** is not stabilized and removed from the heme pocket under aerobic condition. In addition, it is of particular interest that cyanide binding for ferrous rMb(**FeOP**) was 150-fold faster than that for ferric native Mb (nMb).

Chapter 3. *Evaluation of Catalytic Properties of Myoglobin Reconstituted with an Iron Porphycene as an Artificial Metalloenzyme toward Cyclopropanation of Styrene*

The chapter 3 describes the investigation of catalytic behavior of Mb reconstituted with iron porphycene (rMb(**FePc**)) toward the cyclopropanation of styrene with ethyl diazoacetate.[28] rMb(**FePc**) shows significantly enhanced catalytic activity compared to nMb. Mechanistic studies indicate that the reaction of rMb(**FePc**) with ethyl diazoacetate was 615-fold faster than that of nMb to afford the active carbene species. Complementary theoretical calculation indicates that the strong ligand field of the porphycene support the efficient formation of the active carbene species of rMb(**FePc**).

Chapter 4. *Mechanistic Investigations of Myoglobin Reconstituted with a Manganese Porphycene toward Development of an Artificial Monooxygenase*

The chapter 4 describes the mechanistic study of H_2O_2-dependent C–H bond hydroxylation of external substrates by Mb reconstituted with manganese porphycene (rMb(**MnPc**)).[29] rMb(**MnPc**) shows the highest catalytic activity toward hydroxylation of ethylbenzene at pH 8.5 with turnover number of 13. Spectroscopic studies clarified that the Mn^V-oxo species is capable of promoting H-atom abstraction and C–H bond hydroxylation of external substrates.

References

(1) (a) Meunier, B.; de Visser, S. P.; Shaik, S. *Chem. Rev.* **2004**, *104*, 3947 – 3980. (b) Zanger, U. M.; Schwab, M. *Pharmacology & Therapeutics* **2013**, *138*, 103 – 141.

(2) (a) Ankel-Fuchs, D.; Thauer, R. K. *Eur. J. Biochem.* **1986**, *156*, 171 – 177. (b) Goubeaud, M.; Schreiner, G.; Thauer, R. K. *Eur. J. Biochem.***1997**, *243*, 110 – 114.

(3) (a) Bertini, I.; Gray, H. B.; Lippard, S. J.; Valentine, J. S. "Bioinorganic Chemistry ", University Science Books, California, **1994**. (b) Lippard, S. J.; Berg, J. M. "Principles of Bioinorganic Chemistry", University Science Books, California, **1994**.

(4) Wilson, M. E.; Whitesides, G. M. *J. Am. Chem. Soc.* **1978**, *100*, 306 − 307.

(5) Büller, H.; Gallus, A.; Pillion, G.; Prins, M.; Raskob, G. *Lancet* **2012**, *379*, 123 – 129.

(6) Skander, M.; Malan, C.; Ivanova, A.; Ward, T. R. *Chem. Commun.* **2005**, 4815 − 4817.

(7) Shang, G.; Li, W.; Zhang, X.; "Catalytic Asymmetric Synthesis,- Transition Metal-Catalyzed Homogeneous Asymmetric Hydrogenation", John Wiley & Sons, Hoboken, **2010**.

(8) Kandemir, B.; Chakraborty, S.; Guo, Y. X.; Bren, K. L. *Inorg. Chem.* **2016**, *55*, 467 − 477.

(9) Sommer, D. J.; Vaughn, M. D.; Ghirlanda, G. *Chem. Commun.* **2014**, *50*, 15852 − 15855.

(10) Onoda, A.; Kihara, Y.; Fukumoto, K.; Sano, Y.; Hayashi, T. *ACS Catal.* **2014**, *4*, 2645 – 26480.

(11) Abe, S.; Hirata, K.; Ueno, T.; Morino, K.; Shimizu, N.; Yamamoto, M.; Takata, M.; Yashima, E.; Watanabe, Y. *J. Am. Chem. Soc.* **2009**, *131*, 6958 − 6960.

(12) Onoda, A.; Fukumoto, K.; Arlt, M.; Bocola, M.; Schwaneberg, U.; Hayashi, T. *Chem. Commun.* **2012**, *48*, 9756 − 9758.

(13) Fukumoto, K.; Onoda, A.; Mizohata, E.; Bocola, M.; Inoue, T.; Schwaneberg, U.; Hayashi, T. *ChemCatChem* **2014**, *6*, 1229 − 1235.

(14) Reetz, M. T.; Jiao, N. *Angew. Chem., Int. Ed.* **2006**, *45*, 2416 − 2419.

(15) Osseili, H.; Sauer, D. F.; Beckerle, K.; Arlt, M.; Himiyama, T.; Polen, T.; Onoda, A.; Schwaneberg, U.;

Hayashi, T.; Okuda, *Beilstein J. Org. Chem.* **2016**, *12*, 1314 − 1321.

(16) Abe, S.; Niemeyer, J.; Abe, M.; Takezawa, Y.; Ueno, T.; Hikage, T.; Erker, G.; Watanabe, Y. *J. Am. Chem. Soc.* **2008**, *130*, 10512 − 10514.

(17) Chatterjee, A.; Mallin, H.; Klehr, J.; Vallapurackal, J.; Finke, A. D.; Vera, L.; Marsh, M.; Ward, T. R. *Chem. Sci*. **2016**, *7*, 673 − 677.

(18) Rousselot-Pailley, P.; Bochot, C.; Marchi-Delapierre, C.; Jorge-Robin, A.; Martin, L.; Fontecilla-Camps, J. C.; Cavazza, C.; Ménage, S. *ChemBioChem* **2009**, *10*, 545 − 552.

(19) Tang, J.; Huang, F. P.; Wei, Y.; Bian, H. D.; Zhang, W.; Liang, H. *Dalton Trans.* **2016**, *45*, 8061 − 8072.

(20) Oohora, K.; Kihira, Y.; Mizohata, E.; Inoue, T.; Hayashi, T. *J. Am. Chem. Soc.* **2013**, *135*, 17282 − 17285.

(21) Hayashi, T.; Hitomi, Y.; Ando, T.; Mizutani, T.; Hisaeda, Y.; Kitagawa, S.; Ogoshi, H. *J. Am. Chem. Soc.* **1999**, *121*, 7747 – 7750.

(22) Sono, M.; Asakura, T. *J. Biol. Chem.* **1975**, *250*, 5227 – 5232.

(23) Hayashi, T.; Dejima, H.; Matsuo, T.; Sato, H.; Murata, D.; Hisaeda, Y. *J. Am. Chem. Soc.* **2002**, *124*, 11226 – 11227.

(24) Matsuo, T.; Hayashi, A.; Abe, M.; Matsuda, T.; Hisaeda, Y.; Hayashi, T. *J. Am. Chem. Soc.* **2009**, *131*, 15124 – 15125.

(25) Cai, Y.-B.; Yao, S.-Y.; Hu, M.; Liu, X.; Zhang, J.-L. *Inorg. Chem. Front.* **2016**, *3*, 1236 – 1244.

(26) (a) Key, H. M.; Dydio, P.; Clark. D. S.; Hartwig, J. F. *Nature* **2016**, *534*, 534 – 537. (b) Wolf, M. W.; Vargas, D. A.; Lehnert, N. *Inorg. Chem.* **2017**, *56*, 5623–5635. (c) Sreenilayam, G.; Moore, E.; Steck, V.; Fasan, R. *Adv. Synth. Cat.* **2017**, *359*, 2076-2089.

(27) Meichin, H.; Oohora, K.; Hayashi, T *Inorg. Chim. Acta*, **2018**, *472*, 184–191.

(28) Oohora, K.; Meichin, H.; Zhao, L.; Wolf, M. W.; Nakayama, A.; Hasegawa, J.; Lehnert, N. Hayashi, T. *J. Am. Chem. Soc.* **2017**, *139*, 17265 – 17268.

(29) Oohora, K.; Meichin, H.; Kihira, Y.; Sugimoto, H.; Shiro, Y.; Hayashi, T. *J. Am. Chem. Soc.* in press.

Chapter 2

Design, Synthesis, and Characterization of Iron Oxaporphyrin and Evaluation of Physicochemical Properties of Myoglobin Reconstituted with Iron Oxaporphyrin

2-1. Introduction

Porphyrin, a macrocycle with 18 π-electrons, includes four pyrrole rings. Iron protoporphyrin IX complex, heme *b*, plays important roles in binding of small molecules such as O_2, NO and CO[1] as well as in enzymatic activities including biosynthesis of hormones,[2] drug metabolism,[3] and hypochlorite production.[4] These functions harness various redox states of the iron center. Other enzymes utilize different metal porphyrinoid compounds such as a nickel corphin complex (F430) and a cobalt corrinoid complex (cobalamin) (Figure 2-1). F430 is used in the active site of methyl coenzyme M reductase, a methane-evolving enzyme of methanogenic archaea.[5,6] The corphin framework has monoanionic character which stabilizes a Ni(I) species as an active intermediate. Cobalamin is found in cobalamin-dependent enzymes such as diol dehydratase[7-9] and methionine synthase[10,11]. In methionine synthase, a specific Co(I) species is known to be involved in the catalytic cycle. The corrin framework of cobalamin also has monoanionic character.

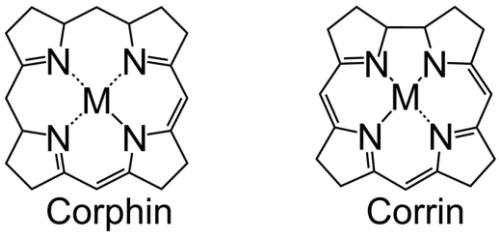

Figure 2-1. Molecular structures of metal complexes of corphin and corrin.

Myoglobin (Mb), a ubiquitous mammalian oxygen storage hemoprotein, uses the heme cofactor which is also used in various oxidative heme enzymes such as cytochrome P450 and heme-containing peroxidases such as horseradish peroxidase. Over several decades, various efforts in the field of protein engineering have demonstrated enhancement of enzymatic activity of Mb as well as ligand binding affinities.[12-27] Furthermore, reconstitution with an artificial cofactor where one of the four pyrrolic nitrogen atoms is substituted with another heteroatom such as oxygen or sulfur is another promising strategy toward development of unique artificial hemoproteins. The O- and S-substituted porphyrins, which are known as oxaporphyrin and thiaporphyrin, respectively, provide the porphyrin with monoanionic character at the

macrocycle core.[28] It is particularly interesting that these porphyrinoids stabilize a low-valent species of a coordinated metal in the framework.[29,30] Therefore, the author describes the preparation of an iron complex of oxaporphyrin (**FeOP**) with a furan ring instead of a pyrrole ring (Figure 2-2). The chapter 2 also describes the physicochemical properties of a new water-soluble iron oxaporphyrin with two propionate side chains and Mb reconstituted with **FeOP** (rMb(**FeOP**)).

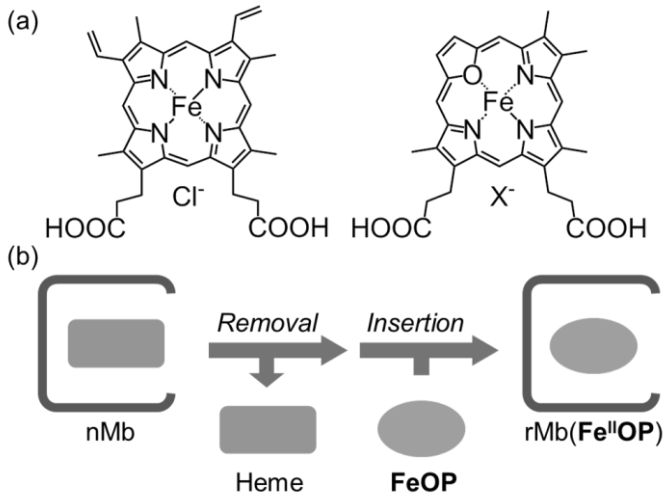

Figure 2-2. (a) Molecular structures of heme and iron oxaporphyrin (**FeOP**) and (b) schematic representation of the reconstitution of Mb.

2-2. Results and Discussions

Preparation and Characterization of FeOP

FeOP was prepared according to the Scheme 2-1. Despite the large number of known porphyrinoid compounds, reports on oxaporphyrin are quite limited.[29-34] In 1971, A. W. Johnson and coworkers reported the synthesis and properties of alkyl group-substituted oxaporphyrin as a monohydrobromide adduct. In the work described in this chapter, oxaporphyrin **7** was isolated in its protonated form. The protonation and deprotonation of the inner nitrogen atom are reversible upon addition of HCl_{aq} or $NaOH_{aq}$ to oxaporphyrin dissolved in methanol, as confirmed by UV-vis spectral changes in Figure 2-3. This behavior is consistent with the report of Johnson *et al*.[31]

Scheme 2-1. Synthesis of **FeOP**.

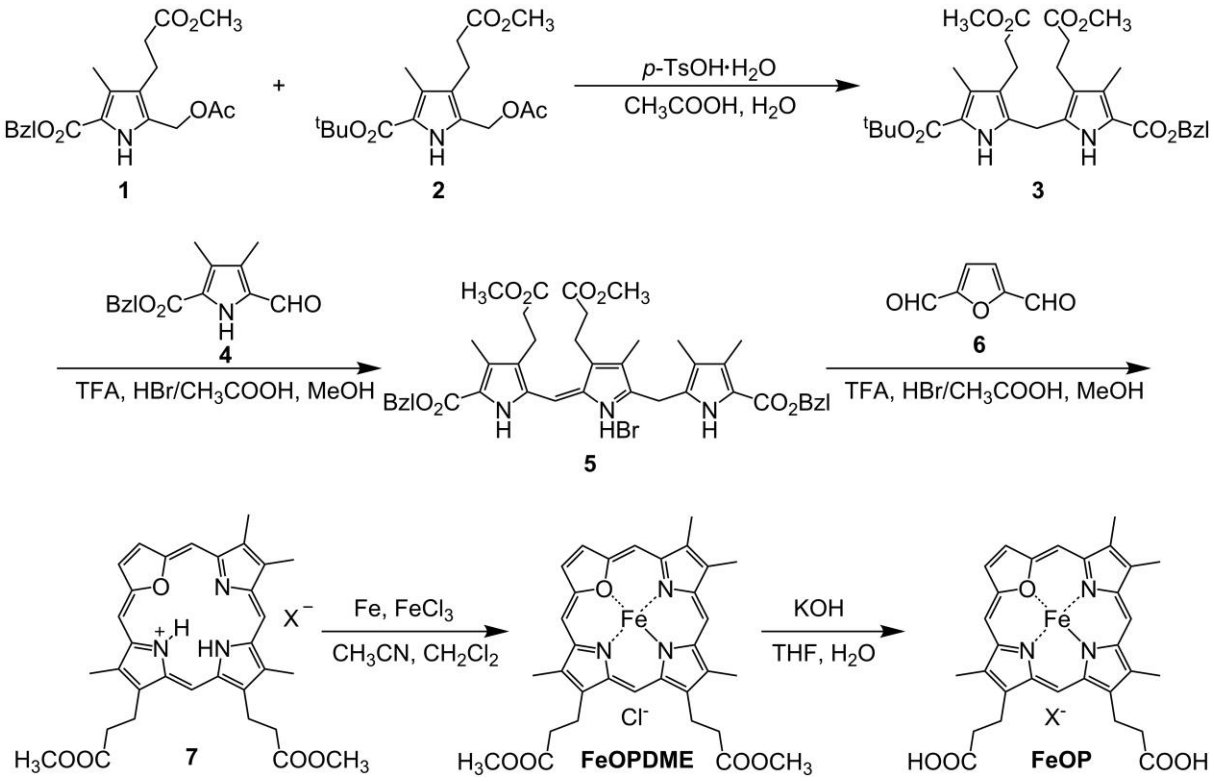

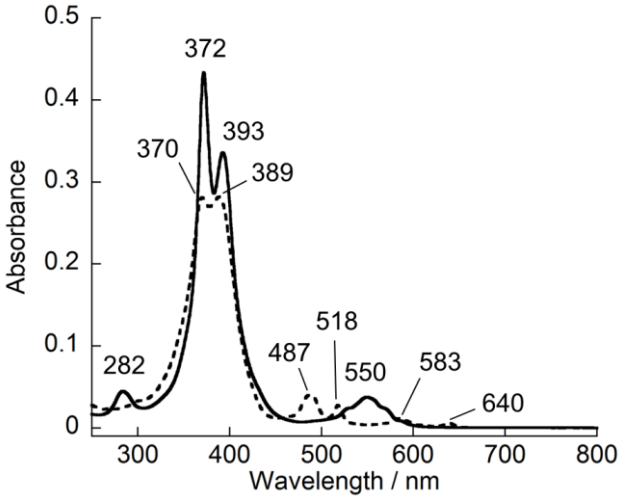

Figure 2-3. UV-vis absorption spectra of oxaporphyrin **7** in methanol with 10 mM hydrochloric acid (solid line) and 50 mM sodium hydroxide (dashed line) containing 1% water at 25 °C.

Insertion of iron into oxaporphyrin **7** was carried out in a similar fashion to generate a thiaporphyrin derivative.[32] The reaction was completed within 2 hours to afford reddish brown compound (**FeOPDME**). The ESI-TOF mass spectrum of **FeOPDME** provides a peak at m/z = 594.169, which is consistent with the calculated exact mass number for $[M–Cl]^+$. This finding supports the formation of a ferrous species in the

macrocycle with consideration of the monoanionic feature of the oxaporphyrin framework. This assignment was also confirmed by measurement of the molar susceptibility of **FeOPDME** using the Evans method.[35] According to the difference of the chemical shift of reference dichloromethane in chloroform-d_1 (Figure 2-19), the molar susceptibility was determined to be 1.25×10^{-7} m^3mol^{-1}, which is in agreement with a complex with $S = 2$. The UV-vis absorption spectrum of **Fe^{II}OPDME** is shown in Figure 2-4. The characteristic split Soret band, two characteristic Q-bands and one shoulder-like Q-band are observed and these are mostly consistent with those of a previously reported iron complex of an oxaporphyrin derivative.[33] The cyclic voltammetries revealed two redox peaks at +0.31 V and -1.1 V vs Ag|AgCl in acetonitrile (Figure 2-18a, b). The former redox peak is assigned to the Fe^{II}/Fe^{III} process, which is positively shifted by 710 mV as compared to that of heme *b*, indicating significant stabilization of the ferrous species in oxaporphyrin. The positive shift of the $E_{1/2}$ value of the Fe^{II}/Fe^{III} process in **FeOPDME** is similar to the observation made in the previous report of a TPP-type oxaporphyrin iron complex.[33] The latter redox peak is attributed to the formation of a one-electron reduced species of the macrocycle, because oxaporphyrin **7** has a redox peak in the cyclic voltammogram at –1.1 V vs Ag|AgCl (Figure 2-18c).

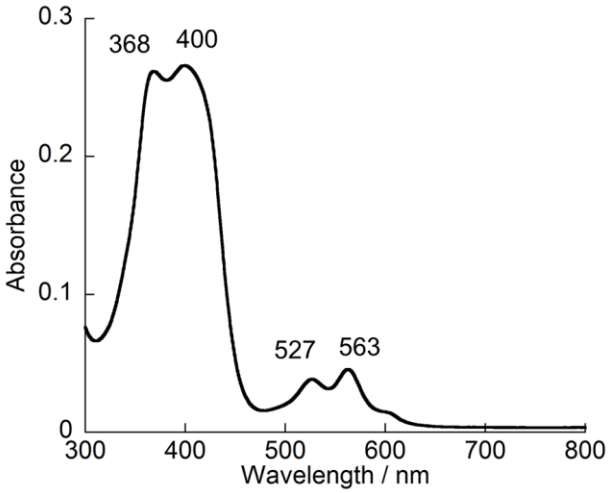

Figure 2-4. UV-vis absorption spectrum of ferrous **FeOPDME** in methanol at 25 °C.

The methyl ester moieties were successfully hydrolyzed under basic conditions to yield **FeOP**. After the reaction, the split Soret band and the characteristic Q-bands disappear in the UV-vis spectrum (Figure 2-5, solid line). This finding suggests that the ferrous state of iron oxaporphyrin is spontaneously oxidized to a ferric μ-oxo dimer product under aerobic conditions.[33] The ESI-TOF mass spectrum of the reaction mixture has a peak with m/z = 574.1349, in which the isotope pattern indicates z = 2+ (Figure 2-17). This value is consistent with the calculated value of the ferric μ-oxo dimer complex (m/z = 574.1347 (z = 2+)). Interestingly, it was found that washing the ferric μ-oxo dimer complex in dichloromethane with 0.1 M HCl removes the iron ion with recovery of the oxaporphyrin free-base species. Instead of employing

acidification, the monomeric ferrous state of **FeOP** complex was obtained by reduction of the μ-oxo dimer complex upon the addition of an excess amount of sodium dithionite. The formation of the ferrous species was confirmed by UV-vis spectroscopy (Figure 2-5, dashed line).

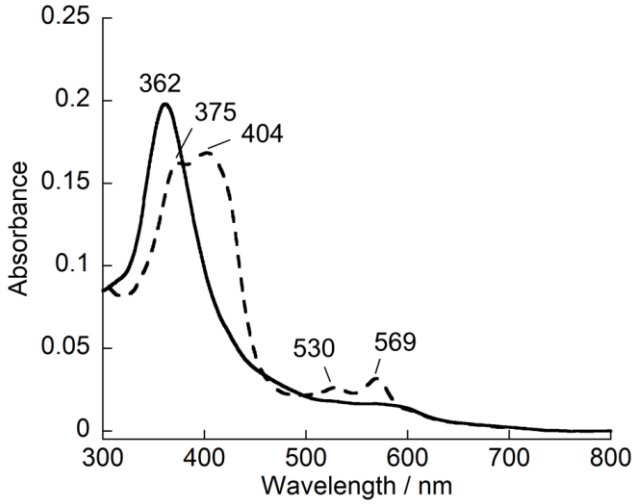

Figure 2-5. UV-vis absorption spectra of the μ-oxo dimer of ferric state of **FeOP** (solid line) and monomer of the ferrous state of **FeOP** (dashed line) in methanol at 25 °C.

Preparation and Characterization of rMb(FeOP)

Insertion of **Fe^{III}OP** μ-oxo dimer into the heme pocket of Mb was attempted after removal of heme. However, a UV-vis spectral change upon the addition of the dimer into the solution of the apoprotein was not observed because of the highly stable μ-oxo bridge structure. Thus, **Fe^{II}OP** was inserted into apoMb in the presence of sodium dithionite (Figure 2-6). The titration curve given in Figure 2-7a clearly shows the curvature at a 1:1 ratio, indicating stoichiometric binding of **Fe^{II}OP** with apoMb. Size exclusion chromatography suggests that the elution volume monitored at 400 nm and 280 nm for the obtained reconstituted protein is consistent with that observed for the native protein (Figure 2-7b). In addition, the ESI-TOF mass spectrum of the reconstituted protein indicated a 9+ ionized form (calcd: 1947.451, found: 1947.351) (Figure 2-20), which confirms formation of rMb(**FeOP**).

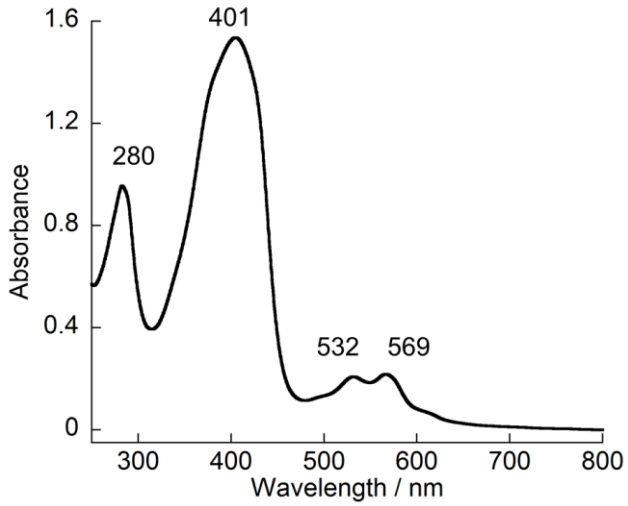

Figure 2-6. UV-vis spectrum of rMb(**FeOP**) in 100 mM potassium phosphate buffer at pH 7.0 at 25 ℃.

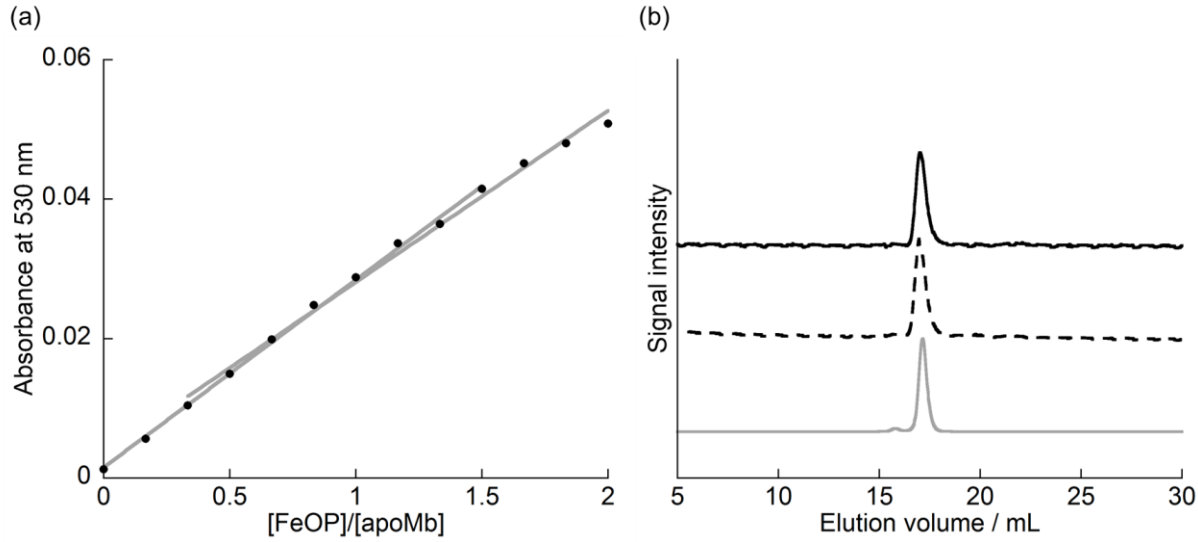

Figure 2-7. (a) Plots of absorbance at 530 nm against the amount of added **Fe^{II}OP** and (b) size exclusion chromatogram of rMb(**FeOP**) (black, solid line: 280 nm, black, dashed line: 400 nm) and nMb (gray, solid line: 409 nm) in 100 mM potassium phosphate buffer at pH 7.0 at 4 ℃.

Investigation of Autooxidation Behavior of rMb(FeOP)

The autoxidation behavior of rMb(**Fe^{II}OP**) was studied. UV-vis spectral changes of rMb(**Fe^{II}OP**) were observed with clear isosbestic points after exposure to air (Figure 2-8a) and characteristic Q-bands essentially disappear within 48 hours. CD spectral changes (Figure 2-8b) suggest that **FeOP** is released from the heme pocket of Mb, because the Cotton effect in the Soret region, which is derived from the chiral environment of the heme pocket, obviously decreases after the reaction. In contrast, the UV-vis spectrum of rMb(**Fe^{II}OP**) under a nitrogen atmosphere does not show any changes over 12 hours (Figure 2-9), supporting the assumption that the spectral changes observed under aerobic conditions are derived from the

autoxidation. Furthermore, UV-vis spectral changes and the disappearance of the CD signal in the Soret region after the addition of potassium ferricyanide indicates that **Fe^{III}OP** is released from the Mb matrix (Figure 2-10). Despite a lot of researches on engineering of Mb, artificial iron complex cofactors which possess dicationic charge are quite limited.[23] It is proposed that the dicationic charged **Fe^{III}OP** significantly decreases in the affinity for the Mb matrix because the hydrophobic interaction between native heme and Mb matrix accounts for the factor of 10^5–10^7 M^{-1} in the overall binding affinity of 1×10^{14} M^{-1}.[36] Similarly, oxidation of ferrous heme to ferric state in soluble guanylyl cyclase, a hemoenzyme, results in release of heme from protein matrix due to lack of hydrophobic interaction.[37]

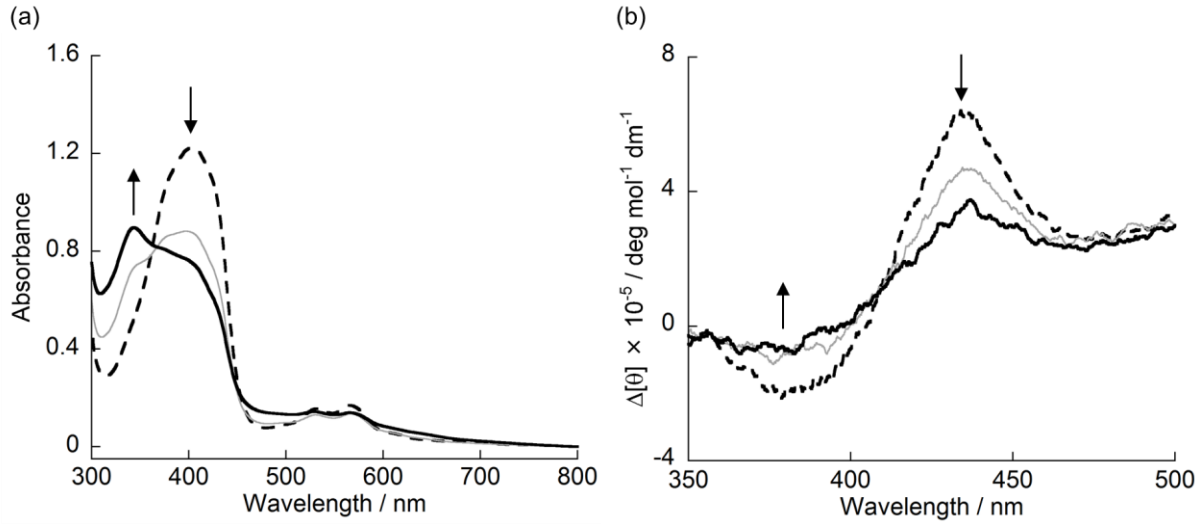

Figure 2-8. (a) UV-vis and (b) CD spectral changes of rMb(**FeOP**) over 48 hours under aerobic conditions in 100 mM potassium phosphate buffer at pH 7.0 at 25 °C.

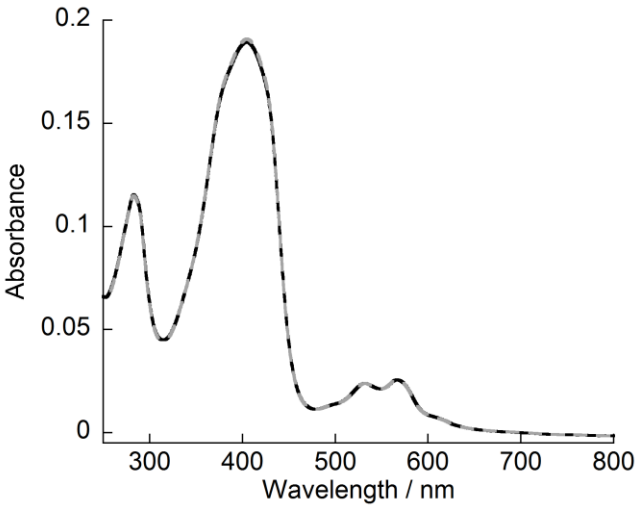

Figure 2-9. UV-vis spectra of rMb(**FeOP**) under anaerobic condition in 100 mM potassium phosphate buffer at pH 7.0 at 25 °C. Spectra were measured at 0 hour (black, solid line) and at 12 hours (gray, dashed line) after preparation of rMb(**Fe^{II}OP**).

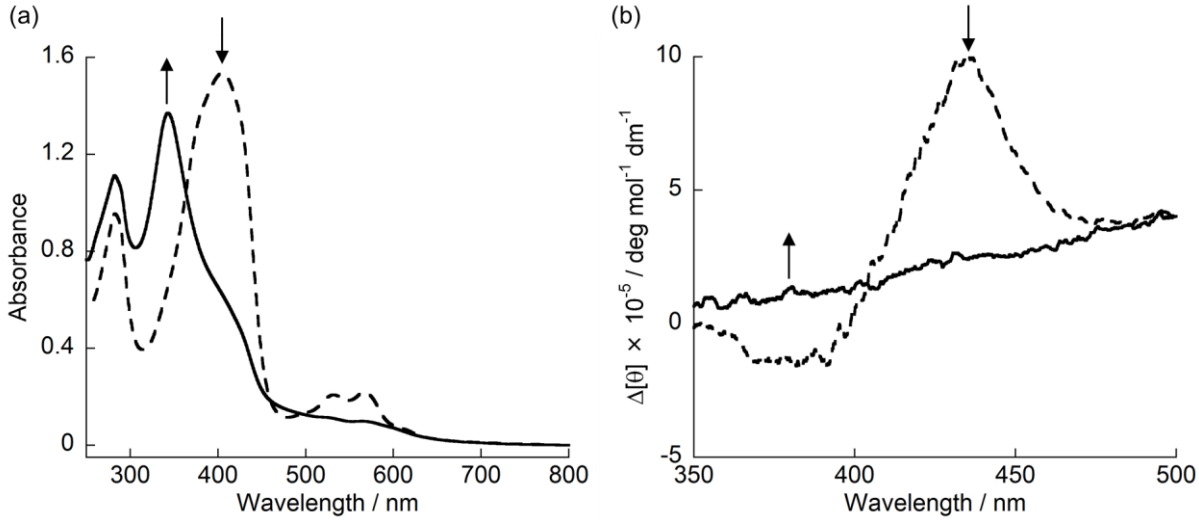

Figure 2-10. (a) UV-vis and (b) CD spectra of rMb(**FeOP**) in the absence (dashed line) and presence (solid line) of potassium ferricyanide under anaerobic conditions in 100 mM potassium phosphate buffer at pH 7.0 at 25 °C. [rMb(**FeOP**)] = 441 μM. [$K_3Fe(CN)_6$] = 860 μM.

Ligand Binding Study to rMb(FeOP)

The addition of potassium cyanide to freshly prepared rMb(**Fe^{II}OP**) induces a color change from brown to pink. UV-vis spectral changes are observed with clear isosbestic points, indicating that cyanide is

capable of binding to the iron center of **Fe^{II}OP** (Figure 2-11) with a binding constant of 1.2×10^4 M^{-1}, although native deoxymyoglobin does not interact with cyanide. Transient absorption spectra were obtained using stopped-flow techniques with various concentrations of potassium cyanide (Figure 2-12). Apparent association and dissociation rate constants, k_{on} and k_{off}, were determined as summarized in Table 2-1. The association of cyanide with rMb(**Fe^{II}OP**) is relatively fast with a k_{on} value of 1.3×10^{-2} $\mu M^{-1}s^{-1}$, which is 150-fold faster than that of ferric nMb. One of the possible reasons for the faster binding may be attributed to the different position of the iron atom in the porphyrinoid plane of **Fe^{II}OP,** relative to its position in heme *b*.[20] The iron atom in **Fe^{II}OP** could be located in the porphyrinoid plane without any deviation from the plane according to the previous report,[39,40] whereas the iron atom in heme *b* is out of plane (with a distance of Δ_{Mb} = 0.29 Å from the protoheme plane).[41] In contrast, the affinity of cyanide for rMb(**Fe^{II}OP**) is 9-fold lower than that of ferric nMb due to its fast dissociation rate.

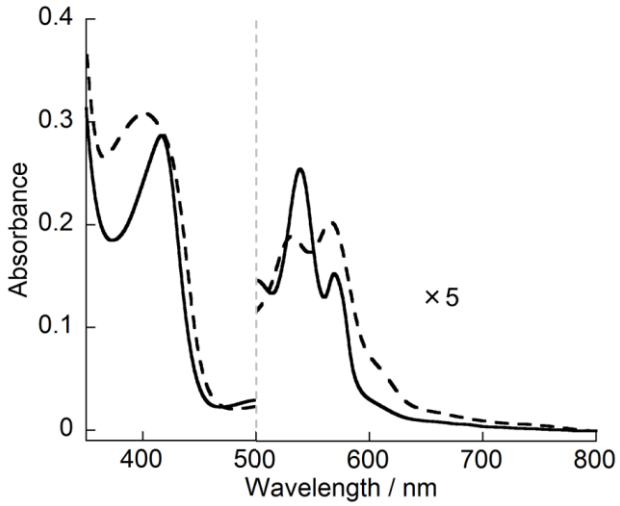

Figure 2-11. UV-vis spectra of 7.8 μM of rMb(**Fe^{II}OP**) in the absence (dashed line) and presence (solid line) of potassium cyanide in 100 mM potassium phosphate buffer at pH 7.0 containing 10 mM sodium dithionite at 25 °C. [rMb(**Fe^{II}OP**)] = 7.8 μM. [KCN] = 770 μM.

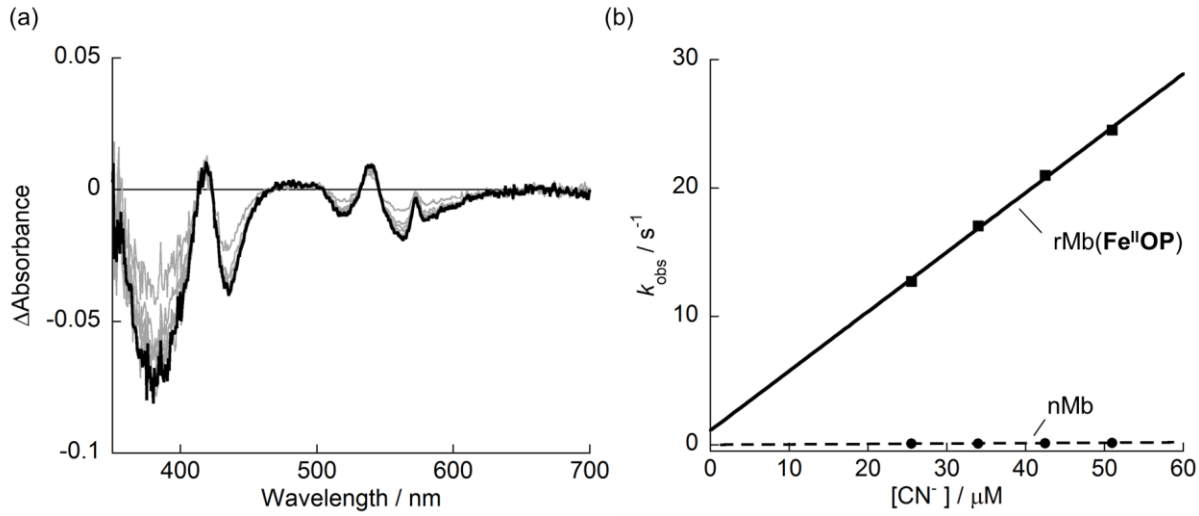

Figure 2-12. (a) Differential transient absorption changes of rMb(**Fe^{II}OP**) during the reaction with potassium cyanide. Spectra were measured every 0.05 s over 0.5 s (solid line: 0.5 s) and (b) plots of rate constants for the reaction of potassium cyanide with (solid line) rMb(**Fe^{II}OP**) and (dashed line) nMb against various concentrations of cyanide ion in 100 mM potassium phosphate buffer at pH 7.0 at 25 °C. In the case of rMb(**FeOP**), the solution contained 10 mM sodium dithionite.

Table 2-1. Cyanide Binding Parameters for nMb and rMb(FeOP).

Protein	k_{on} ($\mu M^{-1}s^{-1}$)[a]	k_{off} (s^{-1})[b]	K_{CN^-} (μM^{-1})
ferric nMb	$8.9 \pm 0.3 \times 10^{-5}$	8.0×10^{-4} [d,e]	0.11
ferrous rMb(**FeOP**) [c]	$1.3 \pm 0.1 \times 10^{-2}$	1.1 ± 0.6	$1.2 \pm 0.6 \times 10^{-2}$

Reaction conditions: 100 mM phosphate buffer (pH 7.0) at 25 °C. [a] Association rate constants of cyanide ligand. [b] Dissociation rate constants of cyanide ligand. [c] in 100 mM potassium phosphate buffer containing 10 mM sodium dithionite. [d] in 110 mM sodium phosphate buffer at pH 6.6 at 25 °C, protein concentration of 5.2 μM. [e] ref 38

2-3. Summary

The work described in this chapter is the first example of the use of iron oxaporphyrin (**FeOP**) as a new myoglobin cofactor. The precursor **FeOPDME** provides a positively shifted Fe^{II}/Fe^{III} redox potential compared to that of heme, indicating that the oxaporphyrin framework clearly stabilizes the ferrous species.

The cofactor, **Fe^{II}OP**, was then successfully incorporated into apoMb to form the reconstituted protein in the presence of dithionite. **Fe^{II}OP** is stable and remains in the protein pocket under a nitrogen atmosphere at room temperature for over 12 hours, whereas under aerobic conditions rMb(**Fe^{II}OP**) releases **FeOP** from the heme pocket via autoxidation. Furthermore, rMb(**Fe^{II}OP**) is capable of binding cyanide as an axial ligand, which is sharply different from nMb. These findings suggest that a metal oxaporphyrin complex has potential for providing new functions as an artificial cofactor of hemoproteins.

2-4. Experimental Section

Instruments

UV-vis spectral measurements were carried out with a UV-2550 or UV-3150 double-beam spectrophotometer (Shimadzu) or V-670 UV-vis-NIR Spectrophotometer (JASCO). pH values were monitored using an F-52 pH meter (HORIBA). ESI-TOF MS analyses were performed on a micrOTOF-II mass spectrometer (Bruker). ^{1}H and ^{13}C NMR spectra were recorded on a DPX 400 or Avance III HD spectrometer (Bruker). Chemical shifts are reported in ppm relative to the internal TMS signal (0.00 ppm). Electrochemical studies were carried out using a potentiostat (CompactStat, Ivium Technologies) using a platinum wire as a counter electrode, an Ag|AgCl (saturated NaClaq: BAS) electrode as a reference and a polished platinum disk as a working electrode under anaerobic conditions. The detection of transiently formed species and kinetic measurements were conducted with a rapid scan stopped-flow system (Unisoku) constructed with a Xe source probe light. CD spectra were recorded at 25 °C on a J-820AC spectropolarimeter (JASCO). Air sensitive manipulations were performed in a UNILab glove box (MBRAUN).

Synthesis of FeOP

All chemicals were purchased from Wako, TCI, Nacalai, and Sigma-Aldrich and used as received unless otherwise noted. Pyrrole derivatives **1**, **2**,[22] **4**,[42] and 1,4-diformylfuran **6** [43] were prepared according to reported procedures. **FeOP** was prepared as described below (Scheme 2-1).

Preparation of Dipyrromethane 3

Pyrrole **1** (1.00 g, 2.68 mmol) and pyrrole **2** (0.91 g, 2.68 mmol) were dissolved in a mixture of glacial acetic acid (65 mL) and water (13 mL). To the solution, *p*-toluenesulfonic acid monohydrate (90 mg, 0.47 mmol) was added and the mixture was stirred for 24 hours at ambient temperature. The reaction mixture was then poured into ice-water (300 mL) and carefully neutralized with sodium bicarbonate, followed by

extraction with dichloromethane. After washing with saturated $NaHCO_{3aq}$ and brine, the organic phase was dried over Na_2SO_4 and dried using a rotary evaporator. The crude product was then purified by silica gel column chromatography (Hexane/AcOEt = 47/3 - 1/1) to afford pure product **3** (544 mg, 0.94 mmol, 35%). ^{1}H NMR (400 MHz, $CDCl_3$) δ = 10.0 (1H, s), 9.31 (1H, s), 7.17-7.09 (5H, m), 5.07 (2H, s), 3.84 (2H, s), 3.49 (3H, s), 3.43 (3H, s) 2.60 (4H, m), 2.25 (4H, m), 2.14 (3H, s), 2.10 (3H, s), 1.36 (9H, s) (Figure 2-13). ^{13}C NMR (100 MHz, $CDCl_3$) δ = 173.49, 173.36, 161.53, 161.18, 136.22, 131.15, 129.59, 128.19, 128.19, 127.67, 127.55, 125.50, 120.05, 119.61, 119.19, 117.47, 79.94, 65.33, 60.13, 51.35, 34.43, 28.19, 22.43, 20.65, 19.15, 13.91, 10.54, 10.45 (Figure 2-14). ESI-TOF MS (positive mode) calculated for $[M+Na]^+$,603.268; found 603.272.

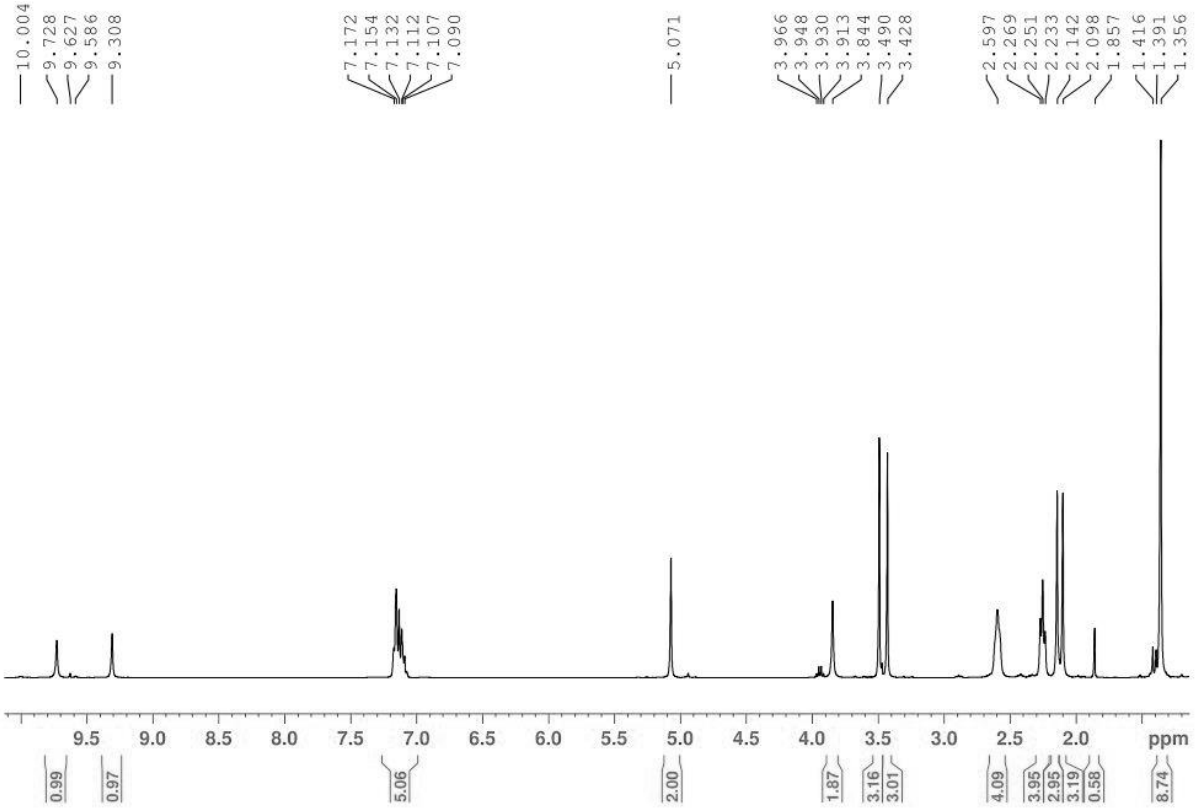

Figure 2-13. ^{1}H NMR (400 MHz) spectrum of **3** in $CDCl_3$.

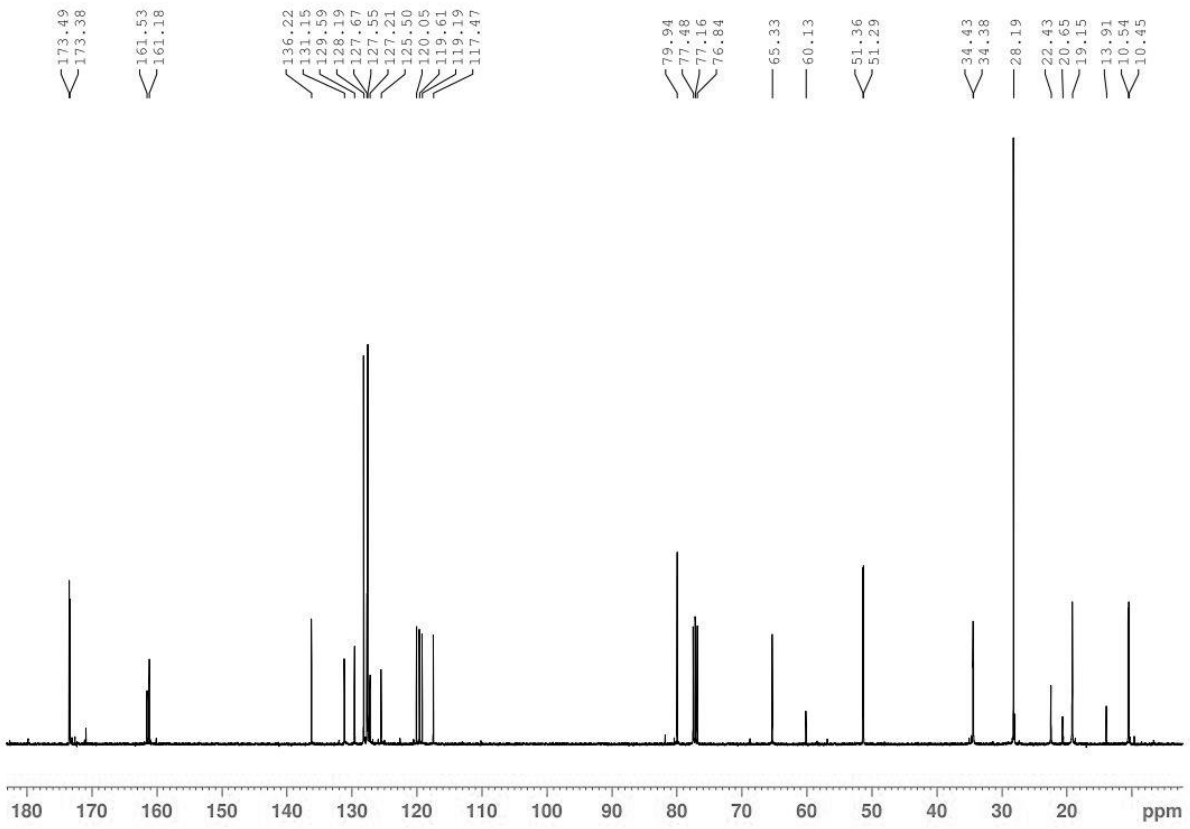

Figure 2-14. ^{13}C NMR (100 MHz) spectrum of **3** in $CDCl_3$.

Preparation of Tripyrrin 5

Dipyrromethane **3** (200 mg, 0.35 mmol) was dissolved in 4 mL of trifluoroacetic acid (TFA) under a nitrogen atmosphere and stirred for 5 min at ambient temperature. To this solution, formylpyrrole **4** (116 mg, 0.45 mmol) in 10 mL of methanol was added and the solution was further stirred for 90 min at ambient temperature. Then 30% HBr/AcOH (70 μL, 0.36 mmol) was added. The solution was then stirred for an additional 30 min before removal of the solvent on a rotary evaporator to provide a red crude oil **5** (381 mg). The obtained oil was then used in the next reaction without purification.

Preparation of Oxaporphyrin 7

Crude tripyrrin **5** (330 mg) was stirred in a mixture of 30% HBr/AcOH (1.4 mL) and TFA (7 mL) for 6 hours under a nitrogen atmosphere. The solution was diluted with 500 mL of methanol and then diformylfuran **6** (54 mg, 0.44 mmol) in 10 mL of methanol was added to this solution. Then the mixture was stirred for 12 hours before removal of the solvent on a rotary evaporator. The obtained red oil was dissolved in dichloromethane and washed with brine three times. The organic phase was dried over Na_2SO_4, evaporated and purified by silica gel column chromatography ($CHCl_3/CH_3OH$ = 49/1 - 3/2) to afford oxaporphyrin **7** (32 mg, 0.059 mmol, 17% in two steps). ^1H NMR (400 MHz, $CDCl_3$) δ = 11.16 (1H, s),

10.82 (1H, s), 10.61 (1H, s), 10.45 (1H, s), 10.36 (1H, s), 10.08 (1H, s), 4.59-4.56 (2H, t, *J* = 6.4 Hz) 4.40-4.37 (2H, t, *J* = 7.2 Hz), 3.89 (3H, s), 3.63 (3H, s), 3.62 (3H, s), 3.59 (3H, s), 3.34-3.27 (4H, m), 1.25 (6H, s) (Figure 2-15). ^{13}C NMR (100 MHz, $CDCl_3$) δ = 173.41, 52.06, 52.00, 36.52, 36.11, 29.85, 21.77, 21.70, 12.50, 12.30, 12.22, 12.04, 1.20, 0.14 (Figure 2-16). ESI-TOF MS (positive mode) calculated for $[M+H]^+$, 540.249; found 540.250.

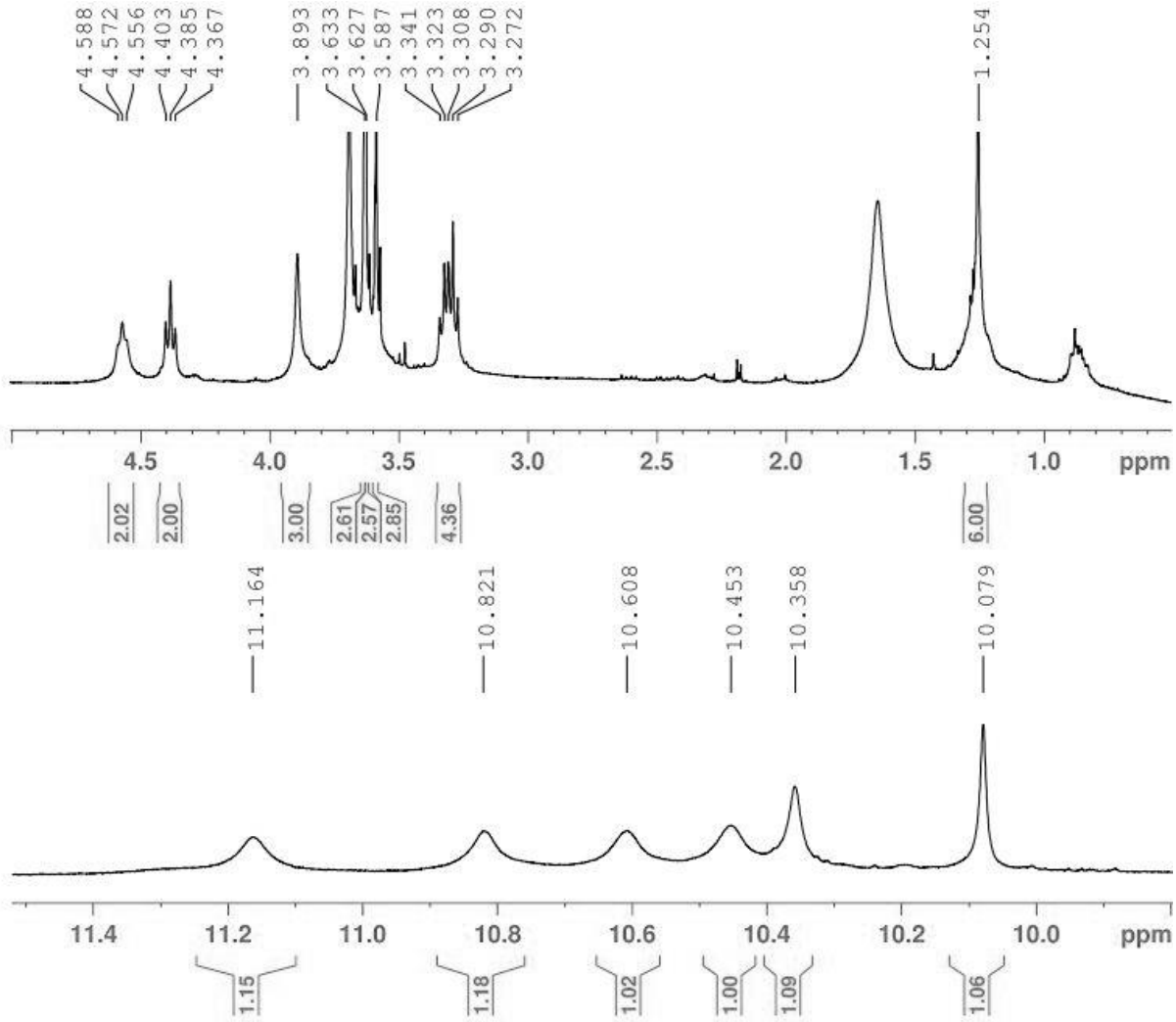

Figure 2-15. ^{1}H NMR (400 MHz) spectrum of **7** in $CDCl_3$.

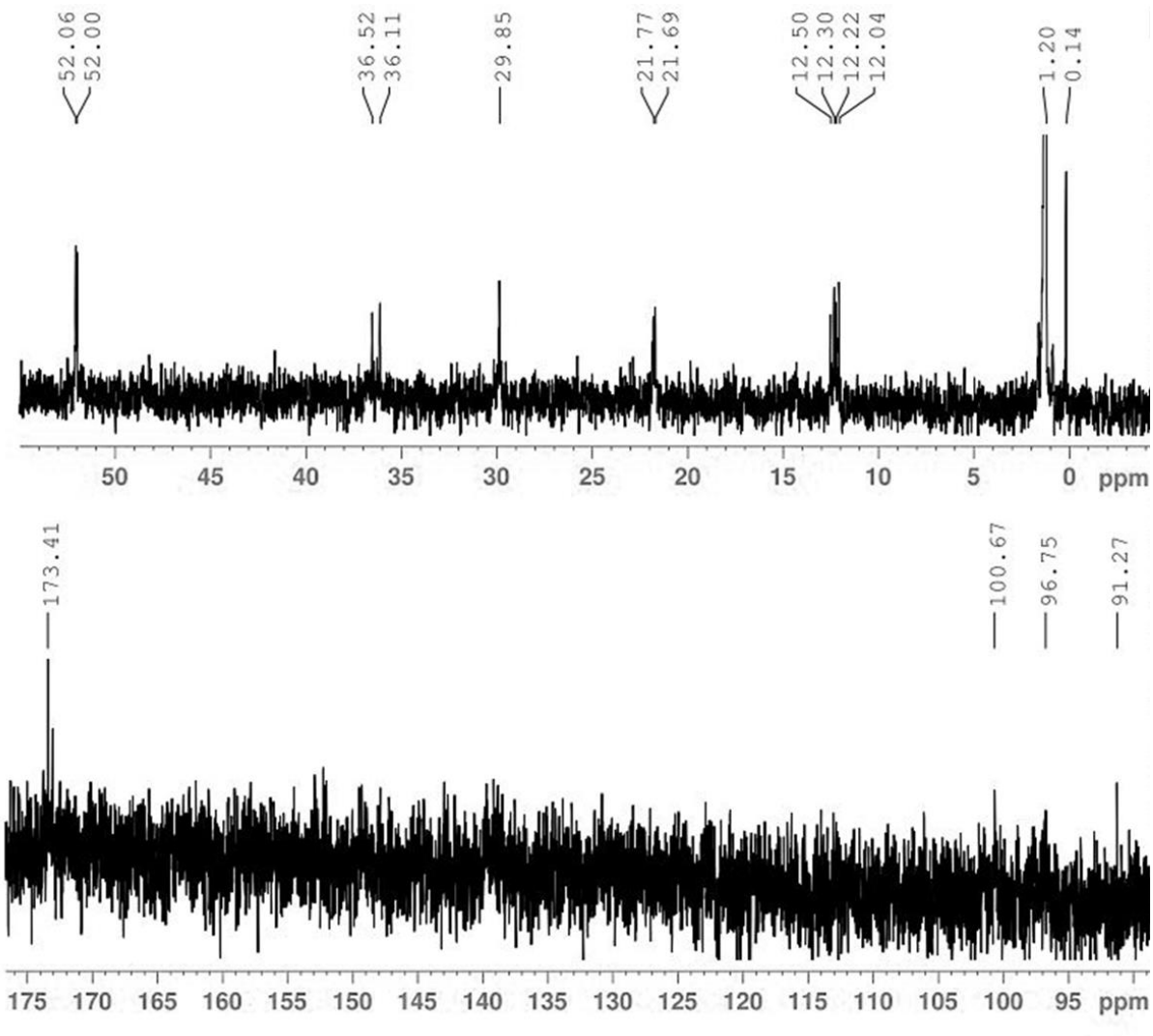

Figure 2-16. ^{13}C NMR (100 MHz) spectrum of **7** in $CDCl_3$.

Preparation of FeOP Dimethyl Ester (FeOPDME)

To oxaporphyrin **7** (6.4 mg, 11.8 μmol) and iron powder (200 mg), degassed acetonitrile (20 mL), dichloromethane (20 mL), and $FeCl_3$ (23 mg, 142 μmol) were added under a nitrogen atmosphere. The solution was refluxed for 2 hours and residual solid iron was filtered and followed by evaporation of solvent. The crude product was purified by gel filtration column chromatography in methanol to give **FeOPDME** (5.5 mg, 8.7 μmol, 74%). HR-ESI-TOF MS (positive mode) calculated for $[M–Cl]^+$, 594.1686; found 594.1690.

Preparation of FeOP

FeOPDME (5.5 mg, 8.7 μmol) was dissolved in 1 mL of THF under a nitrogen atmosphere, and 1 mL of 0.05 M KOH solution was added. This mixture was stirred for 2 hours at ambient temperature. The

reaction mixture was carefully neutralized with 0.05 M HCl solution. After evaporation, the crude product was purified by gel filtration column chromatography in methanol to afford product **FeOP** (1.2 mg, 2.0 μmol, 23%). HR-ESI-TOF MS (positive mode) calculated for $[M–Cl]^+$, 566.1373; found 566.1361 (Figure 2-17).

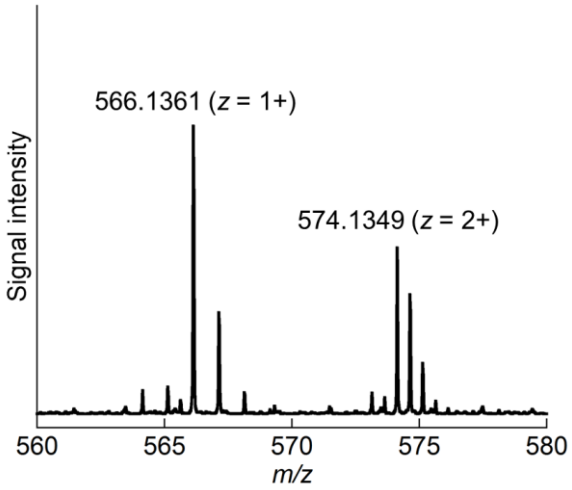

Figure 2-17. ESI-TOF mass spectrum of **FeOP** in methanol.

Electrochemical Measurement of FeOPDME

Cyclic voltammograms (CVs) were taken in the potential range of -1.5 to 0.7 V (vs saturated Ag|AgCl reference electrode) at scan rate of 10 to 300 mV/s in degassed acetonitrile containing 5% DMF and 54 mM of tetrabutylammonium hexafluorophosphate as an electrolyte at 25 °C.

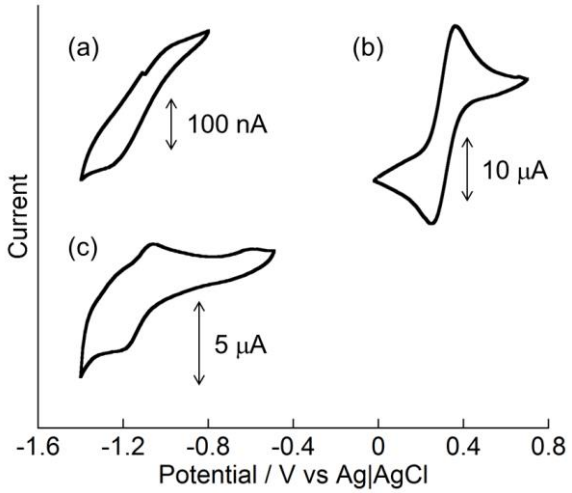

Figure 2-18. CVs of **FeOPDME** ((a), (b)) and **7** (c) in acetonitrile. Scan rate: (a) 300 mV/s and (b) and (c) 10 mV/s in a degassed acetonitrile containing 54 mM tetrabutylammonium hexafluorophosphate as an electrolyte at 25 °C

^{1}H NMR Snalysis of FeOPDME Using Evans Method

The molar susceptibility of **FeOPDME** was determined using the Evans technique (Figure 2-19). ^{1}H NMR spectra of **FeOPDME** (2.5 mM) were measured in chloroform-d_1 solution containing dichloromethane as a reference. The equations below were used in the analysis (eq 2-1, 2-2, 2-3).

$$\chi_M^{para}(m^3/mol) = 3 \times \Delta\delta \times 10^{-6}/(1000 \times M) \quad (2\text{-}1)$$

$$\mu_{eff} = \sqrt{\chi_M^{para} \times 3 \times k \times T/N_A \times \mu_0}/\mu_B \quad (2\text{-}2)$$

$$\mu_{eff} = g\sqrt{S(S+1)} \quad (2\text{-}3)$$

Where $\Delta\delta$ is difference of chemical shift of CH_2Cl_2 in ppm in the presence and absence of **FeOPDME**, M is concentration of **FeOPDME** in mol/L, μ_{eff} is the magnetic susceptibility, k is the Boltzmann constant (1.38×10^{-23} (J/K)), T is temperature in K, N_A is the Avogadro constant ($6.02 \times 10^{23}(\text{mol}^{-1})$), μ_0 is the magnetic permeability of a vacuum ($4 \times \pi \times 10^{-7}$ (T^2m^3/J)), μ_B is the Bohr magneton (9.27×10^{-24} (J/T)), and g is the g value for electron spin (2.002).

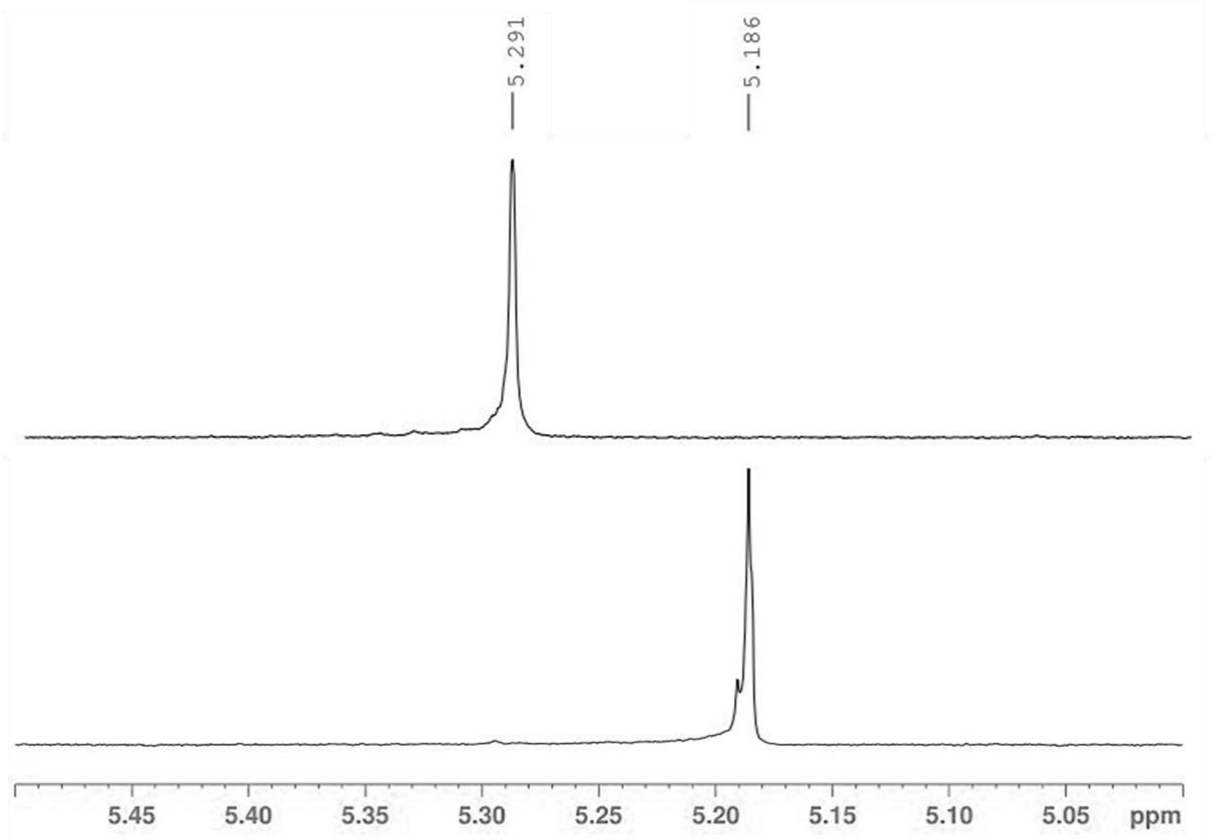

Figure 2-19. ^{1}H NMR (400 MHz) spectra of CH_2Cl_2 in $CDCl_3$: Spectra (a) and (b) are obtained in the presence (2.5 mM) and absence of **FeOPDME**, respectively.

Preparation of rMb(FeOP)

Horse heart Mb was purchased from Sigma-Aldrich and purified by CM-Cellulose cation exchange column (Wako). Removal of the heme molecule from Mb was performed by the reported procedure.[44] An **Fe^{II}OP** solution (60 μL in total, 600 μM in 100 mM potassium phosphate buffer containing 16.7 mM sodium dithionite) was added dropwise to an apoMb solution (3 mL, 6 μM in 100 mM potassium phosphate buffer at pH 7.0) under a nitrogen atmosphere. Excess sodium dithionite and **FeOP** were removed by gel filtration chromatography using a HiTrap desalting column (5 mL, GE Healthcare) with 100 mM potassium phosphate buffer at pH 7.0 under anaerobic conditions. The obtained protein solution was stored anaerobically at 4 °C.

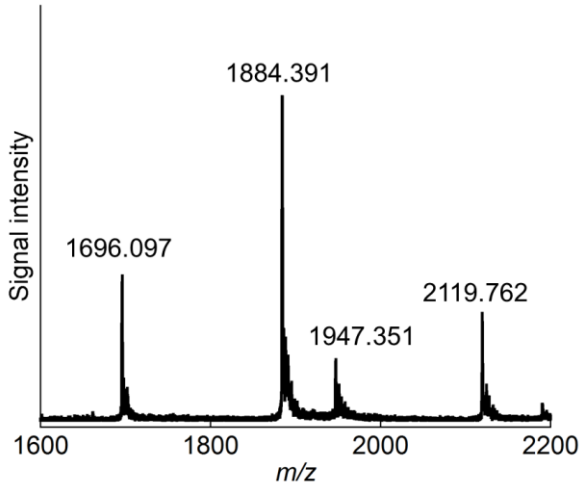

Figure 2-20. ESI-TOF mass spectrum of rMb(**FeOP**) in 10 mM ammonium $acetate_{aq}$.

Oxidation of rMb(Fe^{II}OP) with Potassium Ferricyanide

To a solution of rMb(**Fe^{II}OP**) (400 μL, 450 μM in 100 mM potassium phosphate buffer at pH 7.0), a potassium ferricyanide solution (8.8 μL, 45 mM in 100 mM potassium phosphate buffer at pH 7.0) was added under nitrogen atmosphere. UV-vis and CD spectra were measured before and after addition of potassium ferricyanide.

Ligand binding studies of rMb(Fe^{II}OP)

To a freshly prepared rMb(**Fe^{II}OP**) solution in 100 mM potassium phosphate buffer at pH 7.0 (7.8 μM, 3 mL), potassium cyanide (30 μL, 7.8 mM in 100 mM potassium phosphate buffer at pH 7.0) was added anaerobically and UV-vis spectra were measured. The kinetics of cyanide binding were further studied under anaerobic conditions. The transient absorption spectra of the reaction of rMb(**Fe^{II}OP**) or aqua-met nMb (35 μM) with potassium cyanide (350-1050 μM) were monitored using a stopped-flow rapid scanning apparatus in 100 mM potassium phosphate buffer at pH 7.0 at 25 °C. The absorption changes were fitted to

a single exponential equation to determine apparent rate constants k_{obs} at various concentrations of cyanide anion. The association rate constants k_{on}, dissociation constants k_{off}, and affinities for cyanide anion K_{CN}- were determined with plots of k_{obs} against concentration of cyanide anion. The concentrations of cyanide anion were determined by the following Henderson–Hasselbach equation (eq 2-4).

$$\mathrm{pH} = \mathrm{p}K_\mathrm{a} - \log\left(\frac{[\mathrm{HCN}]}{[\mathrm{CN}^-]}\right) = \mathrm{p}K_\mathrm{a} - \log\left(\frac{\mathrm{C}_0 - [\mathrm{CN}^-]}{[\mathrm{CN}^-]}\right) \qquad (2\text{-}4)$$

where pK_a is 9.2 [45] and C_0 is the concentration of added KCN.

2-5. References and Notes

(1) Ghosh, A. *The Smallest Biomolecules: Diatomics and their Interactions with Heme Proteins*, *Elsevier*, **2008**, 3 – 17.

(2) Meunier, B.; de Visser, S. P.; Shaik, S. *Chem. Rev.* **2004**, *104*, 3947 – 3980.

(3) Zanger, U. M.; Schwab, M. *Pharmacology & Therapeutics* **2013**, *138*, 103 – 141.

(4) Klebanoff, S. J. *J. Leukoc. Biol*. **2005**, *77*, 598 – 625.

(5) Ankel-Fuchs, D.; Thauer, R. K. *Eur. J. Biochem.* **1986**, *156*. 171 – 177.

(6) Goubeaud, M.; Schreiner, G.; Thauer, R. K. *Eur. J. Biochem.* **1997**, *243*, 110 – 114.

(7) Kräutler, B.; Sigel, A. *Metal Ions in Life Science*, *Springer*, **2009**, 1 – 51.

(8) Gruber, K.; Puffer, B.; Kräutler, B. *Chem. Soc. Rev.* **2011**, *40*, 4346 – 4363.

(9) Brown, K. L. *Chem. Rev.* **2005**, *105*, 2075 – 2150.

(10) Drennan, C. L.; Huang, S.; Drummond, J. T.; Matthews, R. G.; Lidwig, M. L. *Science* **1997**, *266*, 1669 – 1674.

(11) Matthews, R. G. *Acc. Chem. Res.* **2001**, *34*, 681 – 689.

(12) Springer, B. A.; Sligar, S. G.; Olson, J. S.; Jr. Phillips, G. N. *Chem. Rev.* **1994**, *94*, 699 – 714.

(13) Draghi, F.; Miele, A. E.; Travaglini-Allocatelli, C.; Vallone, B.; Brunori, M.; Gibson, Q. H.; Olson, J. S. *J. Biol. Chem.* **2002**, *277*, 7509 – 7519.

(14) Sato, H.; Hayashi, T.; Ando, T.; Hisaeda, Y.; Ueno, T.; Watanabe, Y. *J. Am. Chem. Soc.* **2004**, *126*, 436 – 437.

(15) Chakraborty, S.; Reed, J.; Ross, M.; Nilges, M. J.; Petrik, I. D.; Ghosh, S.; Hammes-Schiffer, S.; Sage, J. T.; Zhang, Y.; Schulz, C. E.; Lu, Y. *Angew. Chem. Int. Ed.* **2014**, *53*, 2417 – 2421.

(16) Bröring, M.; Brégier, F.; Burghaus, O.; Kleeberg, C. *Z. Anorg. Allg. Chem.* **2010**, *636*, 1760 – 1766.

(17) Bordeaux, M.; Tyagi, V.; Fasan, R. *Angew. Chem. Int. Ed.* **2015**, *54*, 1744 – 1748.

(18) Hayashi, T.; Hitomi, Y.; Ogoshi, H. *J. Am. Chem. Soc.* **1998**, *120*, 4910 – 4915.

(19) Hamachi, I.; Shinkai, S. *Eur. J. Org. Chem.* **1999,** *1999*, 539 – 549.

(20) Matsuo, T.; Dejima, H.; Hirora, S.; Murata, D.; Sato, H.; Ikegami, T.; Hori, H.; Hisaeda, Y.; Hayashi, T. *J. Am. Chem. Soc.* **2004**, *126*, 16007 – 16017.

(21) Oohora, K.; Kihira, Y.; Mizohata, E.; Inoue, T.; Hayashi, T. *J. Am. Chem. Soc.* **2013**, *135*, 17282 – 17285.

(22) Matsuo, T.; Hayashi, A.; Abe, M.; Matsuda, T.; Hisaeda, Y.; Hayashi, T. *J. Am. Chem. Soc.* **2009**, *131*, 15124 – 15125.

(23) Hayashi, T.; Morita, Y.; Mizohata, E.; Oohora, K.; Ohbayashi, J.; Inoue, T.; Hisaeda, Y. *Chem. Commun.* **2014**, *50*, 12560 – 12563.

(24) Morita, Y.; Oohora, K.; Sawada, A.; Doitomi, K.; Ohbayashi, J.; Kamachi, T.; Yoshizawa, K.; Hisaeda, Y.; Hayashi, T. *Dalton Trans.* **2016**, *45*, 3277 – 2384.

(25) Key, H. M.; Dydio, P.; Clark, D. S.; Hartwig, J. F. *Nature* **2016**, *534*, 534 – 537.

(26) Wolf, M. W.; Vargas, D. A.; Lehnert, N. *Inorg. Chem.* **2017**, *56*, 5623 – 5635.

(27) Sreenilayam, G.; Moore, E. J.; Steck, V.; Fasan, R. *Adv. Synth. Cat.* **2017**, *359*, 2076 – 2089.

(28) Chatterjee, T.; Shetti, V. S.; Sharma, R.; Ravikanth, M. *Chem. Rev.* **2017**, *117*, 3254 – 3328.

(29) Chmielewski, P. J.; Latos-Grażyński, L.; Olmstead, M. M.; Balch, A. L. *Chem. Eur. J.* **1997**, *3*, 268 – 278.

(30) Pacholska, E.; Chmielewski, P. J.; Latos-Grażyński, L. *Inorg. Chim. Acta* **1998**, *273*, 184 – 190.

(31) Broadhurst, M. J.; Grigg, R.; Johnson, A. W. *J. Chem. Soc. C* **1971**, 3681 – 3690.

(32) Latos-Grażyński, L.; Lisowski, J.; Olmstead, M. M.; Balch, A. L. *Inorg. Chem.* **1989**, *28*, 1183 – 1188.

(33) Pawlicki, M.; Latos-Grażyński, L. *Inorg. Chem.* **2002**, *41*, 5866 – 5873.

(34) Stute, S.; Götzke, L.; Meyer, D.; Merroun, M. L.; Rapta, P.; Kataeva, O.; Seichter, W.; Gloe, K.; Dunsch, L.; Gloe, K. *Inorg. Chem.* **2013**, *52*, 1515 – 1524.

(35) Bertini, I.; Luchinat, C.; Turano, P.; Battaini, G.; Casella, L. *Chem. Eur. J.* **2003**, *9*, 2316 – 2322.

(36) Hargrove, M. S.; Barrick, D.; Olson, J. S. *Biochemistry* **1996**, *35*, 11293 – 11299.

(37) Fritz, B. G.; Hu, X.; Brailey, J. L.; Berry, R. E.; Walker, F. A.; Montfort, W. R. *Biochemistry* **2011**, *50*, 5813 – 5815.

(38) Cox, R. P.; Hollaway, M. R. *Eur. J. Biochem.* **1977**, *74*, 575 – 587.

(39) In ferric heme *b*, spin density exists in $d_{x^2-y^2}$ orbital of iron atom and this causes overlap between 2p-orbitals of pyrrole nitrogen atoms. The electron in $d_{x^2-y^2}$ orbital is accommodated in σ^* orbital to weaken the Fe–nitrogen bond, resulted in the out-of-plane position of iron in heme *b*. Latos-Grażyński *et al.* proposed unoccupied $d_{x^2-y^2}$ orbital for bisaryl adduct of Fe(II) oxaporphyrin complex. As a result, the

iron atom is in the plane of oxaporphyrin .

(40) Pawlicki, M.; Latos-Grażyński, L. *Inorg. Chem.* **2004**, *43*, 5564 – 5571.

(41) Kachalova, G. S.; Popov, A. N.; Bartunik, H. D. *Science* **1999**, *284*, 473 – 476.

(42) Battersby, A. R.; Baker, M. G.; Broadbent, H. A.; Fookes, C. J. R.; Leeper, F. J. *J. Chem. Soc. Perkin. Trans. 1* **1987**, 2027 – 2048.

(43) Yoon, D. W.; Gross, D. E.; Lynch, V. M.; Sessler, J. L.; Hay, B. P.; Lee, C. H. *Angew. Chem. Int. Ed.* **2008**, *47*, 5038 – 5042.

(44) Teale, F. W. J. *Biochem. Biophys. Acta* **1959**, *35*, 543.

(45) Izatt, R. M.; Christensen, J. J.; Pack, R. T.; Bench, R. *Inorg. Chem. 1* **1962**, 828 – 831.

Chapter 3.

Evaluation of Catalytic Properties of Myoglobin Reconstituted with an Iron Porphycene as an Artificial Metalloenzyme toward Cyclopropanation of Styrene

3-1. Introduction

Carbene transfer reactions have been investigated as fascinating abiological reactions for artificial metalloenzymes.[1-4] Engineered hemoproteins provide excellent scaffolds for the catalytic activity toward carbene-transfer reactions such as cyclopropanation.[2,3] An artificial metalloenzyme using a cytochrome P450 scaffold has been developed by directed evolution[2] and shows high activity for the abiological cyclopropanation reaction. The modification of myoglobin through mutagenesis is also found to significantly accelerate catalysis in this reaction.[3] Recent efforts have further demonstrated that metal substitution of the heme cofactor is effective for improvement of the catalytic activity.[4] However, detailed investigations on the catalytic mechanism have not been reported. In particular, the carbene species has not been spectroscopically detected in protein-based catalysts. In this study, the author focused on iron porphycene (**FePc,** Figure 3-1a) as an artificial prosthetic group for Mb. Porphycene is a constitutional isomer of porphyrin and its metal complexes exhibit remarkably different physicochemical properties and reactivities relative to the corresponding metal porphyrins.[5] Hayashi *et al.* have previously reported that metalloporphycenes can act as attractive cofactors of myoglobin not only for dioxygen binding but also for enzyme-like catalysis such as peroxidase or hydroxylase reactions.[6] In this chapter, the first spectroscopic observation of the active metallocarbene species is described.[7] In addition, it is shown that the metallocarbene species efficiently promotes the cyclopropanation of styrene, using myoglobin reconstituted with **FePc** (rMb(**FePc**)).

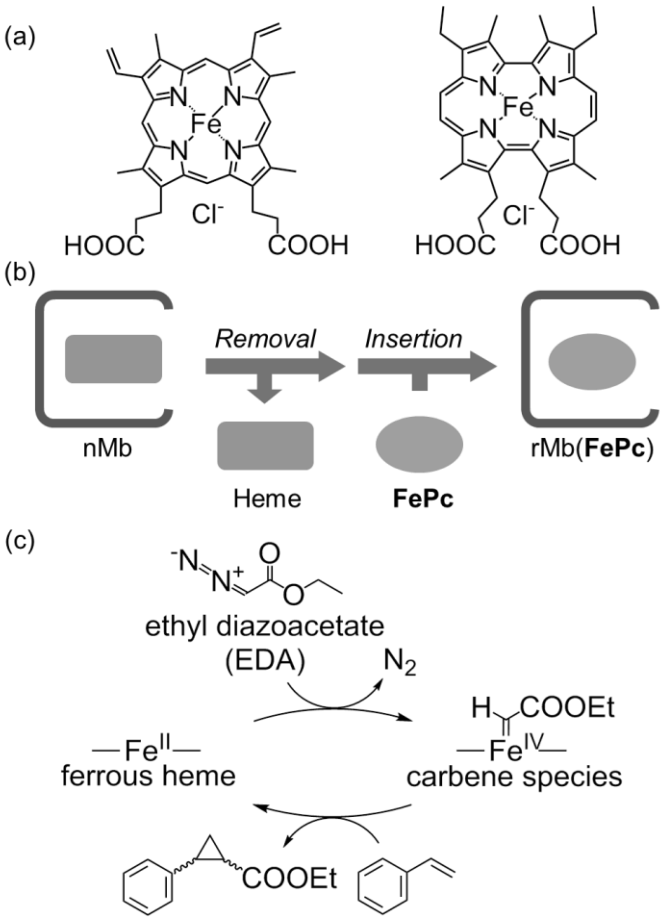

Figure 3-1. (a) Molecular structures of heme and **FePc**, (b) schematic representation of reconstitution of Mb, and (c) plausible reaction mechanism of cyclopropanation of styrene using ethyl diazoacetate catalyzed by hemoproteins.

3-2. Results and Discussions

Evaluation of Catalytic Activities of Mbs Toward Cyclopropanation Reaction of Styrene

The catalytic activities of rMb(**FePc**) and native Mb (nMb) toward cyclopropanation reaction of styrene with ethyl diazoacetate (EDA) as a carbene source were examined in the presence of dithionite.[8] The product, (*E*)-ethyl 2-phenylcyclopropanecarboxylate, was quantified by GC−MS analysis. Excitingly, rMb(**FePc**) shows 99% formation of the trans isomer, without the need for any modification of the myoglobin matrix (Figure 3-2).[9,10] In addition, a turnover frequency (TOF) of 2.2 s^{-1} at the initial stage of catalysis was observed (Figure 3-3). This value is 35 times higher than the TOF nMb under the same conditions.[11] At various concentrations of styrene and 20 mM EDA, TOFs were determined and Michaelis−Menten curves were plotted (Figure 3-4a and Table 3-1).[12] The plots of the TOF values for both rMb(**FePc**) and nMb were fitted in the conventional manner, and k_{cat} values of rMb(**FePc**) and nMb were determined to be 1.7 and 0.06 s^{-1} , respectively. In contrast to the obvious difference in k_{cat}, both K_m values

are almost the same, suggesting that styrene binding occurs at the distal site in the heme pocket of the myoglobin matrix.[3] Similarly, the Michaelis−Menten parameters at various concentrations of EDA and 2.0 mM of styrene were evaluated (Figure 3-4b and Table 3-2). Interestingly, the kinetic curve of nMb does not show saturation behavior of the reaction rate, even upon addition of 20 mM EDA. When 40 mM EDA is employed for the Michaelis−Menten plots at various concentrations of styrene, the k_{cat} value increases to 0.19 s^{-1} , whereas the K_m value exhibits only a small change (Table 3-3). Because the k_{cat} value for nMb depends on the EDA concentration, the reaction of the ferrous state of nMb with EDA dominantly limits the rate of product formation. Several reports also support this suggestion.[12] In the case of rMb(**FePc**), k_{cat} and K_m were determined to be 2.1 s^{-1} and 1.9 mM^{-1} , respectively. The k_{cat} values were consistently above one, indicating that the typical steady state analysis can successfully be applied to catalysis by rMb(**FePc**).

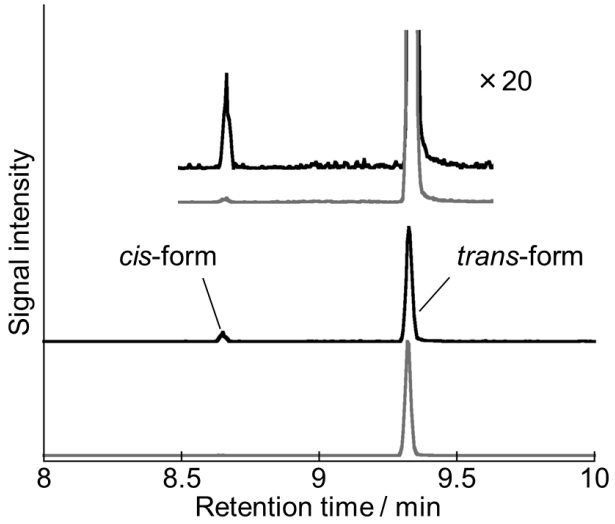

Figure 3-2. GC-MS traces for the product of the cyclopropanation reaction catalyzed by rMb(**FePc**) (gray) and nMb (black). Reaction conditions: [Mb] = 4.3 μM, [dithionite] = 8.6 mM, [styrene] = 2 mM, [EDA] = 20 mM in 100 mM potassium phosphate buffer containing 5% methanol at pH 8.0 and 25 °C. Reaction time: 1 min.

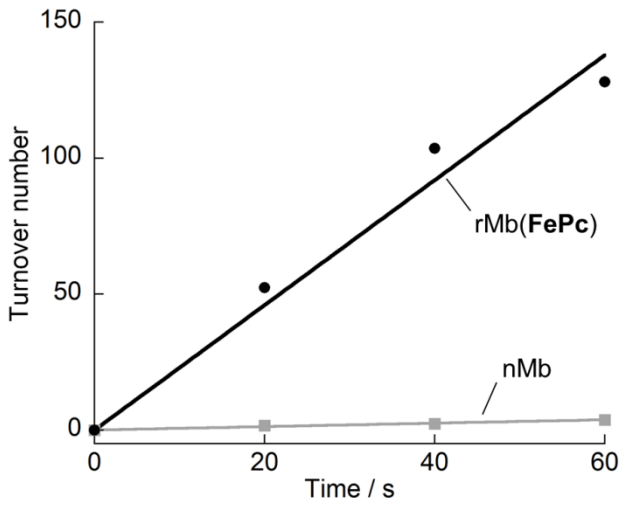

Figure 3-3. Time course plots of the turnover number (TON) for the cyclopropanation reaction of styrene using EDA. Conditions: [Mb] = 4.3 μM, [dithionite] = 8.6 mM, [EDA] = 20 mM, [styrene] = 2.0 mM in 100 mM potassium phosphate buffer containing 5% methanol at pH 8.0, and 25 °C.

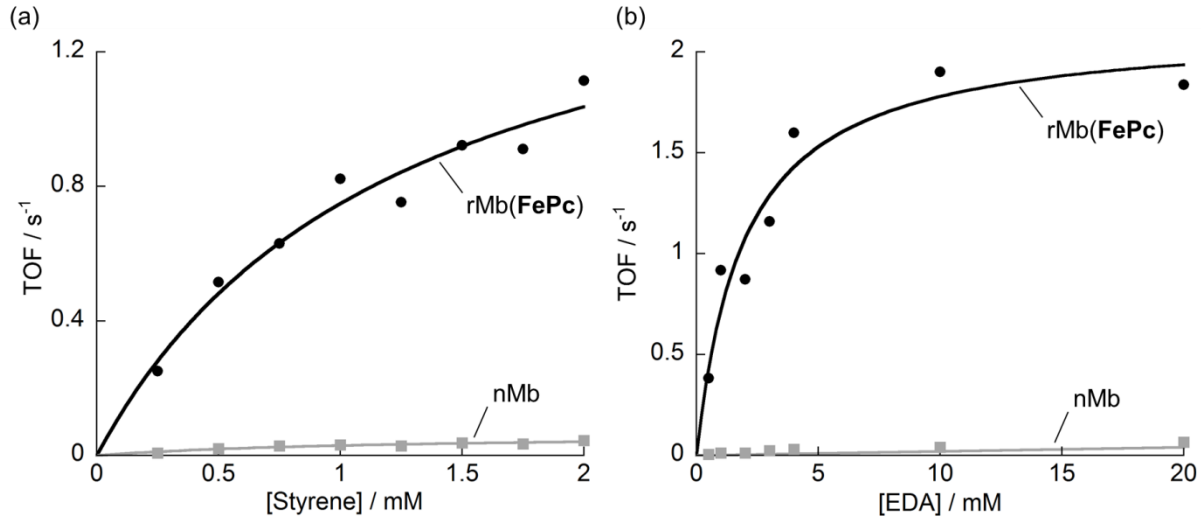

Figure 3-4. Plots of the TOF for the cyclopropanation reaction of styrene using EDA. General conditions: [Mb] = 4.3 μM, [dithionite] = 8.6 mM in 100 mM potassium phosphate buffer containing 5% methanol at pH 8.0 and 25 °C. TOFs were determined by the reaction rate of a period of 1 min. (a) [EDA] = 20 mM and [styrene] = 0.25−2.0 mM. (b) [styrene] = 2.0 mM and [EDA] = 0.5−20 mM.

Table 3-1. Michaelis-Menten Parameters for rMb(FePc) and nMb with Various Concentrations of Styrene.[a]

Protein	k_{cat} (s^{-1})	K_m (mM)	k_{cat}/K_m ($mM^{-1} s^{-1}$)
rMb (**FePc**)	1.7 ± 0.3	1.3 ± 0.4	1.3 ± 0.5
nMb	0.06 ± 0.01[b]	1.2 ± 0.5[b]	0.05 ± 0.02[b]

[a]Conditions are described in the caption of Figure 3-4a. [b]pseudo Michaelis-Menten parameters under the condition of unsaturated concentration of EDA.

Table 3-2. Michaelis-Menten Parameters for rMb(FePc) and nMb with Various Concentrations of EDA.[a]

Protein	k_{cat} (s^{-1})	K_m (mM)	k_{cat}/K_m ($mM^{-1} s^{-1}$)
rMb(**FePc**)	2.1 ± 0.2	1.9 ± 0.6	1.1 ± 0.4
nMb	n.d.[b]	n.d.[b]	0.002 ± 0.0001[c]

[a]Conditions are described in the caption of Figure 3-4b. [b]Not determined. [c]The k_{cat}/K_m value was determined from the slope of the linear relationship.

Table 3-3. Michaelis-Menten Parameters for nMb using Different Concentrations of EDA and Various Concentrations of Styrene.[a]

[EDA] (mM)	k_{cat} (s^{-1})	K_m (mM)	k_{cat}/K_m ($mM^{-1} s^{-1}$)
20	0.06 ± 0.01	1.2 ± 0.5	0.05 ± 0.02
40	0.19 ± 0.04	1.6 ± 0.6	0.1 ± 0.05

[a]Conditions: [Mb] = 4.3 μM, [dithionite] = 8.6 mM, [styrene] = 0.25 - 2.0 mM in 100 mM potassium phosphate buffer containing 5% methanol at pH 8.0 and 25 °C, and reaction time to determine TOF: 1 min.

Observation of the Formation of Active Carbene Species

The reaction of rMb(**FePc**) and nMb with EDA was further evaluated with stopped flow techniques. Figure 3-5a shows the transient absorption spectral changes of ferrous-rMb(**FePc**) after addition of 68.8 mM EDA. The decrease in the absorbance at 587 nm, originating from the ferrous state, was observed with the concomitant increase in an absorbance at 620 nm with clear isosbestic points, suggesting the formation of a new species, putatively assigned as the metallocarbene intermediate.[13] The time-dependent absorption changes at 620 nm were analyzed with a single exponential equation (Figure 3-9). Obtained kinetic constants, k_{obs}, are plotted against various EDA concentrations and show linear relationships (Figure 3-5b,

black line). Similarly, the reaction of nMb with EDA was evaluated (Figure 3-10 and Figure 3-5b, gray line). The second-order rate constants k_1 for rMb(**FePc**) and nMb are determined to be 2.5×10^{-1} and 4.0×10^{-4} mM^{-1} s^{-1}, respectively. The much higher k_1 value for rMb(**FePc**) compared to nMb is consistent with the higher k_{cat} value observed for rMb(**FePc**). Furthermore, the reaction of the detectable carbene intermediate of rMb(**FePc**) (Figure 3-5a: solid line) with styrene was monitored by UV−vis spectroscopy as shown in Figure 3-6 (the experimental setup is shown in Figure 3-11).[14] Interestingly, the addition of styrene resulted in the spectral changes from the dashed line to the solid line, with the latter being similar to that observed for ferrous rMb(**FePc**) (see Figure 3-6a). The observed rate constants, k'_{obs}, are determined by single exponential fits of the absorption changes at 620 nm. It is found that an increase in the concentration of styrene linearly accelerates the reaction (Figure 3-6b). The apparent second order rate constant k_2 was determined to be 28 mM^{-1} s^{-1} at pH 8.0 from the obtained slope. Taken together, it is inferred that the catalytic reaction by rMb(**FePc**) smoothly proceeds via the carbene intermediate to yield the cyclopropane derivatives as shown in Figure 3-1c. Under catalytic conditions ([EDA] = 20 mM and [styrene] = 2 mM), the k_{obs} and k'_{obs} values are calculated to be 5.0 and 45 s^{-1}, respectively, using the apparent second-order rate constants due to the low solubility of styrene in water. These values are larger than k_{cat} (1.7 s^{-1}). These findings indicate that the reaction rate of the catalytic cyclopropanation by rMb(**FePc**) is not limited by the reaction of the ferrous state with EDA and the reaction of the carbene species with styrene. Therefore, the release of the product is suggested to be the overall rate-limiting step. The pH of the solution seems to be a key factor for the reactivity of the metallocarbene intermediate (Figure 3-6b, Table 3-4). At higher pH, a larger apparent second-order rate constant is observed, which is consistent with a larger TOF at higher pH under catalytic conditions.

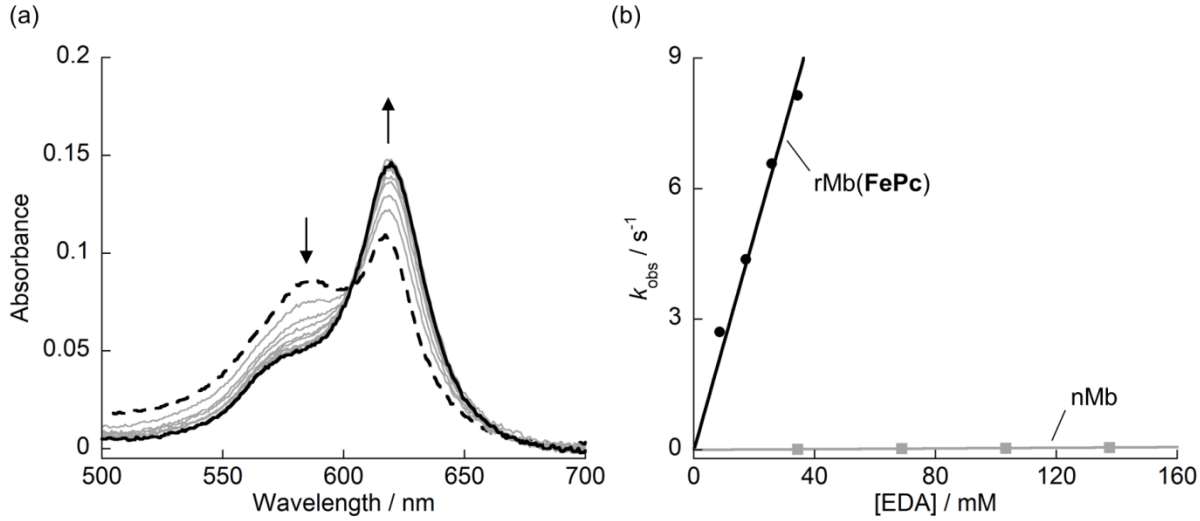

Figure 3-5. (a) Absorption spectra of the ferrous state of rMb(**FePc**) monitored every 0.05 s for 0.5 s after the addition of 68.8 mM EDA (dashed line: 0 s and solid line: 0.5 s). (b) Plots of rate constants (determined from the absorption changes) against various concentrations of EDA (black line: rMb(**FePc**) and gray line: nMb). Conditions: [Mb] = 4.3 μM, [dithionite] = 8.6 mM, [EDA] = 8.6−34.4 mM (for rMb(**FePc**)) or 34.4−137.6 mM (for nMb) in 100 mM potassium phosphate buffer containing 5% methanol at pH 8.0 and 25 °C.

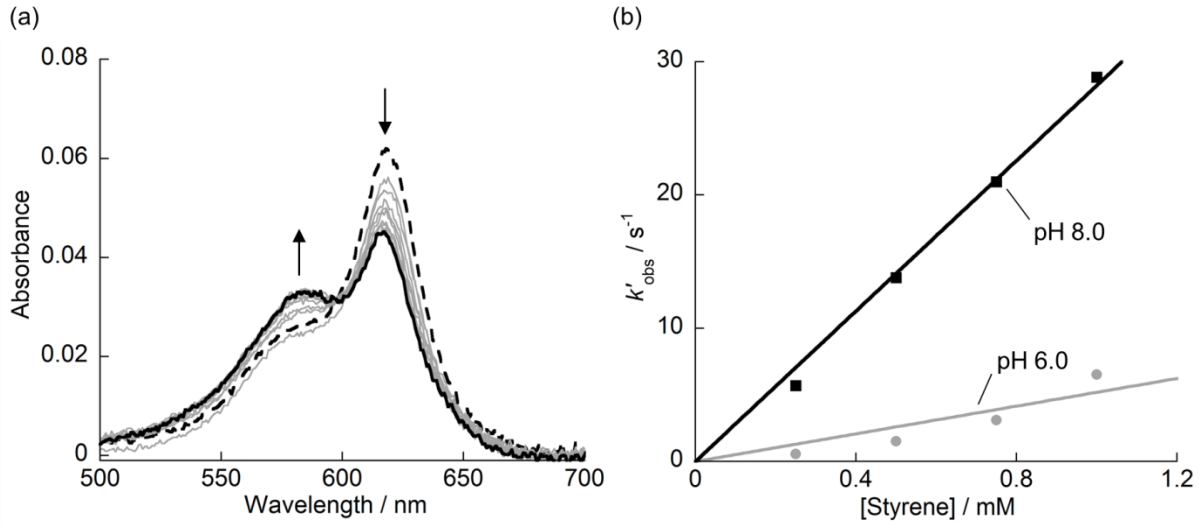

Figure 3-6. (a) Absorption spectra of the product obtained by the reaction of rMb(**FePc**) with EDA monitored every 0.05 s for 0.5 s after addition of 2.0 mM styrene (dashed line: 0 s and solid line: 0.5 s). (b) Plots of apparent rate constants (determined from the absorption changes) against various concentrations of styrene at pH 8.0 (black) and pH 6.0 (gray). Conditions: [rMb(**FePc**)] = 2.2 μM, [dithionite] = 8.6 mM, [EDA] = 4 mM, [styrene] = 0.25−1.0 mM in 100 mM potassium phosphate buffer containing 5% of methanol at 25 °C. Aging time: 1 s.

Theoretical Calculation of Formation of the Carbene Species

To understand the different reactivity of rMb(**FePc**) and nMb with EDA, the potential energy profiles for the cyclopropanation reaction were estimated by DFT calculations at the B97D/6-31g* level. Although there are several DFT studies on the electronic structure and energy profile for the carbene species with a porphyrin ligand,[16] the present one is the first report on the comparison between the porphyrin and porphycene ligands and also on the reaction pathway via intersystem crossing. In these calculations, the cofactors, heme and **FePc**, with an imidazole ligand, were utilized as the simplified active site models (details are given in Figure 3-12). The optimized structures and relative potential energies of the ferrous state, the EDA adduct, and the carbene species were calculated for each spin state, singlet, triplet, and quintet. The estimated energy diagrams for rMb(**FePc**) and nMb are summarized in Figure 3-7, showing the key structures at each step (all optimized structures of stable intermediates in different spin states are shown in Figure 3-13). In the case of nMb, the stable quintet state of the catalytically active ferrous state converts to the quintet EDA adduct, and then a quintet/triplet transition occurs via the Q/T crossing point, which is the minimum energy intersystem crossing point (MEISCP). However, the structure at the Q/T point and its potential energy are both similar to those of the optimized triplet EDA adduct, indicating that the triplet species is efficiently quenched to the stable quintet state of the EDA adduct via a negligible kinetic barrier. The inefficiently generated triplet EDA adduct must overcome an energy barrier of 4.0 kcal/mol (MEISCP T/S) to produce the singlet EDA adduct, which is allowed to transform to the singlet carbene species over an energy barrier of 7.0 kcal/mol. The total barrier for the transition from the quintet state to the singlet state of the EDA adduct is estimated to be 8.2 kcal/mol, because the direct transition from a quintet to a singlet state is prohibited by the selection rule of spin−orbit coupling (the suggested overall pathway to form the carbene species is summarized in Figure 3-13). In contrast to nMb, the stable triplet state of ferrous rMb(**FePc**),[17] which results from the strong ligand field of the porphycene relative to the porphyrin, yields the triplet state of the EDA adduct. The triplet adduct is converted to the singlet adduct via MEISCP T/S (energy barrier = 6.2 kcal/mol), and then, the singlet carbene species is produced from the singlet EDA adduct via an energy barrier of 4.6 kcal/mol. Therefore, fewer steps in intersystem crossing are observed for rMb(**FePc**), and the smaller kinetic barriers in rMb(**FePc**) relative to nMb strongly support the larger rate constants for the reaction of rMb(**FePc**) with EDA compared to that of nMb.

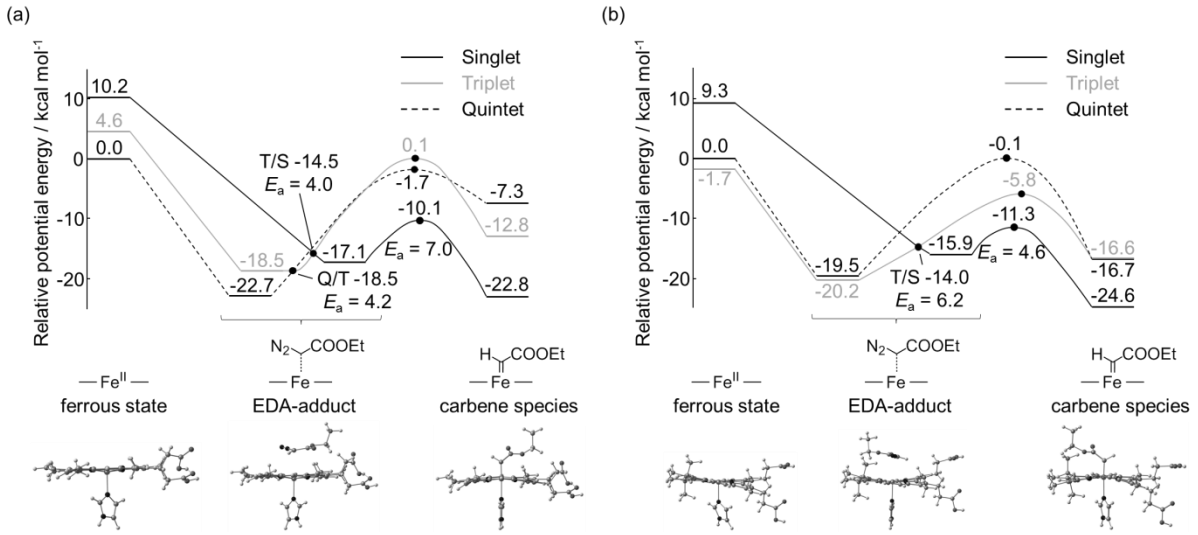

Figure 3-7. Potential energy diagrams for the reactions of (a) the native heme-imidazole complex with EDA and (b) the **FePc**-imidazole complex with EDA. Optimized structures of stable intermediates in different spin states at each step in the reaction are shown below the diagrams.

3-3. Summary

FePc in the myoglobin matrix is found to efficiently react with ethyl diazoacetate to generate the active carbene species for the cyclopropanation of styrene. The catalytic activity of rMb(**FePc**) with **FePc** is 26-fold higher than that observed for the native iron porphyrin in the protein matrix. The present result constitutes the first spectroscopic characterization of the active carbene intermediate of a metal porphyrinoid complex in the protein matrix. Theoretical investigations strongly support the fact that the strong ligand field of porphycene is useful for the efficient formation of the central carbene intermediate. This finding contributes to the rational design of highly active artificial metalloenzymes that can catalyze abiological reactions.

3-4. Experimental Section

Instruments

UV-vis spectral measurements were conducted with V-670 UV-vis-NIR Spectrophotometer (JASCO). pH measurements were carried out using an F-52 pH meter (HORIBA). Detection of transiently formed species and kinetic measurements were conducted with a rapid scan stopped-flow system (Unisoku) constructed with a Xe light source. Air sensitive manipulations were performed in a vinyl anaerobic chamber (Coy Laboratory Products). GC-MS (EI) analyses were performed using a Shimadzu GC 2010

equipped with a Restek Rxi-5Sil MS column. Separation method: 1 μL injection for rMb(**FePc**) and 2 μL injection for nMb, injector temp.: 250 ˚C, detector temp.: 250 ˚C. Gradient: column temperature set to 80 ˚C, then to 180 ˚C at 10 ˚C/min, and then to 250 ˚C at 50 ˚C/min and held at 250 ˚C for 5 min. Total run time was 16.40 min.

Materials

All chemicals were purchased from Wako, TCI, Nacalai, and Sigma-Aldrich and used as received unless otherwise noted. **FePc** was synthesized as described in previous literature.[18] Removal of heme from nMb and preparation of rMb(**FePc**) were performed according to reported procedures.[18,19] The conversion of apoMb to rMb(**FePc**) upon the addition of **FePc** was confirmed by the R_z value, which is determined from the ratio of A_{Soret} and A_{280}, where A_{Soret} and A_{280} represent the absorbance at 387 nm (Soret band) and 280 nm (protein), respectively (Figure 3-8).

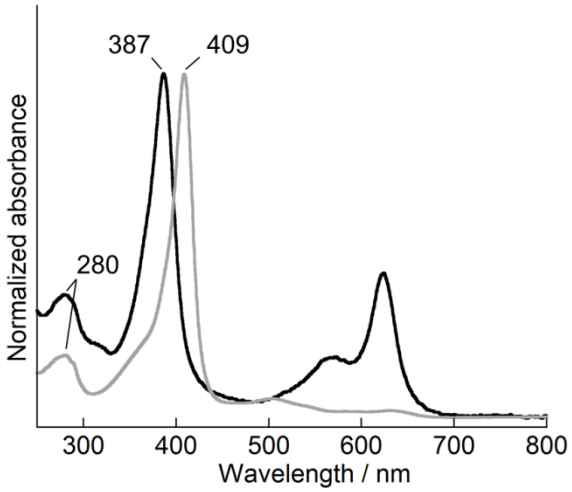

Figure 3-8. UV-vis spectra of rMb(**FePc**) (black) and nMb (gray) measured immediately after purification in 100 mM potassium phosphate buffer at pH 7.0 at 25 ℃. R_z values for rMb(**FePc**) ($A_{387\ \text{nm}}/A_{280\ \text{nm}}$) and for nMb ($A_{409\ \text{nm}}/A_{280\ \text{nm}}$) are 2.8 and 5.5, respectively. The value of rMb(**FePc**) is consistent with that of a solution in which crystals of rMb(**FePc**) were dissolved, supporting the quantitative cofactor loading into the protein.

Evaluation of Catalytic Activities for Cyclopropanation Reaction

Reactions were conducted in a mixture of 4.3 μM of nMb or rMb(**FePc**), 8.6 mM of dithionite, 2 mM of styrene and 20 mM ethyl diazoacetate (EDA) in 100 mM potassium phosphate buffer at pH 6.0 or 8.0 containing 5% methanol at 25 ℃. To the mixture, 10 μL of benzyl alcohol (100 mM for rMb(**FePc**) and 50 mM for nMb) in methanol was added as an internal standard, followed by extraction with 500 μL of ethyl

acetate. The organic layer was then analyzed with GC-MS. To conduct a time course study, reactions were quenched 20 s, 40 s, and 60 s after addition of EDA. To perform Michaelis-Menten kinetic studies, reactions were conducted in various concentrations of styrene (0.25 - 2.0 mM) or EDA (0.5 - 20 mM) in 100 mM potassium phosphate buffer at pH 8.0 containing 5% methanol at 25 °C and organic compounds were extracted at a period of 60 s after addition of EDA. To determine the maximum turnover number, reactions were quenched 6 min (rMb(**FePc**) and **FePc**) or 60 min (nMb and heme) after addition of EDA.

Table 3-4. **Turnover Frequencies of the Cyclopropanation Reaction of Styrene at Various pH Values.**[a]

pH	TOF (min^{-1})
6.0	31 ± 1
8.0	130 ± 3

[a]Condition: [rMb(**FePc**)] = 4.3 μM, [dithionite] = 8.6 mM, [styrene] = 2 mM, [EDA] = 20 mM in 100 mM potassium phosphate buffer containing 5% methanol at pH 6.0 or 8.0 and 25 °C, and reaction time to determine TOF: 1 min.

Table 3-5. Yield, TON, de and Byproduct Yield of the Cyclopropanation Product of Styrene by the Catalysis Using nMb, rMb or Free Cofactors.[a]

Catalyst	TON	*de*[b] (%)
rMb(**FePc**)[c]	130 ± 3	99.5 ± 0.1
nMb[d]	49 ± 1	85 ± 1
FePc[c]	9 ± 1	52.6 ± 0.3
heme[d]	23 ± 1	61.5 ± 0.6

[a]Condition: [catalyst] = 4.3 μM, [dithionite] = 8.6 mM, [styrene] = 2 mM, [EDA] = 20 mM in 100 mM potassium phosphate buffer containing 5% methanol at pH 8.0 and 25 °C under aerobic condition. [b] Diastereomeric excess for (*E*)-ethyl 2-phenylcyclopropanecarboxylate. [c]Reaction time = 6 min. [d]Reaction time = 60 min.

Kinetic Studies of the Reaction of nMb and rMb(FePc) with EDA

A solution containing 8.6 μM of nMb or rMb(**FePc**) and 8.6 mM of sodium dithionite in 100 mM potassium phosphate buffer at pH 8.0 containing 5% methanol was mixed anaerobically with a solution containing various concentration of EDA (17.2 - 68.8 mM for rMb(**FePc**) and 68.8 - 275.2 mM for nMb) and 8.6 mM of sodium dithionite in 100 mM potassium phosphate buffer at pH 8.0 containing 5% methanol. Transient absorption spectra were monitored using a stopped-flow rapid scanning apparatus at 25 °C. The

absorption changes were fitted with a single exponential equation to determine apparent reaction rate constants k_{obs} at various concentrations of EDA. The second-order rate constant, k_1, was determined with plots of k_{obs} against the concentration of EDA.

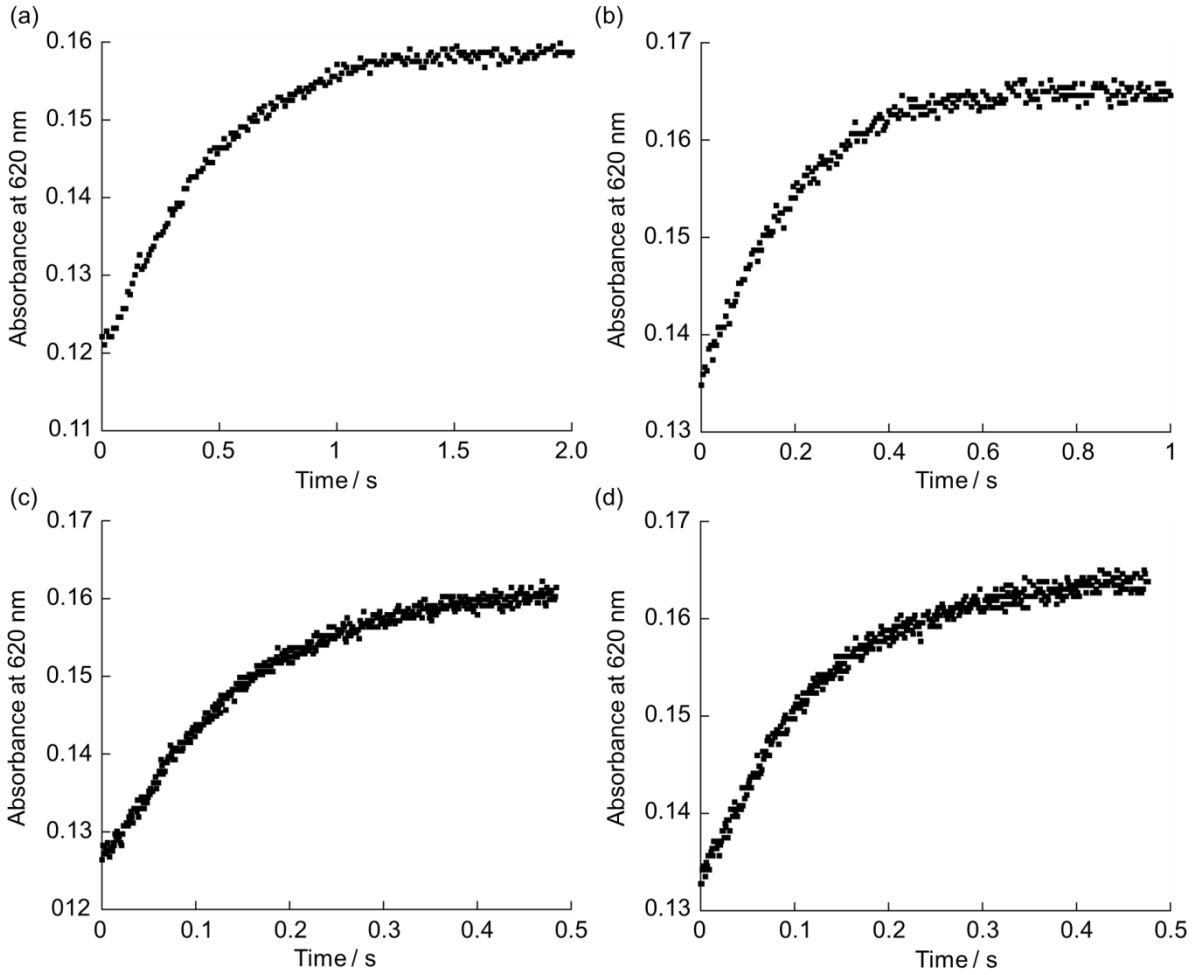

Figure 3-9. Time course plots of the absorption changes of rMb(**FePc**) after addition of (a) 17.2 mM, (b) 34.4 mM, (c) 51.6 mM, and (d) 68.8 mM EDA, measured at 620 nm. Conditions: [rMb(**FePc**)] = 4.3 μM, [dithionite] = 8.6 mM, [EDA] = 8.6 - 34.4 mM in 100 mM potassium phosphate buffer containing 5% methanol at pH 8.0, and 25 °C.

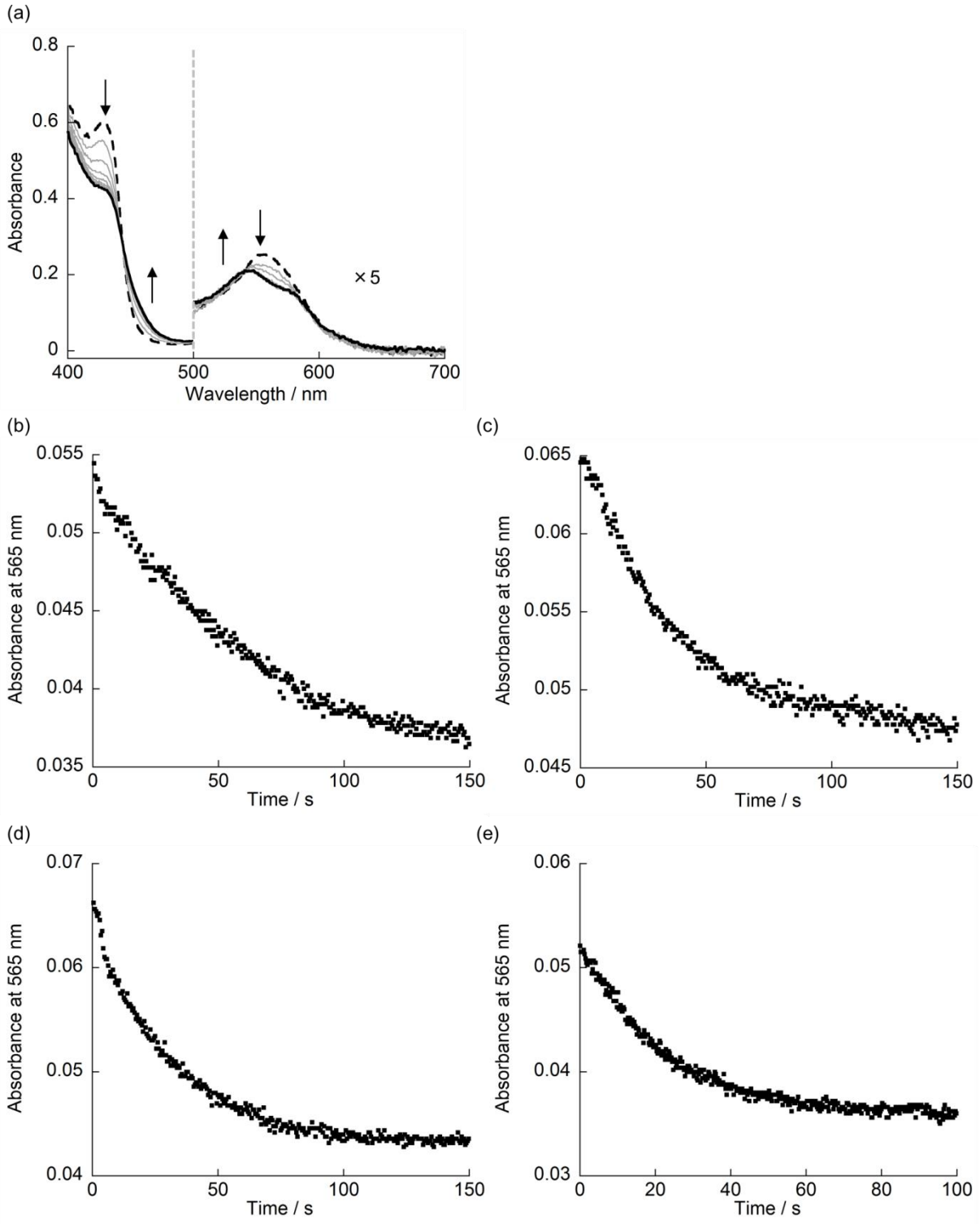

Figure 3-10. (a) Absorption spectra of ferrous nMb measured every 12 s over 120 s after the addition of 275.2 mM EDA (dashed line: 0 s and solid line: 120 s). Time course plots of the absorption changes of ferrous nMb after addition of (b) 68.8 mM, (c) 137.6 mM, (d) 206.4 mM, and (e) 275.2 mM of EDA, monitored at 565 nm. Conditions: [nMb] = 4.3 μM, [dithionite] = 8.6 mM, [EDA] = 34.4 – 137.6 mM in 100 mM potassium phosphate buffer containing 5% methanol at pH 8.0, and 25 °C.

Evaluation of the Reaction of the Carbene Intermediate of rMb(FePc) with Styrene

Reactivity of a transiently formed carbene species with styrene was evaluated in rMb(**FePc**) using a stopped-flow double mixing apparatus under anaerobic condition. To a solution of rMb(**FePc**) (8.6 μM) containing 8.6 mM of sodium dithionite and 5% of methanol in 100 mM potassium phosphate buffer at pH 6.0 or 8.0, 8.0 mM of EDA containing 8.6 mM of sodium dithionite and 5% of methanol in 100 mM potassium phosphate buffer at pH 6.0 or 8.0 was added and incubated for 1 second at 25 °C. To the mixture, a solution containing various concentrations of styrene (0.5 – 2.0 mM) and 8.6 mM sodium dithionite with 5% of methanol in 100 mM potassium phosphate buffer at pH 6.0 or 8.0 was added and transient spectra were recorded. Spectral changes were fitted to a single exponential equation to determine apparent reaction rate constants k'_{obs} in various concentrations of styrene. The second-order rate constant k_2 was determined with plots of k'_{obs} against the concentration of styrene.

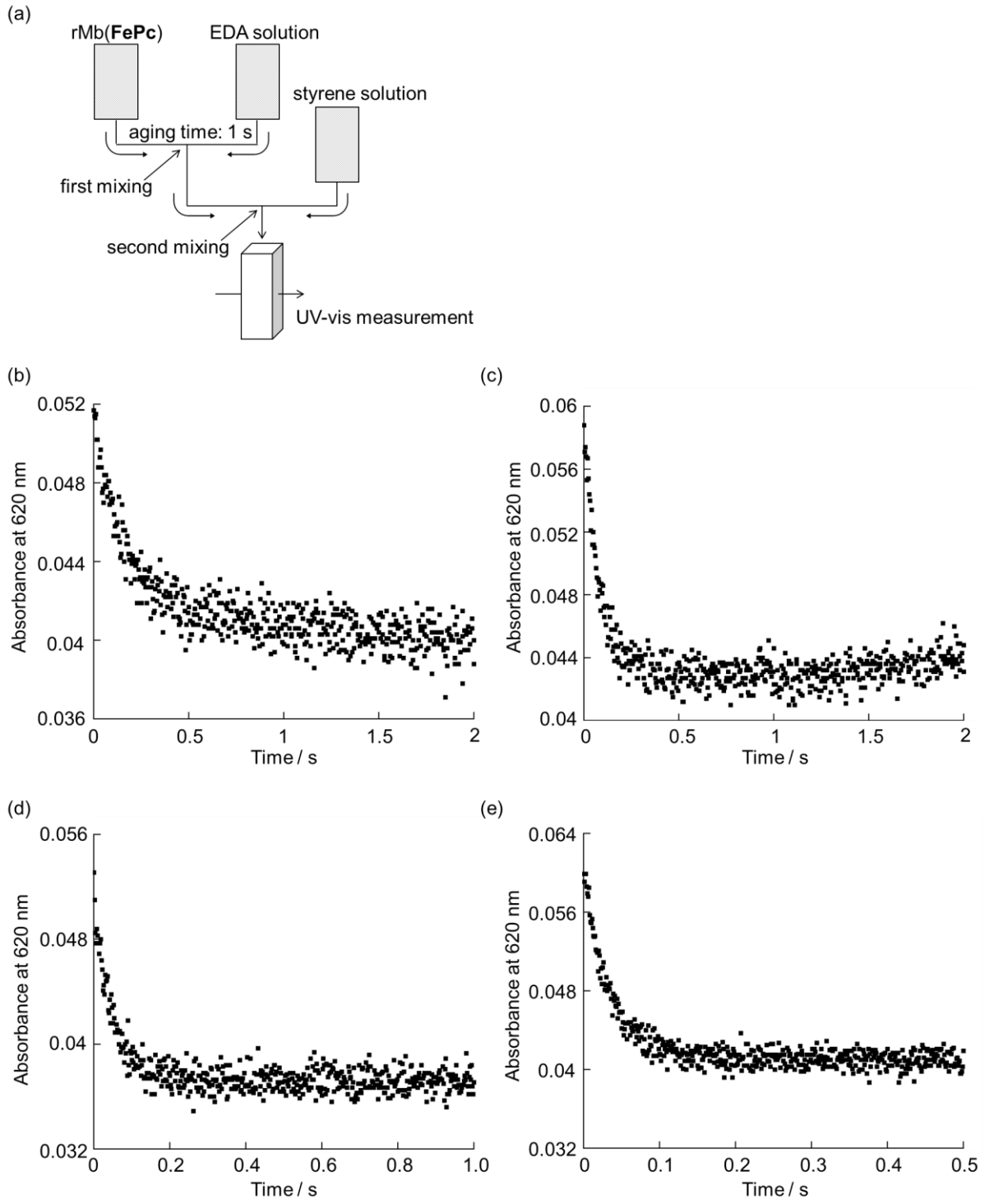

Figure 3-11. (a) Schematic representation of the stopped-flow double-mixing apparatus, and time course plots of the absorption changes of the active carbene complex of rMb(**FePc**) after addition of (b) 0.5 mM, (c) 1 mM, (d) 1.5 mM, and (e) 2 mM of styrene, monitored at 620 nm. Conditions: [rMb(**FePc**)] = 2.2 μM, [dithionite] = 8.6 mM, [EDA] = 4 mM, [styrene] = 0.25 - 1 mM in 100 mM potassium phosphate buffer containing 5% methanol at pH 8.0, and 25 °C. Aging time: 1 s.

DFT Calculations on the Formation of Iron Carbene Species

For the computational models of Fe(II)-porphyrin-imidazole and Fe(II)-porphycene-imidazole complexes, the structures shown in Figure 3-12 were used. The structure of EDA is also shown. All the structures described in this chapter were fully optimized with DFT method using the unrestricted B97D functional.[20] As for the basis sets, Stuttgart/Dresden (611111/22111/411) sets of the effective-core potential and valence sets were adopted for Fe,[21] while the 6-31g* basis set was used for the other atoms. This functional and basis sets were chosen because this computational method reproduced the energy difference between the spin states of oxyheme (O_2FePorIm) in a previous study.[22] Frequency calculations and IRC analyses were conducted to ascertain that proper energy minima and transition states were obtained. All of the above calculations were performed with the Gaussian 09 program package.[23] In finding the minimum energy intersystem crossing point (MEISCP), the geometries were optimized under the constraint that the two states have to be energetically degenerate. Such optimizations were carried out with a program package developed by Hasegawa's group, which allows for the identification of minimum energy crossing points.[24,25] Previously, DFT calculations on the iron carbene species with the porphyrin ligand were reported.[26,27] In these studies, only the porphyrin ligand was investigated, and porphyrin derivatives like the porphycene ligand were not considered. Zhang *et al.* also calculated the energy profile of the carbene formation process for the porphyrin ligand.[26] However, their calculations omitted the intersystem crossing processes from the quintet state to the triplet state and then to the singlet state. Therefore, the calculations presented here provide new insight into the ligand effect (nMb vs rMb(**FePc**)) on the intersystem crossing pathway, which is one of the essential points of the carbene formation process. A previous study by Shaik *et al.* focused on the electronic structure of the iron carbene porphyrin with a negatively charged cysteine ligand $[SCH_3]^-$.[27] They obtained the open-shell ground state which is about 5 kcal/mol lower than the closed-shell ground state. On the other hand, the system presented here features the neutral imidazole ligand. The change of the ligand affects the stability. With the imidazole ligand, the ground state is calculated to be a closed-shell singlet state. When the same calculation are conducted as the previous one (stable=opt),[27] the open-shell singlet state was 6.2 kcal/mol and 11.5 kcal/mol higher than the closed-shell singlet state in the nMb and rMb(**FePc**) systems, respectively.

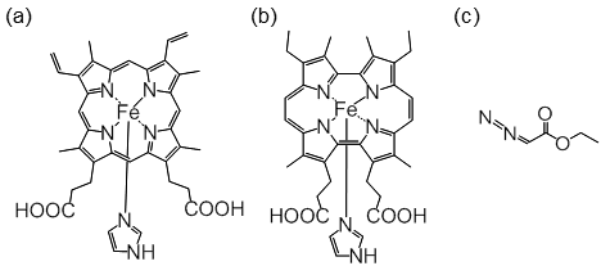

Figure 3-12. Computational models for the (a) Fe(II)-porphyrin-imidazole and (b) Fe(II)-porphycene-imidazole complexes, and (c) EDA.

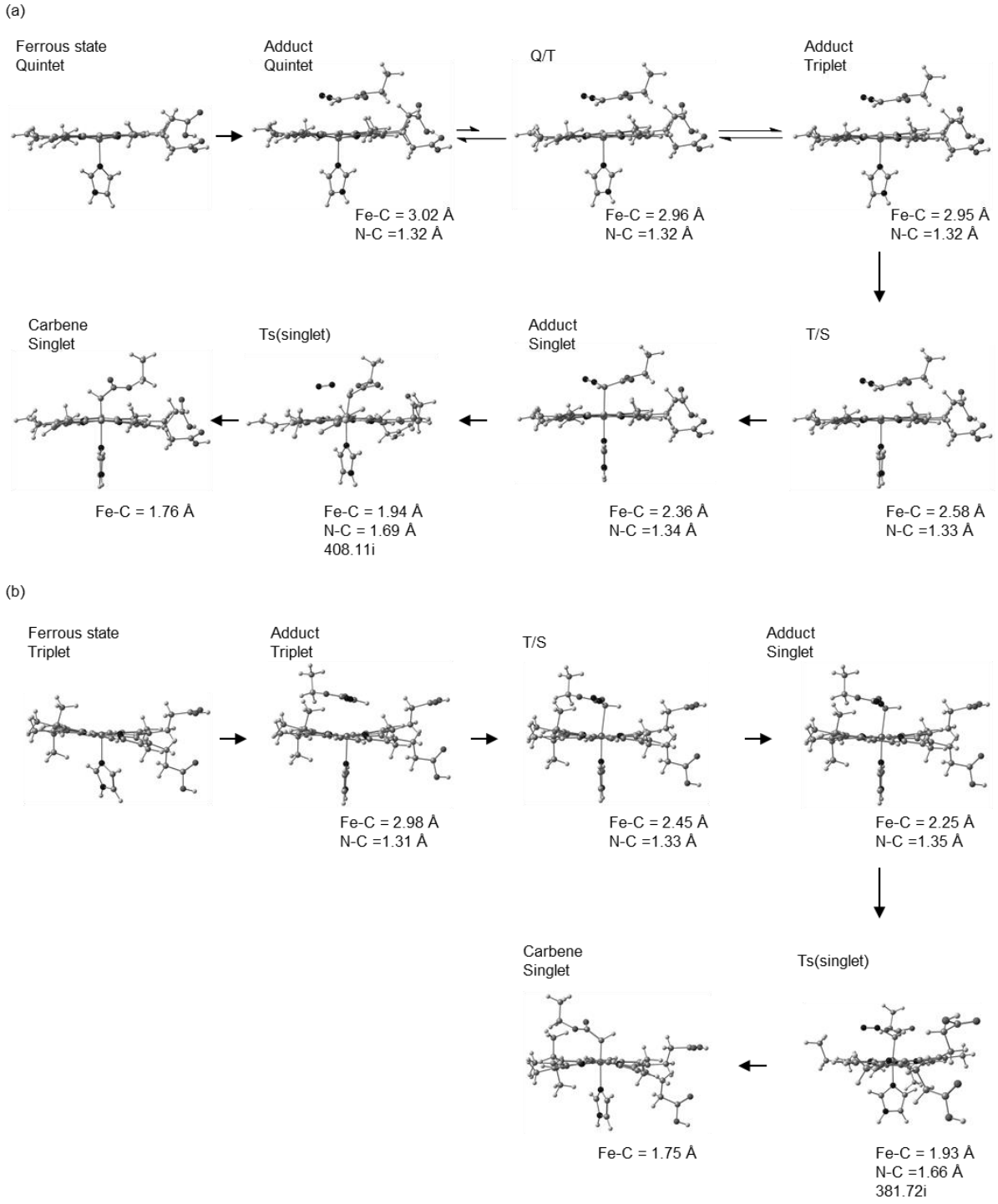

Figure 3-13. DFT-optimized structures of stable intermediates and transition states in different spin states at each step in the reaction of (a) nMb and (b) rMb(**FePc**) with EDA.

3-5. References and Notes

(1) (a) Coelho, P. S.; Brustad, E. M.; Kannan, A.; Arnold, F. H. *Science* **2013**, *339*, 307–310. (b) Coelho, P. S.; Wang, Z. J.; Ener, M. E.; Baril, S. A.; Kannan, A.; Arnold, F. H.; Brustad, E. M. *Nat. Chem. Biol.* **2013**, *9*, 485–487. (c) Gober, J. G.; Brustad, E. M. *Curr. Opin. Chem. Biol.* **2016**, *35*, 124–132. (d) Srivastava, P.; Yang, H.; Ellis-Guardiola, K.; Lewis, J. C. *Nat. Commun.* **2015**, *6*, 7789. (e) Schwizer, F.; Okamoto, Y.; Heinisch, T.; Gu, Y.; Pellizzoni, M. M.; Lebrun, V.; Reuter, R.; Köhler, V.; Lewis, J. C.; Ward, T. R. *Chem. Rev.* **2018**, *118*, 142–231.

(2) (a) Wang, Z. J.; Renata, H.; Peck, N. E.; Farwell, C. C.; Coelho, P. S.; Arnold, F. H. *Angew. Chem. Int. Ed*. **2014**, *53*, 6810–6813. (b) Renata, H.; Wang, Z. J.; Kitto, R. Z.; Arnold, F. H. *Catal. Sci. Technol.* **2014**, *4*, 3640–3643. (c) Heel, T.; McIntosh, J. A.; Dodani, S. C.; Meyerowitz, J. T.; Arnold, F. H. *ChemBioChem* **2014**, *15*, 2556-2562. (d) Gober, J. G.; Ghodge, S. V.; Bogart, J. W.; Wever, W. J.; Watkins, R. R.; Brustad, E. M.; Bowers, A. A. *ACS Chem. Biol.* **2017,** *12* , 1726–1731.

(3) Bordeaux, M.; Tyagi, V.; Fasan, R. *Angew. Chem. Int. Ed.* **2015**, *54*, 1744–1748.

(4) (a) Key, H. M.; Dydio, P.; Clark, D. S.; Hartwig, J. F. *Nature* **2016**, *534*, 534–537. (b) Sreenilayam, G.; Moore, E. J.; Steck, V.; Fasan, R. *Adv. Synth. Catal.* **2017**, *359*, 2076–2089. (c) Wolf, M. W.; Vargas, D. A.; Lehnert, N. *Inorg. Chem.* **2017**, *56*, 5623–5635. (d) Key, H. M.; Dydio, P.; Liu, Z.; Rha, J. Y.-E.; Nazarenko, A.; Seyedkazemi, V.; Clark, D.S.; Hartwig, J. F. *ACS Cent. Sci.* **2017**, *3*, 302–308.

(5) Sessler, J. L.; Gebauer, A.; Vogel, E. In Porphyrin Handbook; Kadish, K. M., Smith, K. M., Guilard, R., Eds.; Academic Press: San Diego, CA, 2000; Vol. 2, pp 1−54.

(6) (a) Matsuo, T.; Dejima, H.; Hirota, S.; Murata, D.; Sato, H.; Ikegami, T.; Hori, H.; Hisaeda, Y.; Hayashi, T. *J. Am. Chem. Soc.* **2004**, *126*, 16007–16017. (b) Hayashi, T.; Murata, D.; Makino, M.; Sugimoto, H.; Matsuo, T.; Sato, H.; Shiro, Y.; Hisaeda, Y. *Inorg. Chem.* **2006**, *45*, 10530–10536. (c) Oohora, K.; Kihira, Y.; Mizohata, E.; Inoue, T.; Hayashi, T. *J. Am. Chem. Soc.* **2013**, *135*, 17282–17285. (d) Morita, Y.; Oohora, K.; Sawada, A.; Doitomi, K.; Ohbayashi, J.; Kamachi, T.; Yoshizawa, K.; Hisaeda, Y.; Hayashi, T. *Dalton Trans.* **2016**, *45*, 3277–3284.

(7) Examples of stable metallocarbene porphyrinoids: (a) Jennings, G. K.; Ritchie, C. M.; Shock, L. S.; Lyons C. E.; Hackett, J. C. *Mol. Pharmacol.* **2016**, *90*, 42–51. (b) Lange, M.; Battioni, J. P.; Mansuy, D.; Lexa D.; Saveant, J. M. *J. Chem. Soc., Chem. Commun.* **1981**, 888–890. (c) Mansuy, D. ; Battioni, J. P.; Chottard, J. C.; Ullrich V. *J. Am. Chem. Soc.* **1979**, *101*, 3971–3973.

(8) In this chapter, horse heart myoglobin was used as a scaffold protein.

(9) The main product was (*E*)-ethyl 2-phenylcyclopropanecarboxylate, whereas (*Z*)-ethyl 2-phenylcyclopropanecarboxylate was obtained as a minor product. The diastereomeric excess (*de*) value for nMb is 86%, whereas *de* for rMb(**FePc**) is 99% (Figure 3-2a).

(10) TON and *de* values of **FePc** without the protein matrix are obviously low, indicating significance of the heme-binding site similar to the situation of the reported nMb-based system (Table 3-5).

(11) The myoglobin mutant catalyze the same reaction in this work with the high catalytic activity (TOF = 15 - 20 s^{-1}).[3]

(12) (a) Mbuvi, H. M.; Woo, L. K. *Organometallics* **2008**, *27*, 637–645. (b) Dzik, W. I.; Xu, X.; Zhang, X. P.; Reek, J. N. H.; de Bruin, B. *J. Am. Chem. Soc.* **2010**, *132*, 10891–10902.

(13) The obtained carbene species of rMb(**FePc**) gradually converts to an unknown inactive species within 20 seconds and the rate is independent of EDA concentration.

(14) The transient species generated by the reaction of ferrous Mb with EDA does not react with styrene. The author proposes extremely rapid conversion of the carbene intermediate to inert species such as *N*-alkylated porphyrin.[15]

(15) Renata, H.; Lewis, R. D.; Sweredoski, M. J.; Moradian, A.; Hess, S.; Wang, Z. J.; Arnold, F. H. *J. Am. Chem. Soc.* **2016**, *138*, 12527–12533.

(16) (a) Khade, R. L.; Zhang, Y. *J. Am. Chem. Soc.* **2015**, *137*, 7560−7563. (b) Sharon,D. A.; Mallick, D.; Wang, B.; Shaik, S. *J. Am. Chem. Soc.* **2016**, *138*, 9597−9610.

(17) (a) Ikeue, T.; Ohgo, Y.;Takahashi, M.; Takeda, M.; Neya, S.; Funasaki, N.; Nakamura, M. *Inorg. Chem.* **2001**, *40*, 3650–3652. (b) Ohgo, Y.; Neya, S.; Ikeue, T.; Takahashi, M.; Takeda, M.; Funasaki, N.; Nakamura, M. *Inorg. Chem.* **2002**, *41*, 4627–4629.

(18) Hayashi, T.; Dejima, H.; Matsuo, T.; Sato, H.; Murata, D.; Hisaeda, Y. *J. Am. Chem. Soc.* **2002**, *124*, 11226–11227.

(19) Teale, F. W. J. *Biochem. Biophys. Acta* **1959**, *35*, 543.

(20) Grimme, S. *J. Comput. Chem.* **2006**, *27*, 1787-1799.

(21) Watanabe, K.; Nakatani, N.; Nakayama, A.; Higashi, M.; Hasegawa, J. *Inorg. Chem.* **2016**, 55, 8082-8090.

(22) Dolg, M.; Wedig, U.; Stoll, H.; Preuss, H. *J. Chem. Phys.* **1987**, *86*, 866-872.

(23) Frisch, M. J.; Trucks, G. W.; Schlegel, H. B.; Scuseria, G. E.; Robb, M. A.; Cheeseman, J. R.; Scalmani, G.; Barone, V.; Mennucci, B.; Petersson, G. A.; Nakatsuji, H.; Caricato, M.; Li, X.; Hratchian, H. P.; Izmaylov, A. F.; Bloino, J.; Zheng, G.; Sonnenberg, J. L.; Hada, M.; Ehara, M.; Toyota, K.; Fukuda, R.; Hasegawa, J.; Ishida, M.; Nakajima, T.; Honda, Y.; Kitao, O.; Nakai, H.; Vreven, T.; Montgomery, J. A.; Peralta, J. E.; Ogliaro, F.; Bearpark, M.; Heyd, J. J.; Brothers, E.; Kudin, K. N.; Staroverov, V. N.;

Kobayashi, R.; Normand, J.; Raghavachari, K.; Rendell, A.; Burant, J. C.; Iyengar, S. S.; Tomasi, J.; Cossi, M.; Rega, N.; Millam, J. M.; Klene, M.; Knox, J. E.; Cross, J. B.; Bakken, V.; Adamo, C.; Jaramillo, J.; Gomperts, R.; Stratmann, R. E.; Yazyev, O.; Austin, A. J.; Cammi, R.; Pomelli, C.; Ochterski, J. W.; Martin, R. L.; Morokuma, K.; Zakrzewski, V. G.; Voth, G. A.; Salvador, P.; Dannenberg, J. J.; Dapprich, S.; Daniels, A. D.; Farkas; Foresman, J. B.; Ortiz, J. V.; Cioslowski, J.; Fox, D. J. *Gaussian 09*, Revision B.01, Gaussin Inc., Wallingford CT, 2009.

(24) Levine, B. G.; Coe, J. D.; Martínez, T. J. *J. Phys. Chem. B* **2008**, *112*, 405-413.

(25) Nakayama, A.; Harabuchi, Y.; Yamazaki, S.; Taketsugu, T. *Phys. Chem. Chem. Phys.* **2013**, *15*, 12322-12339.

(26) Khade, R. L.; Zhang, Y. *J. Am. Chem. Soc.* **2015**, *137*, 7560−7563.

(27) Sharon,D. A.; Mallick, D.; Wang, B.; Shaik, S. *J. Am. Chem. Soc.* **2016**, *138*, 9597−9610.

Chapter 4.

Mechanistic Investigations of Myoglobin Reconstituted with a Manganese Porphycene toward Development of an Artificial Monooxygenase

4-1. Introduction

It is known that various heme-containing enzymes such as monooxygenases and peroxidases utilize an Fe^{IV}-oxo porphyrin π-cation radical known as compound I as a common key intermediate in oxidation reaction. In particular, cytochrome P450s catalyze important hydroxylation reaction via activation of an inert C–H bond without using precious metals.[1] To mimic and elucidate the functions of cytochrome P450, a series of metal complexes of porphyrin derivatives[2] and porphyrinoids such as corrole,[3] corrolazine[4] and porphycene[5] have been investigated. It has been found that certain protein matrices are useful for stabilization and/or activation of reactive species.[6] A previous study reported by Hayashi and his coworkers demonstrated that Mb reconstituted with manganese porphycene (**MnPc**, Figure 4-1a and b), rMb(**MnPc**), is capable of hydroxylation of a C(sp^3)–H bond of hydrocarbons such as ethylbenzene, toluene and cyclohexane using H_2O_2 as an oxidant, although native Mb (nMb) does not show monooxygenase activity for inert alkane substrates.[7] In this chapter, a high-resolution crystal structure of the resting state of rMb(**Mn^{III}Pc**), and a spectroscopic investigation of the high-valent intermediate, rMb(**Mn^{V}**(O)**Pc**) which activates an inert C–H bond (Figure 4-1c) are described.[8]

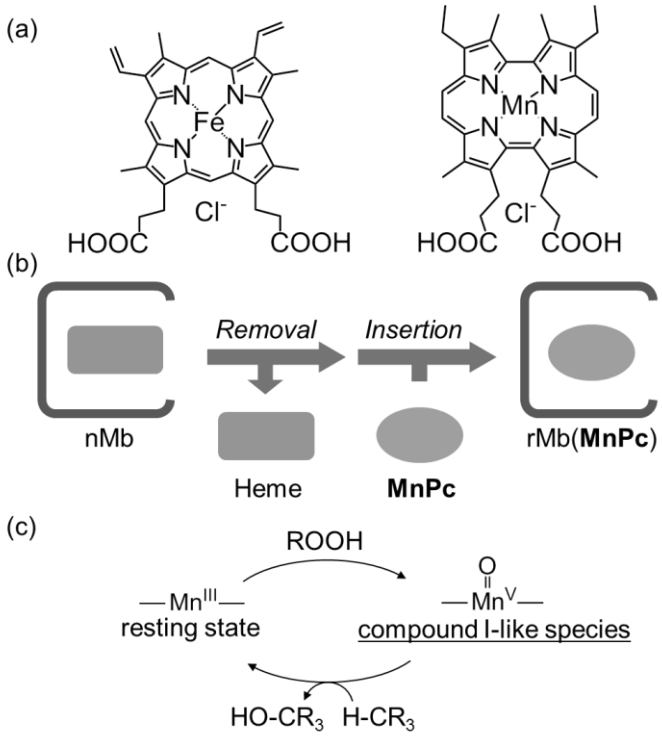

Figure 4-1. (a) Molecular structures of heme and **MnPc**, (b) schematic representation of reconstitution of Mb and (c) plausible reaction mechanism of catalytic C–H bond hydroxylation by rMb(**MnPc**).

4-2. Results and Discussions

Investigation of Catalytic Activity and X-ray Crystal Structure of rMb(MnPc)

The catalytic acitivities of rMb(**MnPc**) toward hydroxylation of ethylbenzene were evaluated at various pH value. The highest turnover number was obtained at pH 8.5 (Table 4-1).[9] Therefore, the crystal of rMb(**Mn^{III}Pc**) was prepared at pH 8.5. The structure with 1.5 Å resolution reveals ligation of His93 and one water molecule[10] to the Mn center in the intrinsic heme pocket (Figure 4-2a). The main chain structure of rMb(**Mn^{III}Pc**) is superimposable on the reported nMb structure[9] with an RMSD (root-mean-square deviation) value of 0.3 Å (Figure 4-2b). Comparing the crystal structure with a previous crystal structure obtained at pH 7.0 with 2.2 Å resolution,[7] no alternative conformation of His64 were found in the structure at pH 8.5 (Table 4-3).[11] From these findings, it appears that stable binding of the cofactor in the heme pocket is important for promotion of the hydroxylation reaction catalyzed by rMb(**MnPc**).

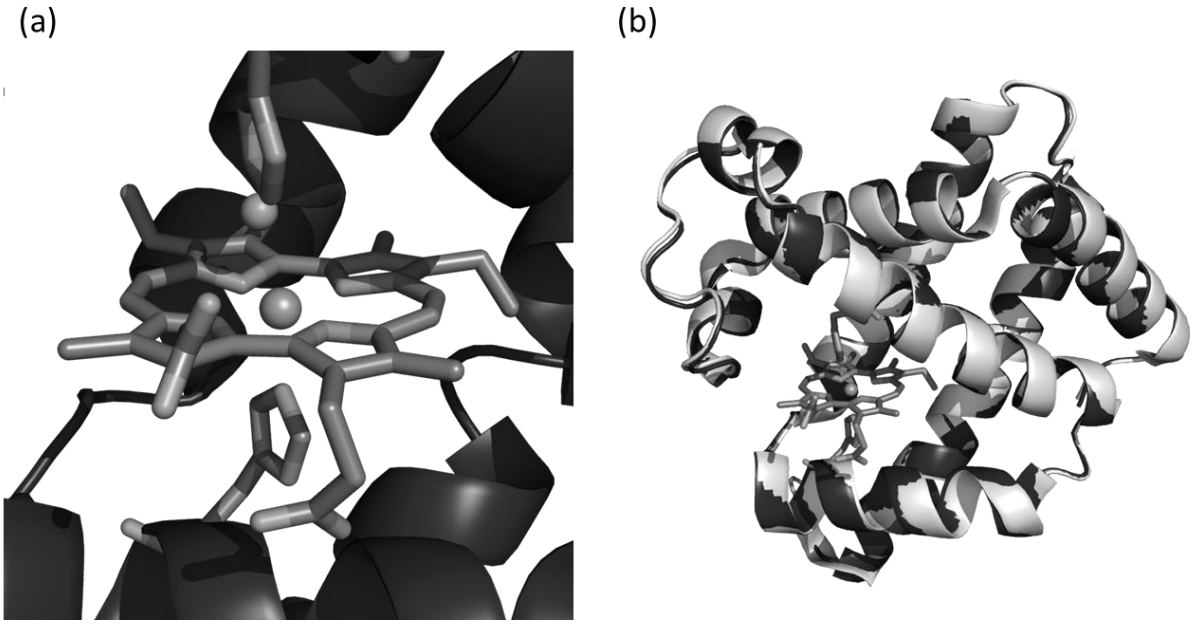

Figure 4-2. (a) Crystal structure of rMb(**Mn^{III}Pc**) around the **MnPc**, His64, His93, and water molecule. (b) Superimposed structures of rMb(**Mn^{III}Pc**) (black) and nMb (white, PDB ID: 1YMB).

Table 4-1. Catalytic Activity of rMb(MnPc) toward Hydroxylation of Ethylbenzene at Various pH Values[a]

entry	pH	TON[b]	$t_{1/2}$ (s)[c]
1	7.0	3.8	20
2	8.0	7.9	33
3	8.5	13	38
4	9.0	12	n.d.[d]

[a]Reaction conditions: [rMb(**MnPc**)] = 20 μM, [H_2O_2] = 10 mM, [ethylbenzene] = 8.0 mM, in 100 mM potassium phosphate buffer containing 8% acetonitrile at 25 ºC. [b]Turnover number after completion of the reaction. [c]Half-life time of two-electron oxidative intermediate measured by the reaction with m-chloroperoxybenzoic acid, (*m*CPBA). Conditions: [rMb(**MnPc**)] = 4 μM, [*m*CPBA] = 10 μM, in 100 mM potassium phosphate buffer at 10 ºC. [d]The value was not determined due to lower formation yield of intermediate.

Observation of Transiently-formed High-valent Species

The reaction of rMb(**Mn^{III}Pc**) with *m*CPBA was monitored using a stopped flow apparatus (Figure 4-3).[12] A decrease in absorbance at 427 nm and 568 nm, originating from the resting state, was observed with a concomitant increase in new absorbance at 382 nm and 618 nm, accompanied by clear isosbestic points within 2 seconds at 10 ºC. The detected intermediate (black, solid spectrum in Figure 4-3a, b) was then evaluated in a double-mixing reaction with ABTS (2,2'-azino-bis(3-ethylbenzothiazoline-6-sulphonic acid)), a typical substrate for peroxidases (Figure 4-7). Spectral changes resulting from this reaction indicate a biphasic profile, suggesting that the intermediate produced by the reaction with *m*CPBA has the potential for two-electron oxidation. Thus, this intermediate should be a Mn^{V}-oxo species or a Mn^{IV}-oxo with π-cation radical on the porphycene ring (similar to compound I of the native hemoprotein).[1,2] This intermediate has no obvious absorption peaks in the near infrared region as shown in Figure 4-3c, although the spectrum of the porphycene π-cation radical is known to have a strong absorption band near 830 nm.[5b,13] These findings provide strong support for assignment of the observed intermediate as a Mn^{V}-oxo species. Further spectral changes occurring after formation of the Mn^{V}-oxo species without addition of substrate indicate quantitative recovery of the resting states with half-life time ($t_{1/2}$) between 20 to 38 seconds (Table 4-1). Longer $t_{1/2}$ values were observed at higher pH and the Mn^{V}-oxo species is not completely formed at pH 9.0, the highest pH value in the investigated range. Thus, pH 8.5 is a suitable pH value for quantitative formation and the longest half-life of the Mn^{V}-oxo species. It was found that the longer half-life of the intermediate provides a higher turnover number, suggesting that the detectable Mn^{V}-oxo species can react with an external substrate in the Mb-based system to replicate the function of monooxygenases.

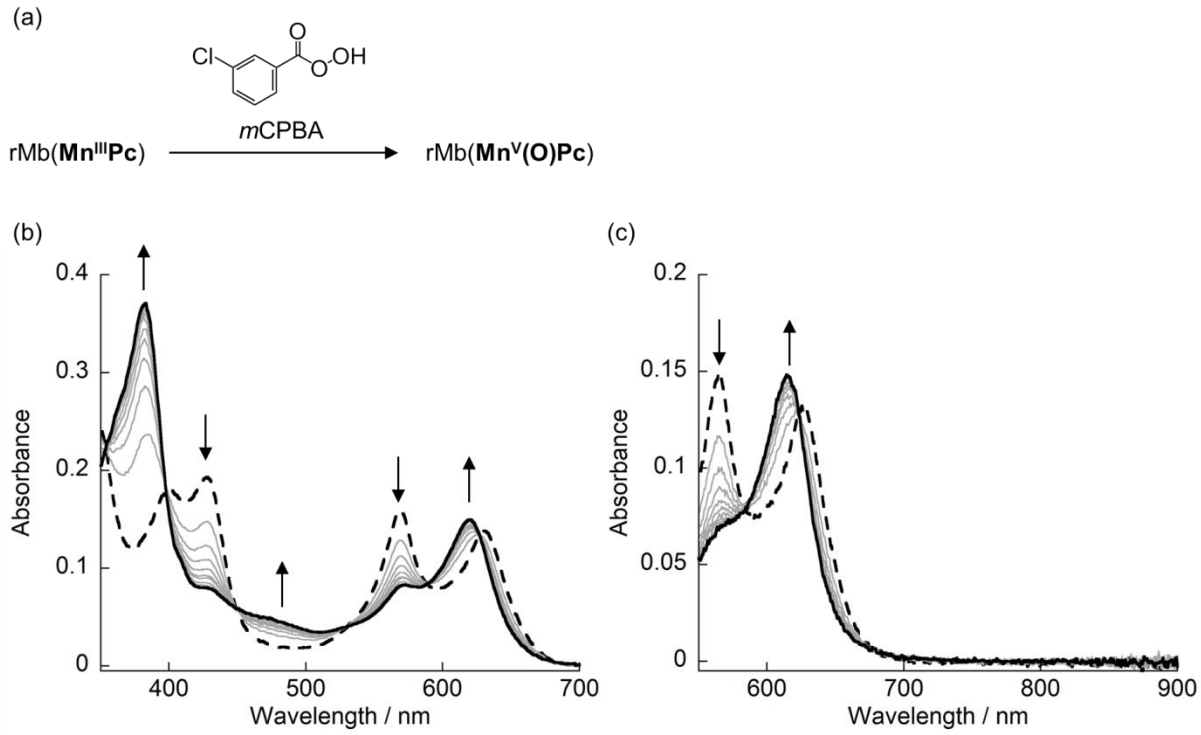

Figure 4-3. (a) Reaction of rMb(**Mn^{III}Pc**) with *m*CPBA. (b) UV-vis and (c) NIR spectral changes occurring upon addition of 10 μM *m*CPBA to a solution of rMb(**Mn^{III}Pc**) (4 μM) every 0.2 s for 2 s (black, dashed line: 0 s and black, solid line: 2 s) in 100 mM potassium phosphate buffer, pH 7.0, at 10 ºC.

Investigation of Electronic Structure of the High-valent Species

To gain insights into the electronic structure of rMb(**MnPc**), electron paramagnetic spin (EPR) spectra were recorded. Figures 4-4a and 4-4b show EPR spectra of the resting state of rMb(**MnPc**) in perpendicular- and parallel- mode measurements, respectively, to assign the electronic states of the intermediate. The integer spin (S = 2) is expected for the resting state according to a previous report of Mn-substituted Mb.[14] In the case of the rMb(**Mn^{III}Pc**), the broad signals are only observed in the spectrum using the perpendicular mode, whereas the parallel mode obviously demonstrates characteristic EPR signals, which are typical for the integer spin species. The sextet peaks at g = 8.3 with hyperfine splitting indicate coupling with the nuclear spin of Mn (I = 5/2). This result clearly confirms that the Mn^{III} species represents the resting state of rMb(**MnPc**). Next, EPR spectra of the rapidly freeze-quenched sample were measured 2 seconds after mixing of rMb(**Mn^{III}Pc**) with 2 equivalents of peracetic acid (Figure 4-4c, d). Interestingly, both perpendicular- and parallel-mode spectra provide no signal. This indicates that the intermediate is a low-spin Mn^{V} species, because the generation of π-cation radical at the porphycene ring is ruled out due to no characteristic absorption at NIR region (*vide supra*). The possibility of the presence of the Mn^{IV}-oxo species at this stage is ruled

out because the Mn^{IV} porphyrinoid is known to be an EPR-active high-spin species (S = 3/2) with typical signals ranging from 1000 to 2000 Gauss.[2b,c,15]

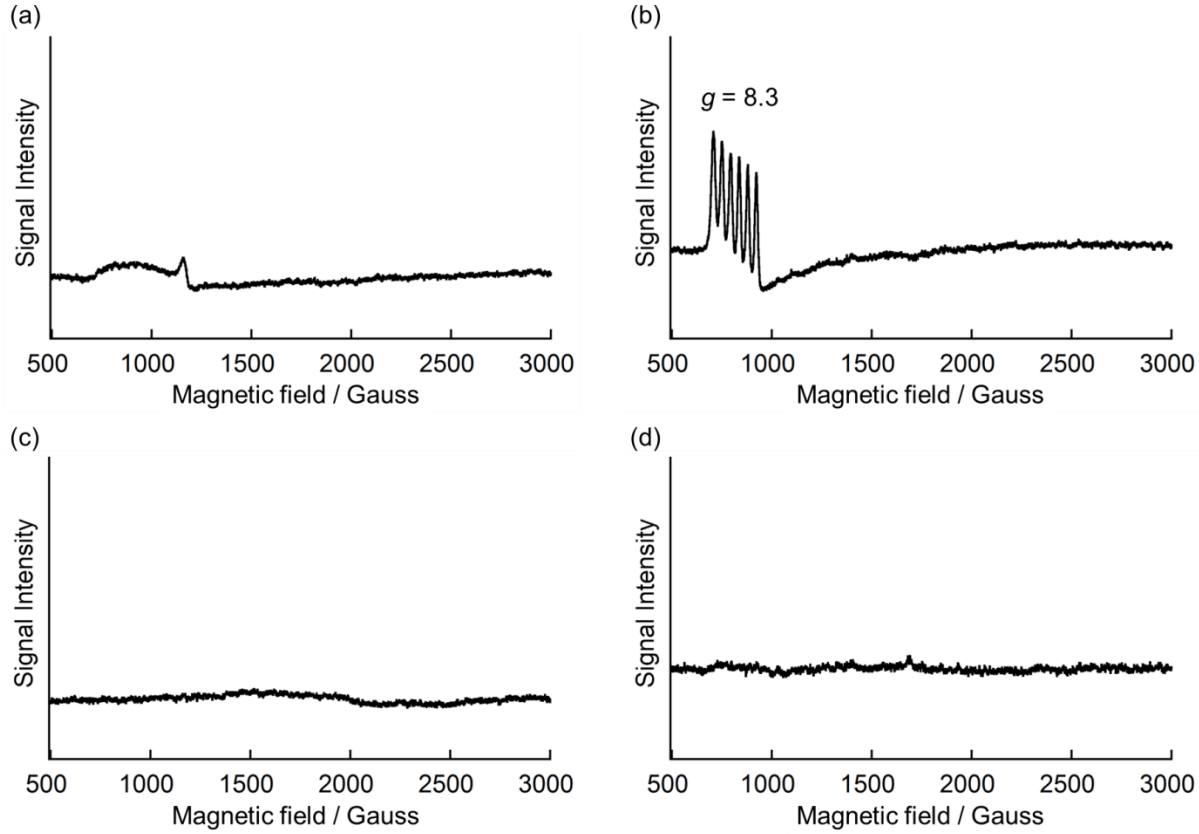

Figure 4-4. X-band EPR spectra of rMb(**Mn^{III}Pc**) (a, b) and the intermediate after the reaction with 2 equivalents of peracetic acid (c, d). Conditions: [rMb(**MnPc**)] = 0.3 mM in potassium phosphate buffer (100 mM, pH 7.0), microwave frequency = 9.68 GHz (perpendicular mode; (a) and (c)) and 9.52 GHz (parallel mode; (b) and (d)), microwave power = 2.0 mW, temperature = 5 K, modulation amplitude = 10 G and modulation frequency = 100 kHz.

Evaluation of the Reactivity of Mn^{V} species

For evaluation of the reactivity of the Mn^{V}-oxo porphycene in the Mb matrix, investigation of single turnover kinetics for hydroxylation of the ethylbenzene derivative were conducted. In this experiment, sodium 4-ethylbenzenesufonate was employed as a substrate due to its high solubility in water. The reaction of the transiently-formed rMb(**Mn^{V}**(O)**Pc**) with sodium 4-ethylbenzenesufonate was monitored using stopped-flow double mixing techniques (Figure 4-5a and 4-8). Figure 4-5a shows the decrease of the characteristic bands at 382 nm and 618 nm and concomitant increase of absorptions bands at 427 and 568 nm accompanied by isosbestic points to recover rMb(**Mn^{III}Pc**). HPLC analysis of the reaction mixture determined the quantitative formation of sodium 4-(α-hydroxyethyl)benzenesulfonate (Figure 4-11).

Furthermore, time course plots of absorbance at 380 nm (Figure 4-8) were analyzed by single exponential decay to determine the reaction rate constant, k_{obs}. The k_{obs} values are plotted against the concentration of sodium 4-ethylbenzenesufonate (Figure 4-5b). The slope of linear relationship provides the apparent second-order rate constant, k_{app}, of 2.0 $M^{-1}s^{-1}$ for 4-ethylbenzenesulfonate at 25 ºC. Furthermore, the reactions with sodium 4-toluenesulfonate (Figure 4-9) and sodium cyclohexanesulfonate (Figure 4-10) were similarly evaluated to determine the k_{app} values to be 0.29 $M^{-1}s^{-1}$ and 0.092 $M^{-1}s^{-1}$, respectively, at 25 ºC (Figures 4-5b). As shown in Figure 4-5c, the linear relationship of the plots of log k_{app} against the $C(sp^3)$–H bond dissociation energy, BDE_{C-H}, indicates that H-abstraction is one of the rate limiting steps.[16] The slope of -0.13 is relatively moderate compared with the reported typical values (-0.4 to -0.2).[16] This indicates that the k_{app} value also depends on the accessibility of the substrate into the active site of rMb.[1c]

Generally, in the hydroxylation reaction catalyzed by cytochrome P450, the rate-determining step is H-abstraction of the substrate by the compound I species.[1] In nMb, the reduction of compound I by amino acid residues such as tyrosine is extremely fast (<< 1 ms).[18] Similarly, Mbs reconstituted with iron porphycene and manganese protoporphyrin IX do not generate detectable compound I-like species and lose the opportunity to abstract a hydrogen atom from an external substrate.[1cd,5a,14,19] Thus, detection of desired intermediate is important to determine the possibility of hydroxylation of external substrates in the Mb-based system. Although the stable intermediate is generally less reactive from the viewpoint of C–H bond activation, the basicity of the Mn^{V}-oxo species appears to be high to compensate for the disadvantage of the redox potential.[20,21] In the case of the present system, longer half-life, which is equivalent with the less non-productive decay of the Mn^{V}-oxo species, and higher TON are observed at higher pH, whereas the pH value does not affect the reactivity of the Mn^{V}-oxo species (Figure 4-12). OH-rebound from the Mn^{IV}-hydroxo species follows H-abstraction to provide the hydroxylated product and the Mn^{III} species, which is supported by the isotope-labeling experiment in the previous study.[7]

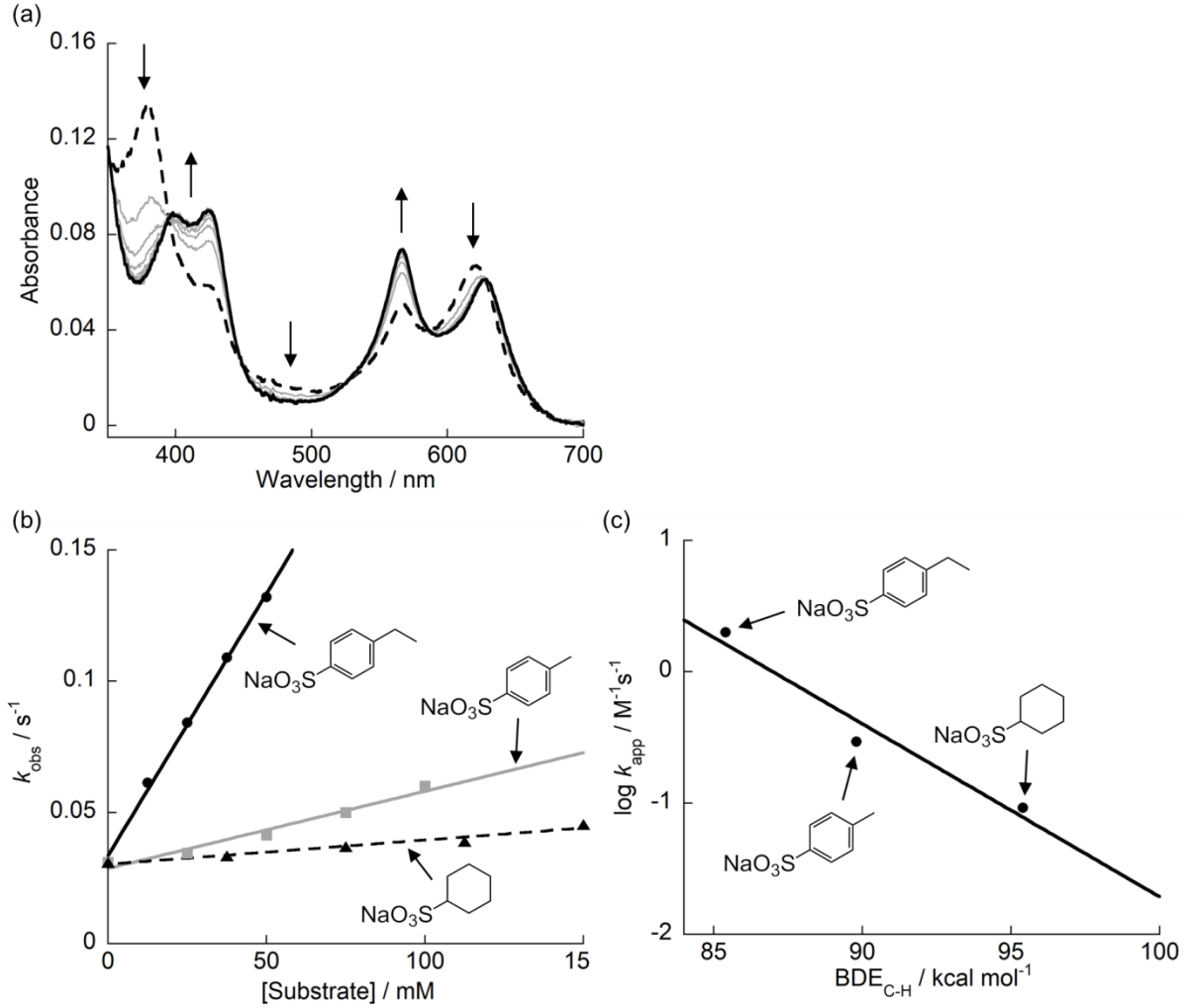

Figure 4-5. (a) UV-vis spectral changes of the intermediate monitored at 6 s intervals for 60 s after addition of sodium 4-ethylbenzenesulfonate (100 mM) as a substrate in 100 mM potassium phosphate buffer, pH 8.5, at 25 ºC (dashed line; 0 s and solid line; 60 s). The substrate was mixed 3 s after the reaction of rMb(**Mn^{III}Pc**) (4.3 μM) with *m*CPBA (6.5 μM). (b) Plots of k_{obs} determined from the absorption changes against various concentrations of the substrates at pH 8.5 and 25 ºC. Black, solid line: sodium 4-ethylabenzenesulfonate, gray, solid line: sodium 4-toluenesulfonate, and black, dashed line: sodium cyclohexanesulfonate. (c) Plots of log k_{app} against the $BDE_{C–H}$. The $BDE_{C–H}$ values of ethylbenzene, toluene and cyclohexane are utilized for the corresponding derivatives.[16,17]

4-3. Summary

Myoglobin reconstituted with manganese porphycene forms a detectable Mn^{V}-oxo species, which was characterized by a single turnover reaction and EPR spectroscopy. This finding clarifies that the lifetime of the intermediate is an important factor for C–H bond activation in a myoglobin-based artificial monooxygenase. To the best of our knowledge, the study described in this chapter is the first example of detection of a high-valent species of a chemically engineered hemoprotein during catalysis of a C–H bond hydroxylation reaction similar to hydroxylation reactions catalyzed by cytochrome P450s.

4-4. Experimental Section

Instruments

UV-vis spectral measurements were carried out with a UV-2700 spectrophotometer (Shimadzu) or V-670 UV-vis-NIR Spectrophotometer (JASCO). pH values were monitored using an F-52 pH meter (HORIBA). ESI-TOF MS analyses were performed on a micrOTOF-II mass spectrometer (Bruker). ^{1}H and ^{13}C NMR spectra were recorded on an Avance III HD spectrometer (Bruker). Chemical shifts are reported in ppm relative to the internal 1,4-dioxane signal (3.75 ppm in ^{1}H NMR and 67.19 ppm in ^{13}C NMR)[22]. The GC/FID measurements were made with a Shimadzu GC-2014 gas chromatography system. The detection of transiently formed species and kinetic measurements were conducted with a rapid scan stopped-flow system (Unisoku) constructed with a Xe or halogen light source. HPLC analyses were conducted with a Shimadzu HPLC Prominence system equipped with a YMC-Triart C18 column (150 × 10 mmI.D. or 150 × 4.6 mmI.D.). EPR spectra were measured using a Bruker EMX Plus spectrometer at the Instrument Center of the Institute for Molecular Science (Okazaki, Japan).

Materials

All chemicals were purchased from Wako, TCI, Nacalai, and Sigma-Aldrich and used as received unless otherwise noted. Manganese porphycene (**MnPc**) was synthesized as described in a previous literature.[7] Removal of heme from native myoglobin (nMb) and preparation of reconstituted myoglobin with **MnPc** (rMb(**Mn^{III}Pc**)) were performed according to reported procedures.[7,23] Sodium 4-(α-hydroxyethyl)benzenesulfonate was prepared as described below.

Synthesis of Sodium 4-(α-hydroxyethyl)benzenesulfonate

Sodium 4-styrenesulfonate hydrate (333 mg, 1.57 mmol) was dissolved in 5 mL distilled water,

followed by addition of 50% H_2SO_{4aq} (3 mL). The solution was then refluxed for 16 h. The reaction mixture was allowed to cool to ambient temperature and carefully neutralized with 1 M $NaOH_{aq}$. To the solution, 50 mL of methanol was added and inorganic salt was removed by suction filtration. The solution was allowed to dryness by rotary evaporator to afford white solid. The crude product was purified with a reverse phase HPLC (CH_3CN/H_2O eluent) to give pure sodium 4-(α-hydroxyethyl)benzenesulfonate as white powder (120 mg, 0.54 mmol, 34%). ^{1}H NMR (400 MHz, D_2O) δ (ppm) = 7.79 (2H, d, *J* = 8.4 Hz), 7.53 (2H, d, *J* = 8.4 Hz), 4.97 (1H, q, *J* = 6.4 Hz), 1.48 (3H, d, *J* = 6.4 Hz). ^{13}C NMR (100 MHz, D_2O) δ (ppm) = 148.50, 141.23, 125.94, 125.58, 66.45, 23.48.

Evaluation of Activity of Catalytic Hydroxylation at Various pH

The reactions were carried out in 100 mM potassium phosphate buffer at various pH (from 7.0 to 9.0) containing 8% CH_3CN at 25 ºC for 3 h. A buffer solution of rMb(**MnPc**) (20 μM) and ethylbenzene (8.0 mM) was incubated for 5 min prior to the addition of H_2O_2 (10 mM). After the reaction, benzyl alcohol as an internal standard and diethyl ether were added, and the reaction mixture was vigorously shaken using a vortex mixer to extract the organic materials. The separated organic phase was concentrated by evaporation with streaming N_2 gas, and the residue was analyzed with a GC/FID system equipped with a DB-1 column.

Crystallization of rMb(Mn^{III}Pc)

A solution of rMb(**Mn^{III}Pc**) in 10 mM potassium phosphate buffer at pH 7.0 was passed through a HiTrap SP sepharose FF cation exchange column to remove the residual apoprotein. The purified protein was crystallized at 25 °C using the hanging-drop vapor diffusion method with cross-seeding of microcrystals of nMb. The crystals were obtained using a reservoir solution containing 3.0 M ammonium sulfate and 100 mM Tris-HCl buffer at pH 8.5 and a hanging drop solution containing 1.5 M ammonium sulfate, 5 mg/mL of the protein, 50 mM Tris-HCl buffer and 5 mM potassium phosphate buffer at pH 8.5.

Data Collection, Structure Determination and Refinement

The crystal was soaked into cryobuffer (crystallization buffer with 18% (w/v) sucrose) and flash-cooled in liquid N_2. X-ray diffraction data were collected at the beamline BL26B1, SPring-8, Japan. The dataset was integrated and scaled with the HKL2000 program. The coordinate of Protein Data Bank (PDB) ID 3WI8 was used as the starting model in the structure refinement. Structure was manually rebuilt in the program COOT and refined with REFMAC5. Data collection and refinement statistics are summarized in Table S1. The final atomic coordinates and structure factor amplitudes were deposited in the PDB with ID 5YL3.

Table 4-2. Data Collection Statistics for rMb(Mn^{III}Pc)

	rMb(**Mn^{III}Pc**)
Data collection	
X-ray source	BL26B1
Wavelength (Å)	1.0
Resolution (Å)	30 - 1.50
Space group	$P2_1$
Cell dimensions (Å, deg.)	a = 34.58, b = 28.71, c = 62.70, β = 106.2
No. of total reflections	135,739
No. of unique reflections	19,335
Completeness (%)	99.6 (93.8)
R_{sym}	7.5 (52.6)
$I/\sigma(I)$	22.4 (2.3)
Refinement	
R_{work}/R_{free}	0.168/0.208
Mean B-factor (Å^2)	16.6
Rmsd from ideal	
Bonds (Å)/angles (deg)	0.016/2.95

Table 4-3. Geometry of Cofactor and Comparison of *B* Factors of MnPc in rMb(Mn^{III}Pc)

	This Work	Ref. 9
PDB ID	5YL3	3WI8
sample	aquomet	aquomet
space group	$P2_1$	$P2_1$
resolution (Å)	1.5	2.2
pH of crystallization	8.5	7.0
distances		
His93 Nε–Mn (Å)	2.31	2.58
Wat O–Mn (Å)	2.36	2.79
His64 Nε–Mn (Å)	4.48	4.72, 8.90[a]
B_{MnPc}/B_{prot} [b]	1.0	1.8

[a]Two alternative conformations exist.

[b]B_{prot} is an averaged B factor of Cα carbon of the protein main chain. B_{MnPc} is the averaged B factor of carbon atoms in the framework of porphycene and the metal atom.

Alkali titration of rMb(Mn^{III}Pc)

To a solution of rMb(**Mn^{III}Pc**) (2.4 μM, 3 mL in 10 mM potassium phosphate buffer at pH 7.0), 1 M or 100 mM of KOH_{aq} was added at 25 °C. The UV-vis spectra and pH values of the protein solution were monitored and a pK_a value of H_2O coordinating to the metal center was determined by fitting the titration curve to the modified Henderson-Hasselbach equation.[24] The spectral changes and titration curve are shown in Figure 4-6.

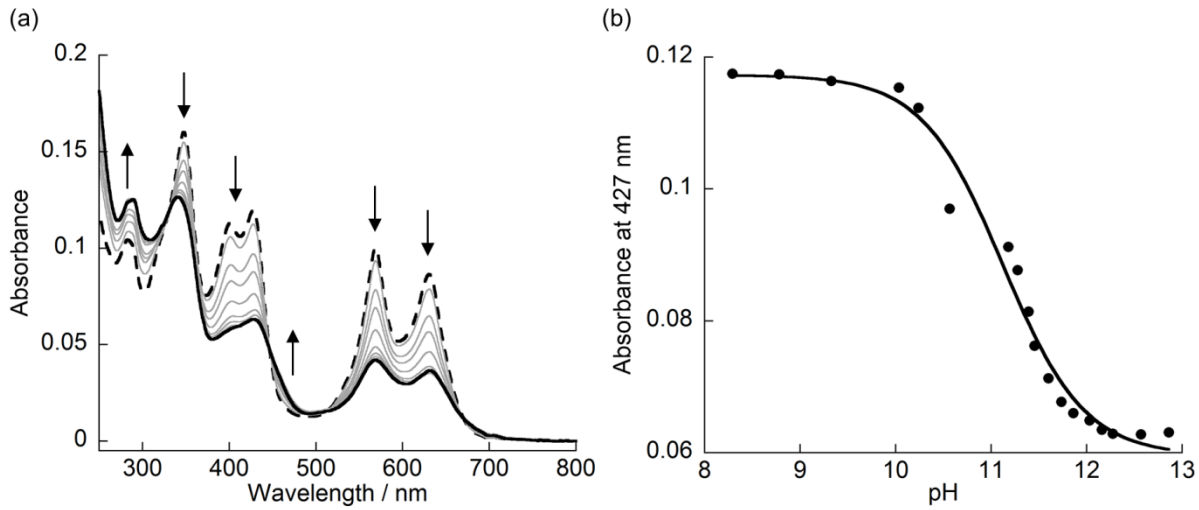

Figure 4-6. (a) UV-vis spectral changes of rMb(**Mn^{III}Pc**) during alkali titration. Dashed line and solid line are obtained at pH 7.0 and 12.9, respectively. (b) Plots of absorbances monitored at 427 nm against pH value during the titration.

Observation of Transiently Formed High-valent Species in rMb(MnPc)

A solution containing rMb(**Mn^{III}Pc**) (8 μM) in 100 mM potassium phosphate buffer at various pH from 7 to 9 was mixed with a solution containing *m*-chloroperoxybenzoic acid (*m*CPBA) (20 μM) in 100 mM potassium phosphate buffer at the same pH with the protein solution. Transient absorption changes were recorded using stopped-flow rapid scanning apparatus at 10 °C.

Analysis of the Reactivity toward Oxidation Reaction of 2,2'-azino-bis(3-ethylbenzothiazoline-6-sulfonic acid) (ABTS)

A solution of rMb(**Mn^{III}Pc**) (16 μM) in 100 mM potassium phosphate buffer at pH 7.0 was mixed with an *m*CPBA solution (24 μM) in 100 mM potassium phosphate buffer at pH 7.0 and incubated for 2 s at 10 °C. To the mixture, a solution containing 1 mM ABTS in 100 mM potassium phosphate buffer at pH 7.0 was mixed and transient absorption spectra were monitored at 10 °C. Transient absorption spectra and time course plots are shown in Figure 4-7.

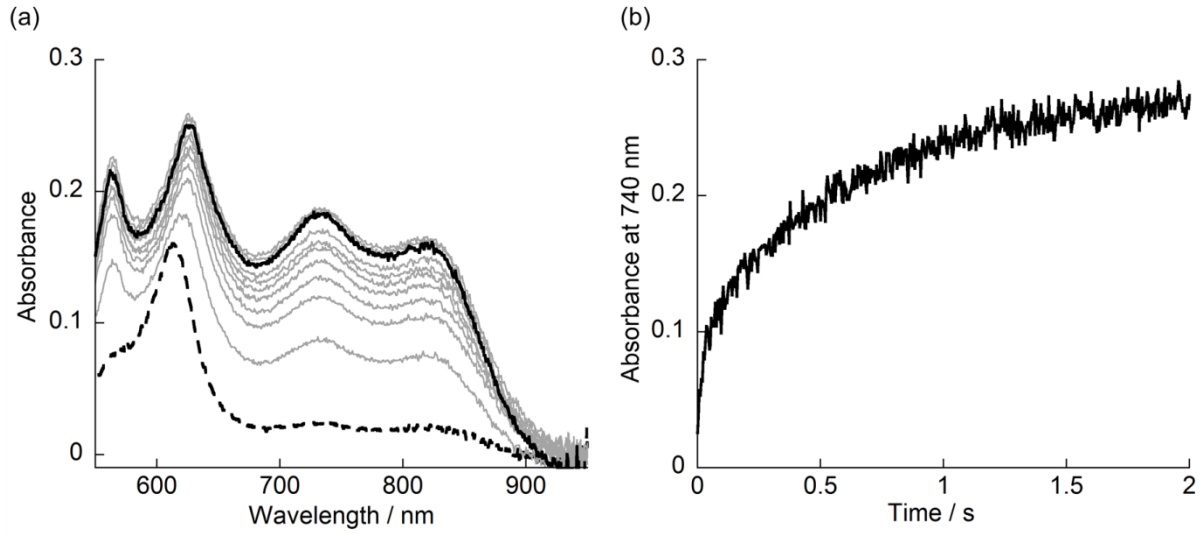

Figure 4-7. (a)Transient absorption spectra of rMb(**Mn**$^{\mathbf{V}}$(O)**Pc**) after addition of 1.0 mM ABTS monitored every 0.2 s for 2.0 s and (b) time course plots of absorption changes monitored at 740 nm. The bend of the slope at 0.3 s supports the biphasic reaction. Conditions: [rMb(**Mn**$^{\mathbf{III}}$**Pc**)] = 4 μM, [*m*CPBA] = 6 μM and [ABTS] = 0.5 mM in 100 mM potassium phosphate buffer at pH 7.0 and 10 °C. Aging time: 2 s.

Evaluation of Hydroxylation Reactivity of rMb(Mn$^{\mathbf{V}}$(O)Pc)

Reaction of a transiently formed rMb(**Mn**$^{\mathbf{V}}$(O)**Pc**) with substrates was evaluated using a stopped-flow double mixing apparatus. To a solution of rMb(**Mn**$^{\mathbf{III}}$**Pc**) (8.6 μM) in 100 mM potassium phosphate buffer at pH 8.5, a solution of *m*CPBA (12.9 μM) in 100 mM potassium phosphate buffer at pH 8.5 was added and incubated for 3 s at 25 °C. To the mixture, a solution containing various concentration of sodium 4-ethylbenzenesulfonate (25 - 100 mM) (Figure 4-8), sodium 4-toluenesulfonate (50 - 200 mM) (Figure 4-9) or sodium cyclohexanesulfonate (75 - 300 mM) (Figure 4-10) in 100 mM potassium phosphate buffer at pH 8.5 was added and transient absorption spectra were monitored at 25 °C. Transient absorption changes were fitted with a single exponential equation to determine apparent reaction rate constants k_{obs}. The second-order rate constants, k_{app}, were determined with plots of k_{obs} against the concentration of substrates.

Hydroxylated product of sodium 4-ethylbenzenesulfonate was analyzed under a single turnover condition. To a solution of rMb(**Mn**$^{\mathbf{III}}$**Pc**) (4.3 μM, 500 μL) containing 100 mM sodium 4-ethylbenzenesulfonate in 100 mM potassium phosphate buffer at pH 8.5, a solution of *m*CPBA (6.5 μM, 500 μL) in 100 mM potassium phosphate buffer at pH 8.5 was added and incubated for 3 minutes at 25 °C. To the reaction mixture, 10 μL of 100 mM benzyl alcohol in acetonitrile was added as an internal standard. The product, sodium 4-(α-hydroxyethyl)benzenesulfonate was quantified using a reverse-phase HPLC (CH_3CN/H_2O eluent). The HPLC traces are shown in Figure 4-11.

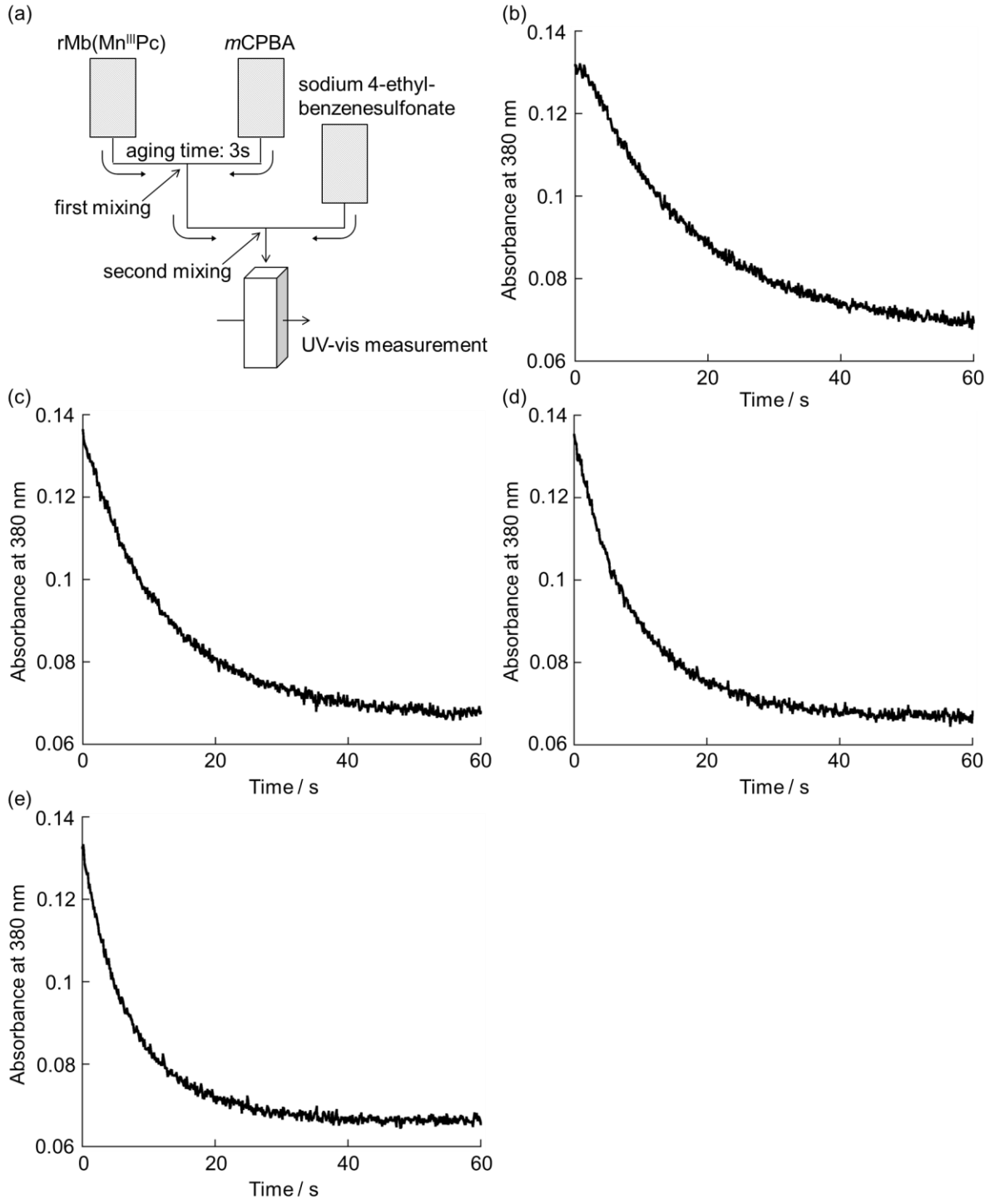

Figure 4-8. (a) Schematic representation of the stopped-flow double-mixing apparatus. Time course plots of the absorption changes of rMb(**Mn^{V}**(O)**Pc**) after addition of (b) 25 mM, (c) 50 mM, (d) 75 mM, and (e) 100 mM of sodium 4-ethylbenzenesulfonate, monitored at 380 nm. Conditions: [rMb(**Mn^{III}Pc**)] = 2.2 μM, [*m*CPBA] = 3.2 μM and [sodium 4-ethylbenzenesulfonate] = 12.5 – 50 mM in 100 mM potassium phosphate buffer at pH 8.5 and 25 °C. Aging time: 3 s.

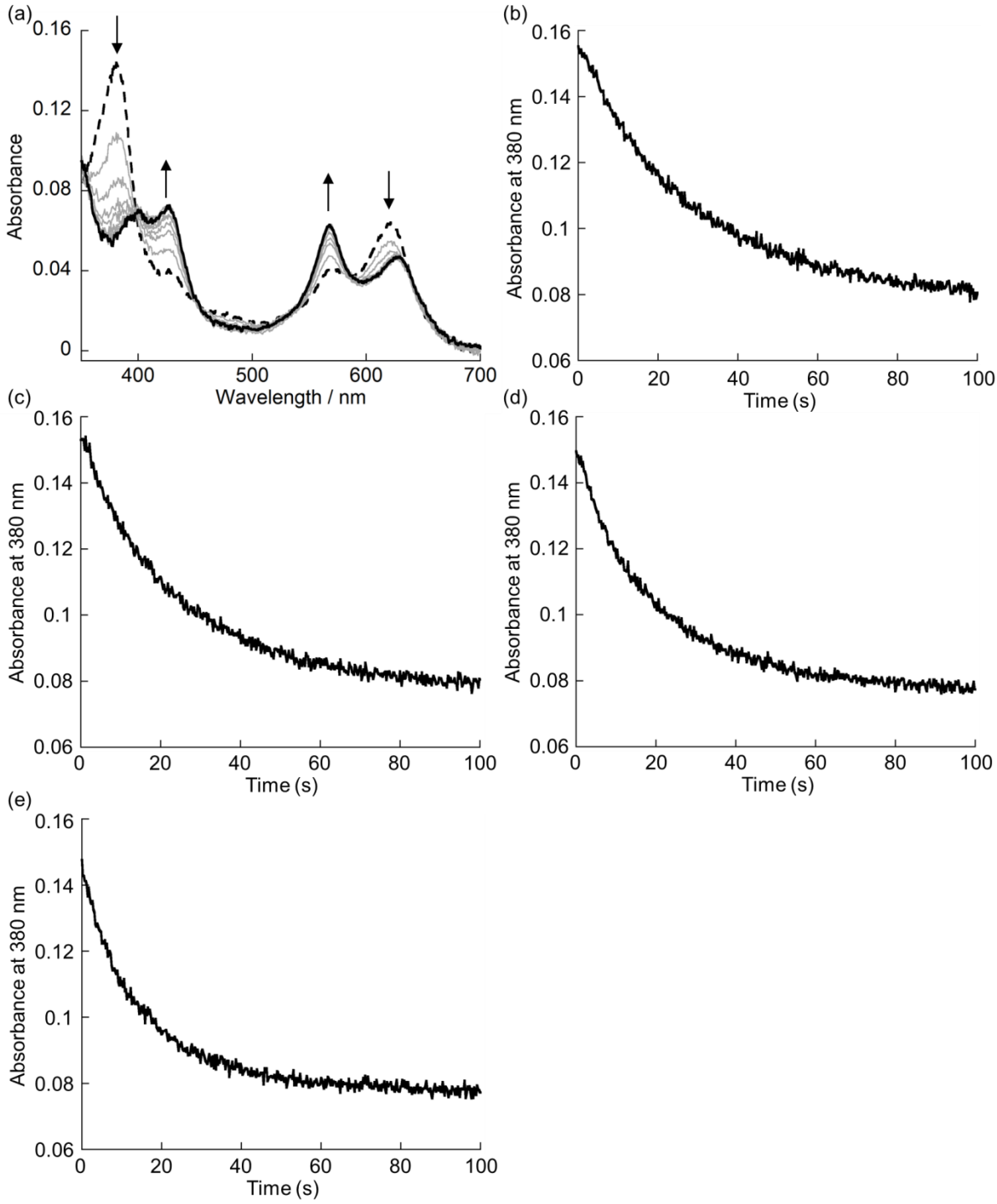

Figure 4-9. (a) Transient absorption spectra of rMb(**Mn**$^{\mathbf{V}}$(O)**Pc**) monitored every 12 s for 120 s after addition of 200 mM sodium 4-toluenesulfonate (dashed line: 0s and solid line: 120 s). Time course plots of the absorption changes of monitored at 380 nm after addition of (b) 50 mM, (c) 100 mM, (d) 150 mM, and (e) 200 mM of sodium 4-toluenesulfonate. Conditions: [rMb(**Mn**$^{\mathbf{III}}$**Pc**)] = 2.2 μM, [*m*CPBA] = 3.2 μM and [sodium 4-toluenesulfonate] = 25 - 100 mM in 100 mM potassium phosphate buffer at pH 8.5 and 25 °C. Aging time: 3 s.

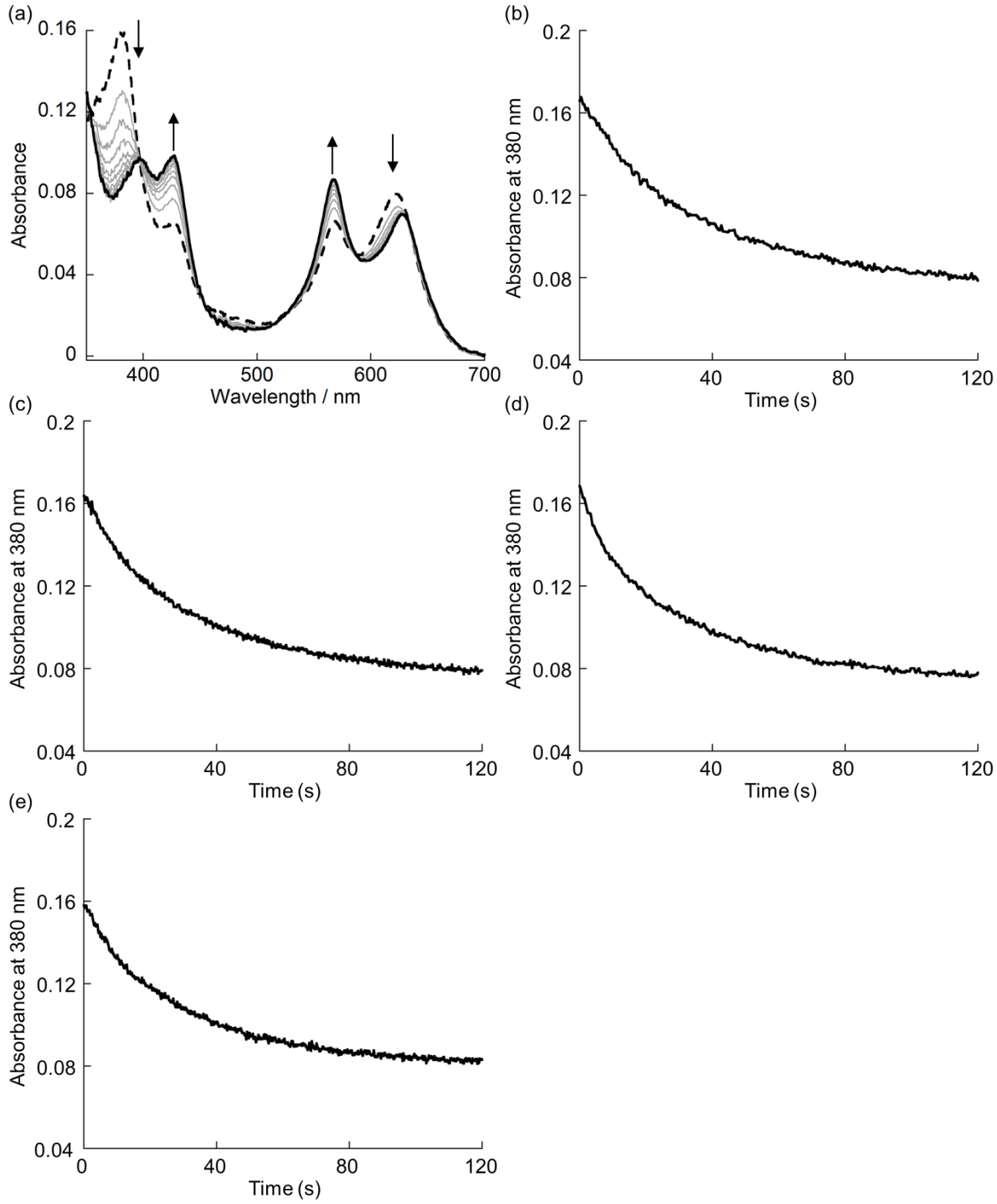

Figure 4-10. (a) Transient absorption spectra of rMb(**Mn**$^{\mathbf{V}}$(O)**Pc**) monitored every 12 s for 120 s after addition of 300 mM sodium 4-cyclohexanesulfonate (dashed line: 0s and solid line: 120 s). Time course plots of the absorption changes of monitored at 380 nm after addition of (b) 75 mM, (c) 150 mM, (d) 225 mM, and (e) 300 mM of sodium cyclohexanesulfonate. Conditions: [rMb(**Mn**$^{\mathbf{III}}$**Pc**)] = 2.2 μM, [*m*CPBA] = 3.2 μM and [sodium cyclohexanesulfonate] = 37.5 - 150 mM in 100 mM potassium phosphate buffer at pH 8.5 and 25 °C. Aging time: 3 s.

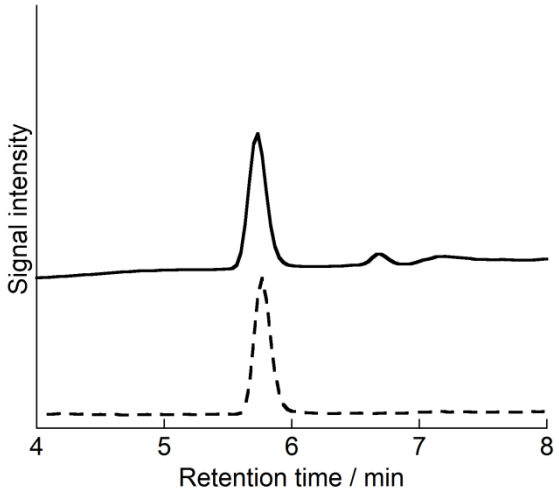

Figure 4-11. HPLC traces for reaction mixture of rMb(**Mn^{III}Pc**) with *m*CPBA and sodium 4-ethylbenzenesulfonate (solid line) and for chemically-synthesized sodium 4-(α-hydroxyethyl)benzenesulfonate solution (dahed line). The analyses were performed at a flow rate of 1 mL/min of water/acetonitrile co-solvent (from 100:0 to 20:80) containing 0.1% TFA for 30 min using a column oven at 50 °C. Reaction conditions: [rMb(**Mn^{III}Pc**)] = 2.2 μM, [*m*CPBA] = 3.2 μM, [substrate] = 50 mM in 100 mM potassium phosphate buffer at pH 8.5 and 25 °C. Reaction time: 3 min. Detection: absorption at 220 nm.

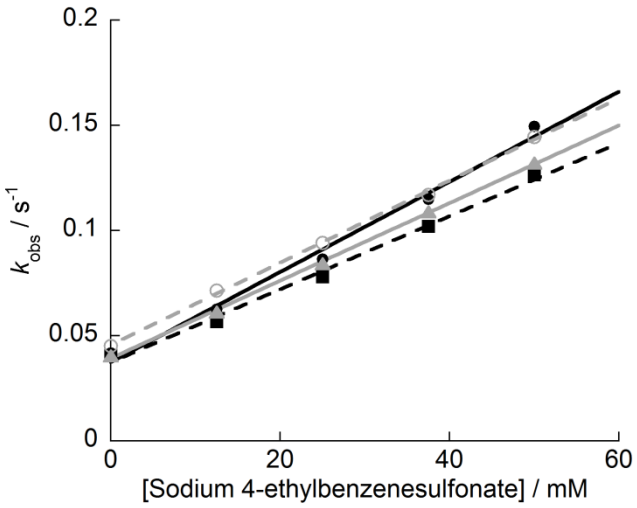

Figure 4-12. Plots of k_{obs} determined from the absorption changes against various concentrations of sodium 4-ethylbenzenesulfonate at pH 7.0 - 9.0. (Black, solid line: pH 7.0, black, dashed line: pH 8.0, gray, solid line: pH 8.5 and gray, dashed line: pH 9.0). Conditions: [rMb(**Mn^{III}Pc**)] = 4.3 μM, [*m*CPBA] = 6.5 μM in 100 mM potassium phosphate buffer at 25 ºC.

EPR Measurements

The measurements of EPR spectra were carried out at the X-band microwave frequency (perpendicular mode: 9.35 GHz and parallel mode: 9.65 GHz) with 100 kHz field modulation and 10 G of modulation amplitude. During EPR measurements, the sample temperature was maintained at 5 K by an Oxford Instruments ESR900 cryostat equipped with a turbo pump to lower vapor pressure of the liquid He. Each protein solution (final concentration: 0.3 mM) in 0.1 M potassium phosphate buffer (pH 7.0) was placed in a 5 mm EPR tube. The sample was quickly frozen in a cold pentane bath chilled with liquid N_2. The intermediate was prepared using a manual mixer equipped with a PEEK tube inserted into the EPR tube and the sample was quickly frozen at 2 s after the addition of 2 equivalents of peracetic acid buffer solution into the rMb(**Mn^{III}Pc**) solution (0.6 mM).

4-5. References and Notes

(1) (a) Denisov, I. G.; Makris, T. M.; Sligar, S. G.; Schlichting, I. *Chem. Rev.* **2005**, *105*, 2253–2277. (b) Ortiz de Montellano, P. R. *Chem. Rev.* **2010**, *110*, 932–948. (c) Rittle, J.; Green, M. T. *Science* **2010**, *330*, 933–937. (d) Yosca, T. H.; Rittle, J.; Krest, C. M.; Onderko, E. L.; Silakov, A.; Calixto, J. C.; Behan, R. K.; Green, M. T. *Science* **2013**, *342*, 825–829. (e) Kawakami, N.; Shoji, O.; Watanabe, Y. *Angew. Chem. Int. Ed.* **2011**, *50*, 5315–5318. (f) Prier, C. K.; Zhang, R. K.; Buller, A. R.; Brinkmann-Chen, S.; Arnold, F. H. *Nat. Chem.* **2017**, *9*, 629–634.

(2) (a) Jin, N.; Lahaye, D. E.; Groves, J. T. *Inorg. Chem.* **2010**, *49*, 11516–11524. (b) Arunkumar, C.; Lee, Y.-M.; Lee, J. Y.; Fukuzumi, S.; Nam, W. *Chem. Eur. J.* **2009**, *15*, 11482–11489. (c) Song, W. J.; Seo, M. S.; George, S. D.; Ohta, T.; Song, R.; Kang, M.-J.; Tosha, T.; Kitagawa, T.; Solomon, E. I.; Nam, W. *J. Am. Chem. Soc.* **2007**, *129*, 1268–1277. (d) Srour, H.; Maux, P. L.; Simonneaux, G. *Inorg. Chem.* **2012**, *51*, 5850–5856. (e) Liu, W.; Cheng, M.-J.; Nielsen, R. J.; Goddard, W. A. III, Groves, J. T. *ACS Catal.* **2017**, *7*, 4182−4188.

(3) (a) Harischandra, D. N.; Zhang, R.; Newcomb, M. *J. Am. Chem. Soc.* **2005**, *127*, 13776–13777. (b) Matsuo, T.; Hayashi, A.; Abe, M.; Matsuda, T.; Hisaeda, Y.; Hayashi, T. *J. Am. Chem. Soc.* **2009**, *131*, 15124–15125. (c) Kumar, A.; Goldberg, I.; Botoshansky, M.; Buchman, Y.; Gross, Z. *J. Am. Chem. Soc.* **2010**, *132*, 15233–15245. (d) Zaragoza, J. P. T.; Yosca, T. H.; Siegler, M. A.; Moënne-Loccoz, P.; Green, M. T.; Goldberg, D. P. *J. Am. Chem. Soc.* **2017**, *139*, 13640–13643.

(4) Neu, H. M.; Baglia, R. A.; Goldberg, D. P. *Acc. Chem. Res.* **2015**, *48*, 2754–2764.

(5) (a) Hayashi, T.; Murata, D.; Makino, M.; Sugimoto, H.; Matsuo, T.; Sato, H.; Shiro, Y.; Hisaeda, Y. *Inorg. Chem.* **2006**, *45*, 10530-10536. (b) Matsuo, T.; Murata, D.; Hisaeda, Y.; Hori, H.; Hayashi, T. *J. Am. Chem. Soc.* **2007**, *129*, 12906–12907.

(6) (a) Mahy, J.-P.; Maréchal, J.-D.; Ricoux, R. *J. Porphyrins Phthalocyanines* **2014**, *18*, 1063–1092. (b) Dydio. P.; Key, H. M.; Nazarenko, A.; Rha, J. Y.-E.; Seyedkazemi, V.; Clark, D. S.; Hartwig, J. F. *Science* **2016**, *354*, 102–106. (c) Schwizer, F.; Okamoto, Y.; Heinisch, T.; Gu, Y.; Pellizzoni, M. M.; Lebrun, V.; Reuter, R.; Köhler, V.; Lewis, J. C.; Ward, T. R. *Chem. Rev.* **2017**, *in press*, DOI: 10.1021/acs.chemrev.7b00014. (d) Upp, D. M.; Lewis, J. C. *Curr. Opin. Chem. Biol.* **2017**, *37*, 48–55. (e) Nastri, F.; Chino, M.; Maglio, O.; Bhagi-Damodaran, A.; Lu, Y.; Lombardi A. *Chem. Soc. Rev.* **2016**, *45*, 5020–5054.

(7) First demonstration of catalytic hydroxylation of inert alkanes using an engineered Mb: Oohora, K.; Kihira, Y.; Mizohata, E.; Inoue, T.; Hayashi, T. *J. Am. Chem. Soc.* **2013**, *135*, 17282–17285.

(8) In the porphyrinoid-based system, the bond between Mn and O may be a double or a triple bond.[2-4] In this chapter, the bond between Mn and O is described as Mn=O according to the previous reports for Mn^{V}-oxo porohyrin.[2]

(9) The relatively low TON is derived from the decomposition of the cofactor. The cofactor bound in the protein matrix is found to decompose within several hours under the catalytic conditions.

(10) The alkali titration shown in Figure 4-6 indicates that the pK_a value of the coordinated water molecule is 11.1.

(11) The His64 residue with two conformations was observed in the previously reported structure of rMb(Mn^{III}Pc) at pH 7.0: In one conformation, His64 is located above the cofactor as seen in the nMb structure and on the other His64 is flipped outside near the protein surface.[7]

(12) The highly reactive oxidant, *m*CPBA, was used for detecting the active species under almost stoichiometric conditions because the reaction of rMb(**Mn^{III}Pc**) with a slight excess of hydrogen peroxide did not proceed under the same condition.

(13) Kadish, K. M.; D'Souza, F.; Caemelbecke, E. V.; Boulas, P.; Vogel, E.; Aukauloo, A. M.; Guilard, R. *Inorg. Chem.* **1994**, *33*, 4474–4479.

(14) Horitani, M.; Yashiro, H.; Hagiwara, M.; Hori, H. *J. Inorg. Biochem.* **2008**, *102*, 781–788.

(15) Stone, K. L.; Hua, J.; Choudhry, H. *Inorganics* **2015**, *3*, 219–229.

(16) Xue, X.-S.; Ji, P.; Zhou, B.; Cheng, J.-P. *Chem. Rev.* **2017**, *117*, 8622–8648.

(17) The negligible substituent effects of the sulfonate group for the BDE values are considered because of its small Hammett substituent constant ($\sigma = 0.09$): McDaniel, D. H.; Brown, H. C. *J. Org. Chem.* **1958**, *23*, 420−427.

(18) (a) Adachi, S.; Nagano, S.; Ishimori, K.; Watanabe, Y.; Morishima, I.; Egawa, T.; Kitagawa, T.; Makino, R. *Biochemistry* **1993**, *32*, 241–252. (b) Lardinois, O. M.; Ortiz de Montellano, P. R. *Biochemistry* **2004**, *43*, 4601–4610.

(19) Cai, Y.-B.; Li, X.-H.; Jing, J.; Zhang, J.-L. *Metallomics* **2013**, *5*, 828–835.

(20) Bernard, C.; Gisselbrecht, J. P.; Vogel, E.; Lausmann, M. *Inorg. Chem.* **1994**, *33*, 2393–2401.

(21) Manganese porphyrinoids have been experimentally and theoretically proposed as a promising catalyst that efficiently promotes C−H bond activation: (a) Borovik, A. S. *Chem. Soc. Rev.* **2011**, *40*, 1870–1874. (b) Latifi, R.; Tahsini, L.; Karamzadeh, B.; Safari, N.; Nam, W.; de Visser, S. P. *Arch. Biochem. Biophys*. **2011**, *507*, 4–13.

(22) Fulmer, G. R.; Miller, A. J. M.; Sherden, N. H.; Gottlieb, H. E.; Nudelman, A.; Stoltz, B. M.; Bercaw, J. E.; Goldberg, K. I. *Organometallics* **2010**, *29*, 2176–2179.

(23) Teale, F. W. J. *Biochim. Biophys. Acta* **1959**. *35*, 543.

(24) Lloyd, E.; Burk, D. L.; Ferrer, J. C.; Maurus, R.; Doran, J.; Carey, P. R.; Brayer, G. D.; Mauk, A. G. *Biochemistry* **1996**, *35*, 11901−11912.

Conclusion

In nature, metalloenzymes are known to achieve various sophisticated reactions regulated by the combination of protein matrices and metal ions or complexes. Over several decades, thousands of studies focusing on the structure-function relationships of metalloenzymes have been done, giving a lot of insights into these mechanisms. Then, one of the next aims is the generation of modified and/or artificial metalloenzymes to develop a new biocatalyst. Toward this end, Hayashi *et al.* have devoted their efforts to increase the inherent reactivity and catalytic activities of myoglobin (Mb) by prosthetic group substitutions and/or amino acid mutations. As a result of these studies, it is now appreciated that the replacement of native heme prosthetic group with an appropriate metal complex enhances the enzymatic activities of H_2O_2-dependent peroxidase and peroxygenase reactions. In contrast, the author has focused on the generation of new artificial metalloenzyme capable of promoting reactions which are not seen in biological systems by reconstitution of Mb. In this thesis, the author presents the details of reactivity and physicochemical properties of abiological porphyrinoid prosthetic groups in a Mb matrix toward development of artificial metalloenzymes. From these studies, it is found that the appropriate metal porphyrinoids are capable of converting Mb, an oxygen storage protein, into a new metalloenzyme such as cyclopropanase or hydroxylase as follows.

In chapter 2, the author described the preparation and investigation of physicochemical properties of iron oxaporphyrin (**FeOP**) where one of pyrrole-nitrogens was replaced with oxygen, and Mb was reconstituted with **FeOP** (rMb(**FeOP**)). **FeOP** dimethylester significantly stabilizes the ferrous species. The ferrous species of **FeOP** is also stable in the Mb matrix under anaerobic condition. Under aerobic condition, oxidized ferric species of **FeOP** is released from the protein matrix due to decreasing hydrophobic interaction of **FeOP** with Mb matrix. Furthermore, acceleration of cyanide binding behavior by 150-fold for the ferrous state of rMb(**FeOP**) was observed compared to the ferric nMb. Thus, **FeOP** serves as a new type of abiological cofactor for Mb with the stabilized ferric species and rapid cyanide binding character.

In chapter 3, the author described the catalytic activity of Mb reconstituted with iron porphycene (rMb(**FePc**)) toward the carbene-transfer cyclopropanation reaction of styrene. The catalytic activity of rMb(**FePc**) was significantly enhanced as compared to that of nMb. Spectroscopic investigations demonstrate that the reaction of rMb(**FePc**) with ethyl diazoacetate was 615-fold faster than that of nMb, indicating rapid formation of the active carbene species. Theoretical calculation indicates that the stabilization of the triplet deoxy state of rMb(**FePc**) due to the strong ligand field of porphycene results in the rapid formation of the active carbene species. These findings would open a way for creation of the

highly active hemoprotein-based enzyme for cyclopropanation reaction by substitution of the prosthetic group.

In chapter 4, the author described the investigation of crystal structure and catalytic behavior of Mb reconstituted with manganese porphycene (rMb(**MnPc**)) toward hydroxylation of external substrates. It was found that **MnPc** tightly binds to the Mb matrix in the crystal structure. Spectroscopic investigation revealed that rMb(**MnPc**) generates a two-electron oxidative intermediate upon the reaction with peracids. The high-valent intermediate was characterized as a Mn^{V}-oxo species by UV-vis, NIR and EPR spectroscopic methods. Furthermore, the Mn^{V}-oxo species reacted with inert alkane substrates and was identified as the active intermediate in the catalysis of C–H bond hydroxylation. It is proposed that formation of a reactive high-valent species with a long lifetime is a key for the hydroxylation of external substrates.

Taken together, the obtained results suggest that artificial metal porphyrinoids have a great potential to become an appropriate prosthetic group for dramatically modifying the physiological properties and reactivities of hemoproteins. Particularly, it is of interest to promote a stereo/regio selective non-natural reaction catalyzed by artificial metalloenzymes with various synthetic prosthetic groups, because it could be easy to chemically modify the structure and electronic properties. Thus, the author here concludes that the presented strategy will serve as a new way to create a quite effective biocatalyst by a simple protein with a suitable scaffold.

List of Publications

1. Preparation and Characterization of Myoglobin Reconstituted with Fe(II) Oxaporphyrin: The Monoanionic Macrocycle Provides Unique Cyanide Binding Behavior for the Ferrous Species
Hiroyuki Meichin, Koji Oohora, Takashi Hayashi
Inorganica Chimica Acta, **2018**, *472*, 184–191.

2. Catalytic Cyclopropanation by Myoglobin Reconstituted with Iron Porphycene: Acceleration of Catalysis due to Rapid Formation of the Carbene Species
Koji Oohora, Hiroyuki Meichin, Liming Zhao, Matthew W. Wolf, Akira Nakayama, Jun-ya Hasegawa, Nicolai Lehnert, Takashi Hayashi
Journal of the American Chemical Society, **2017**, *139*, 17265–17268.

3. Manganese(V) Porphycene Complex Responsible for Inert C–H Bond Hydroxylation in a Myoglobin Matrix
Koji Oohora, Hiroyuki Meichin, Yushi Kihira, Hiroshi Sugimoto, Yoshitsugu Shiro, Takashi Hayashi
Journal of the American Chemical Society, **2017**, *139*, 18460–18463.